

Thesis for the Degree of Doctor of Philosophy

**CELLULAR DYES AND BIOACTIVE PEPTIDES**  
- CELL MEMBRANE INTERACTIONS AND CELLULAR UPTAKE

MARIA MATSON DZEBO



**CHALMERS**

Department of Chemical and Biological Engineering  
Chalmers University of Technology  
Gothenburg, Sweden 2014

Cellular Dyes and Bioactive Peptides  
- Cell Membrane Interactions and Cellular Uptake  
MARIA MATSON DZEBO  
ISBN: 978-91-7597-096-7

© MARIA MATSON DZEBO, 2014

Doktorsavhandlingar vid Chalmers tekniska högskola  
Ny serie nr 3777  
ISSN 0346-718X

Department of Chemical and Biological Engineering  
Chalmers University of Technology  
SE-412 96 Gothenburg  
Sweden  
Telephone + 46 (0)31-772 1000

**Front cover:** Four different types of molecules and their membrane interaction and cellular uptake are studied in this thesis. The categories of molecules are illustrated by representative molecules: the ruthenium complex D4 (top), a voltage-sensitive ANEPPS dimer (left), the cell-penetrating peptide RWmix (bottom), and the antisecretory peptide AF-16 (right).

**Back cover:** photograph by Peter Sandin

Printed by Chalmers Reproservice  
Gothenburg, Sweden 2014

# Cellular Dyes and Bioactive Peptides

## - Cell Membrane Interactions and Cellular Uptake

Maria Matson Dzebo

Department of Chemical and Biological Engineering  
Chalmers University of Technology

### Abstract

---

Knowledge about mechanisms behind interactions of molecules with biomembranes and cellular uptake is very important for understanding biological processes and for drug design. The work described in this thesis has focused on interactions of cellular dyes and bioactive peptides with cells and the cell membrane. Cellular dyes can be used to investigate processes occurring in the cell since they enhance the contrast of specific intracellular areas or molecules. Here, two types of dyes have been investigated; ruthenium dipyrrophenazine complexes and voltage-sensitive dyes. Further, bioactive peptides have gained an increased attention for promising therapeutic applications. In this thesis, the cellular uptake of cell-penetrating peptides, interesting as drug delivery systems, and of the antisecretory peptide, AF-16, is examined. For the development of compounds of both categories, a large challenge is to overcome the poor cellular uptake, which is restricted by the cell membrane, and to understand the mechanisms of interactions with the cell membrane.

The results show that ruthenium dipyrrophenazine complexes, interesting as cellular dyes because of their low background emission, have tunable affinity for biomembranes and nucleic acids upon slight changes of their lipophilicity and stereochemistry. These complexes enter cells in two different ways, by endocytosis and by a photoactivated uptake mechanism. The voltage-sensitive dyes, which are used for visualization of the membrane potential variation by microscopy, seem to interact with lipid membranes in a dimeric form. For the studied series of arginine- and tryptophan-rich cell-penetrating peptides, the cellular uptake efficiency was found to be sequence specific, both regarding the number and the position of the tryptophan residues. Concerning the therapeutic peptide AF-16, its cellular uptake is mediated by endocytosis, which is enhanced by the presence of cell-surface proteoglycans. Overall, the results in this thesis give insights into the membrane binding properties and cellular uptake of dyes and bioactive peptides as well as factors influencing these interactions, important knowledge for inspiring in future development of diagnostic and therapeutic molecules.

**Keywords:** *Cell Membrane, Membrane Interactions, Cellular Uptake, Cell Dyes, Ruthenium Complexes, Voltage-Sensitive Dyes, Bioactive Peptides, Cell-Penetrating Peptides, Antisecretory Factor, AF-16, Spectroscopy, Confocal Laser Scanning Microscopy, Flow-Cytometry, Isothermal Titration Calorimetry.*

# List of Publications

---

The thesis is based on the work described in the following papers<sup>1</sup>:

- I. **Lipophilic Ruthenium Complexes with Tuned Cell Membrane Affinity and Photoactivated Uptake**  
Frida Svensson, Maria Matson, Minna Li and Per Lincoln  
*Biophysical Chemistry*, **2010**, 149 (3), 102-106
- II. **Correlation Between Cellular Localization and Binding Preference to RNA, DNA, and Phospholipid Membrane for Luminescent Ruthenium(II) Complexes**  
Maria Matson, Frida Svensson, Bengt Nordén and Per Lincoln  
*Journal of Physical Chemistry B*, **2011**, 115 (7), 1706-1711
- III. **Spectral Properties and Orientation in Lipid Membranes of Voltage-Sensitive Dyes**  
Maria Matson, Nils Carlsson, Tamás Beke-Somfai and Bengt Nordén  
*Langmuir*, **2012**, 28 (29), 10808-10817
- IV. **Effects of Tryptophan Content and Backbone Spacing on the Uptake Efficiency of Cell-Penetrating Peptides**  
Hanna A. Rydberg, Maria Matson, Helene L. Åmand, Elin K. Esbjörner and Bengt Nordén  
*Biochemistry*, **2012**, 51 (27), 5531-5539
- V. **Enhanced Cellular Uptake of Antisecretory Peptide AF-16 through Proteoglycan Binding**  
Maria Matson Dzebo, Anna Reymer, Kristina Fant, Per Lincoln, Bengt Nordén and Sandra Rocha  
*Biochemistry*, **2014**, 53 (41), 6566-6573

---

<sup>1</sup> Papers are published with my maiden name Maria Matson before September 2012 and after 2012 with Maria Matson Dzebo.

# Contribution Report

---

- I. Performed confocal microscopy experiments.
- II. Planned the experiments with FS. Performed the experiments, analyzed the data, and wrote the paper.
- III. Planned and performed the experiments, analyzed the data, and wrote the paper together with NC. Did not contribute to the molecular modeling done by TBS.
- IV. Performed binding isotherm, cellular uptake, and toxicity experiments together with HR. Made the binding isotherm analysis and contributed to the writing of the paper.
- V. Planned and performed all experiments, analyzed the data and wrote the paper. Did not contribute to the molecular modeling done by AR.

# Table of Contents

---

<b>1. INTRODUCTION</b> .....	<b>1</b>
<b>2. THE CELL – BIOLOGICAL MEMBRANES AND NUCLEIC ACIDS</b> .....	<b>3</b>
2.1 THE CELL – THE SMALLEST LIVING UNIT .....	3
2.2 BIOLOGICAL MEMBRANES.....	4
2.2.1 <i>Proteoglycans</i> .....	5
2.2.2 <i>Transport through the Cell Membrane</i> .....	6
2.2.3 <i>Membrane Potential</i> .....	7
2.2.4 <i>Membrane Models</i> .....	8
2.3 NUCLEIC ACIDS .....	10
<b>3. ENHANCING THE VISUALIZATION OF CELLS – CELLULAR DYES ...</b>	<b>13</b>
3.1 RUTHENIUM POLYPYRIDYL COMPLEXES IN BIOLOGICAL SYSTEMS.....	13
3.2 VOLTAGE-SENSITIVE DYES .....	15
<b>4. BIOACTIVE PEPTIDES FOR THERAPEUTIC APPLICATIONS</b> .....	<b>17</b>
4.1 STRUCTURE OF PEPTIDES.....	17
4.2 CELL-PENETRATING PEPTIDES.....	19
4.3 THE ANTISECRETORY PEPTIDE AF-16 .....	20
<b>5. METHODOLOGY AND FUNDAMENTAL CONCEPTS</b> .....	<b>23</b>
5.1 SPECTROSCOPY AND PHOTOPHYSICS .....	23
5.1.1 <i>Absorption Spectroscopy</i> .....	23
5.1.2 <i>Emission Spectroscopy</i> .....	24
5.1.3 <i>Absorption and Emission of Ruthenium dppz Complexes</i> .....	26
5.1.4 <i>Spectral Properties of Voltage-Sensitive Dyes</i> .....	28
5.1.5 <i>Photophysical Properties of Peptides</i> .....	28
5.1.6 <i>Polarized Spectroscopy</i> .....	29
5.1.6.1 <i>Linear Dichroism Spectroscopy</i> .....	29
5.1.6.2 <i>Circular Dichroism Spectroscopy</i> .....	31
5.2 ISOTHERMAL TITRATION CALORIMETRY .....	32
5.3 CONFOCAL LASER SCANNING MICROSCOPY .....	34
5.4 FLOW CYTOMETRY .....	35
<b>6. RESULTS</b> .....	<b>37</b>
6.1 TUNING THE AFFINITY AND CELLULAR LOCALIZATION OF DYES BASED ON RUTHENIUM COMPLEXES .....	37
6.1.1 <i>Lipophilicity of the Complexes and Membrane Charge Influence Binding         Preferences</i> .....	37
6.1.2 <i>Two Different Ways of Cell Internalization</i> .....	41
6.1.3 <i>Enantioselective Binding Preferences</i> .....	43
6.2 MEMBRANE INTERACTION OF VOLTAGE-SENSITIVE DYES .....	44
6.2.1 <i>Dye Dimerization Can Explain Unexpected Spectral Shifts</i> .....	44

6.2.2 Membrane Binding Kinetics Differ Between Dyes but Binding Geometry is Similar .....	46
6.3 AMINO ACID SEQUENCE AFFECTS THE CELLULAR UPTAKE OF CELL-PENETRATING PEPTIDES .....	48
6.3.1 Sequence Dependence of Cellular Uptake Efficiency and Internalization Mechanism.....	48
6.3.2 Membrane Affinity is Similar for All Peptides .....	50
6.4 PROTEOGLYCANS ENHANCE THE CELLULAR UPTAKE OF THE ANTISECRETORY PEPTIDE AF-16.....	51
6.4.1 Electrostatic Interaction of AF-16 and Heparin.....	52
6.4.2 Binding to Proteoglycans Enhances Cellular Uptake .....	54
6.4.3 AF-16 Interacts with Negatively Charged Lipid Membranes .....	55
<b>CONCLUSIONS .....</b>	<b>59</b>
<b>ACKNOWLEDGEMENTS .....</b>	<b>61</b>
<b>LIST OF REFERENCES .....</b>	<b>63</b>

# List of Abbreviations

---

A	Adenine
A745	Proteoglycan deficient CHO-K1 cells
AF	Antisecretory Factor
AF-16	Antisecretory peptide, 16 amino acids long
ATP	Adenosine Triphosphate
BCA	Bicinchoninic Acid
bpy	2,2'-Bipyridine
C	Cytosine
CD	Circular Dichroism
CHO-K1	Chinese Hamster Ovarian cells
CLSM	Confocal Laser Scanning Microscopy
CPP	Cell-Penetrating Peptide
ct-DNA	calf thymus DNA
di-4-ANEPPS	4-(2-(6-(dibutylamino)-2-naphthalenyl)ethenyl)-1-(3-sulfopropyl)-pyridinium
di-8-ANEPPS	4-[2-[6-(dioctylamino)-2-naphthalenyl]ethenyl]-1-(3-sulfopropyl)-pyridinium
DNA	Deoxyribonucleic Acid
DOPC	1,2-oleoyl-sn-glycero-3-phosphocholine
DOPG	1,2-dioleoyl-sn-glycero-3-phospho-(1'-rac-glycerol)
dppz	Dipyrido[3,2a:2',3'-c]phenazine
G	Guanine
GAG	Glycosaminoglycan
GUV	Giant Unilamellar Vesicle
ITC	Isothermal Titration Calorimetry
LC	Ligand Centered
LD	Linear Dichroism
LLC	Lamellar Liquid Crystal
LUV	Large Unilamellar Vesicle
MLCT	Metal-to-Ligand Charge Transfer
phen	1,10-Phenanthroline
RH421	4-{4-[4-(Dipentylamino)phenyl]-1,3-butadienyl}-1-(4-sulfobutyl)pyridinium
RNA	Ribonucleic Acid
SPC	Special Processed Cereals
SUV	Small Unilamellar Vesicles
T	Thymine
U	Uracil

Amino acid abbreviations are found on page 18.

# I. Introduction

---

*Life is amazing.*

Have you ever thought about life as a phenomenon? It is fantastic. As far as we know the existence of life on our planet is unique but on the other hand the variety of life forms found on earth is huge. The size of organisms varies from micrometer scales for one-cell organisms to ten's of meters for animals and plants and additionally life forms come in different shapes and colors. Despite all differences, all organisms are made up from the same essential building blocks, nucleic acids, proteins, and lipids. All organisms are also sharing various basic processes that differentiate life from the dead matter. No wonder that humans always have been interested in life. But even if we are fascinated and have for a very long time been exploring how life actually works, we still have much to learn about life. Sometimes I wonder if we know more about outer space than we do about ourselves. I am, and have always been very curious about life and interestingly, the more I learn, the more I am amazed that it actually works so well. Mother nature is creative and has found interesting ways of solving problems and to adjust to the surrounding conditions. If we consider cells, there is a tremendous amount of different processes carried out simultaneously for conducting the primary function of the cell as well as maintaining its needs. Additionally, there is a huge defense system, making sure that there is little room for mistakes in biological processes. This is clear during the creation of a new life form, which depends on many processes that all have to be carried out in certain way for the new life to be born, but also in processes sustaining the organism such as protection of DNA against mutations. Life is truly vulnerable but still very powerful. If a process is malfunctioning it might lead to a disease, for instance cancer. By understanding the biological processes in detail and the origin of diseases we may have the chance to prevent them and to help people that already suffer for these diseases.

The cell is the smallest living unit. It is surrounded by the semi-permeable cell membrane which restricts the transport in and out of the cell. The barrier function of the membrane is crucial for life but it can also be hard to overcome when we design molecules intended for targeting intracellular regions or molecules. I have had the pleasure to work with two different fields that are associated with their important interactions with cells and the cell membrane, see Figure 1.1. The first part includes two types of dyes that can be used to visualize cells. Cellular dyes are valuable when studying cells and cellular processes since they provide contrast to the otherwise rather transparent sample and can be used to label a specific area or molecule within the cell. Today it is possible to study objects as small as individual molecules in live cells by clever microscopy techniques in combination with fluorescent dyes. The Nobel Prize in Chemistry this year has emphasized the importance of this possibility for studies of cellular mechanisms and origins of diseases. There are various dyes commercially available but there is also a need of new dyes since many of them exhibit problems like photobleaching and poor specificity. It is thus important to continue to study the dyes available as well as new alternatives to improve the toolbox for cell biologists. In *Paper I* and *II*, three ruthenium dipyrrophenazine complexes varying in their lipophilicity are investigated to examine how slight structural alterations affect their relative affinity for biomolecules and biomembranes as well as their cellular uptake. Moreover, three voltage-sensitive styryl dyes and their spectral properties and membrane binding are studied in *Paper III* to understand more about their properties as cellular dyes and their voltage-sensing mechanisms.

In the second part two types of bioactive peptides with potential therapeutic applications are investigated. The market for biomolecular-based drugs is rapidly increasing but there are many bottlenecks that reduce the expansion of this field. For instance, fast degradation of biomolecules by enzymes occurs in the blood stream, which decreases the life time of the molecule in the body. Additionally, in comparison with conventional drugs based on organic molecules, biomolecules generally show poor bioavailability and cellular uptake, because of the higher molecular weight and hydrophilicity. Cell-penetrating peptides (CPPs) are known to enter cells and are able to bring a cargo into the cell interior and can hence be used as drug delivery systems or as models for designing new biomolecular drugs with enhanced cellular uptake. The influence of the amino acid sequence on membrane interaction and cellular uptake is studied in *Paper IV* for a series of arginine- and tryptophan-rich peptides. Furthermore, there are many peptides that can be used as the active therapeutic substance. AF-16 is a peptide derived from the natural protein Antisecretory Factor (AF), which has the ability to cure diseases with secretory and inflammatory conditions, for instance diarrhea. The mechanism of action is still unknown and in *Paper V*, the cellular uptake and membrane interaction of the peptide are investigated.

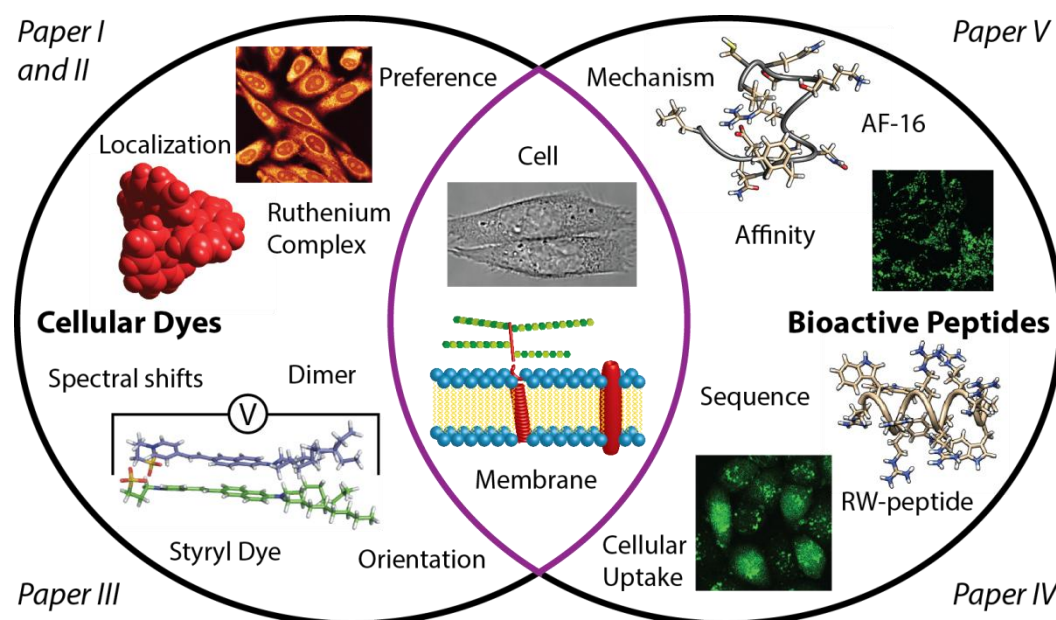


**Figure 1.1.** This thesis focus on membrane and cell interactions of cellular dyes and bioactive peptides. The images and key words represent the different papers.

## 2. The Cell – Biological Membranes and Nucleic Acids

---

*With this part of the thesis I aim to give an overview of the animal cell, the biological membranes and nucleic acids, as well as describe some of their important properties and features. The main focus of this thesis is molecular interactions with the cell and in particular with the cell membrane, and therefore this is more extensively described. Further details can be found in the referred textbooks about general molecular cell biology [1,2], as well as more specialized books about biological membranes [3] and nucleic acids [4].*

### 2.1 The Cell – The Smallest Living Unit

The cell is the smallest unit of life that alone can be regarded as living. A typical animal cell is about 10-20  $\mu\text{m}$  in diameter [1] and is surrounded by a *cell membrane* which defines the border between inside (*intracellular*) and outside (*extracellular*) of the cell. Like the human body, the cell is composed by different organs, so called *organelles* which also are enclosed by membranes providing both structure and function. Figure 2.1 shows a schematic representation of a mammalian cell and many of the important organelles. The *nucleus* is the largest organelle and contains genetic material in the form of DNA. All intracellular material except from the nucleus is referred to as the *cytoplasm* which is composed of intracellular fluid, the *cytosol*, and a number of organelles. The organelle *endoplasmic reticulum*, found close to the nucleus, has a role in transport and modifications of biomolecules and is a site where a lot of *ribosomes* are found. The ribosomes are made up from proteins and RNA and function as the protein factories of the cell. They are produced in an area inside the nucleus called *nucleolus*. The number of nucleoli<sup>2</sup> is varying with the cell cycle and increases when more ribosomes are needed, for instance prior to cell division [5]. The *Golgi apparatus* can be seen as the post office and is found close to the endoplasmic reticulum. Other important organelles are the *mitochondria*, the energy factories, and the *lysosomes*, in which molecules are degraded either for recycling purposes or for protection against toxic compounds.

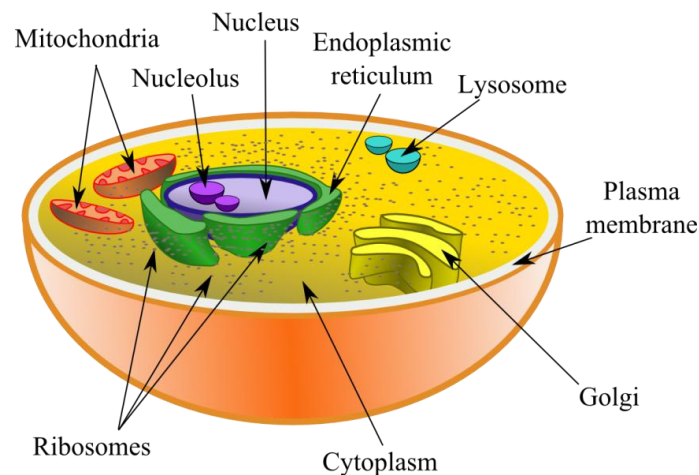


**Figure 2.1.** A schematic illustration of a mammalian cell and some of its important organelles.

---

<sup>2</sup> Nucleoli is the plural form of nucleolus. Nuclei is the plural of nucleus.

## 2.2 Biological Membranes

Biological membranes are important for both the structure and function of cells. They are found both as the cell membrane, also called *plasma membrane*, which surrounds the cell and defines the boundary between the intracellular and extracellular space, and inside the cell enclosing the organelles. Most animal cell membranes are composed of about 50 mass% *lipids* [1], consisting of a hydrophilic head group and one or two hydrophobic tails of saturated or unsaturated fatty acids, that are arranged into a lipid bilayer, see Figure 2.2. The most abundant lipids in animal cells are the *phospholipids* which have two hydrocarbon tails, usually with at least one unsaturated fatty acid. Two other important lipid categories are the *sphingolipids* and the *sterols*. Sphingolipids have usually saturated hydrocarbon chains and they form therefore thicker and more densely packed bilayers compared to phospholipids [6]. The most common sterol in animal cell membranes is cholesterol, which is important for the membrane rigidity [1].

Another major component of the cell membrane is *membrane proteins*. The protein content found in membranes differs a lot between different cell types and organelles and influences the functions carried out by the membrane and the physical properties of the membrane as the density [3]. The proteins can be found embedded in the lipid membrane, either transmembrane proteins spanning across the full lipid bilayer, or extended only on one side of the bilayer, whereas other proteins are associated with the membrane by covalent bonds to lipids or non-covalent interactions with membrane embedded proteins. The proteins are involved in various functions as for example transport of molecules across the membrane, catalysis of reactions and cell signaling.

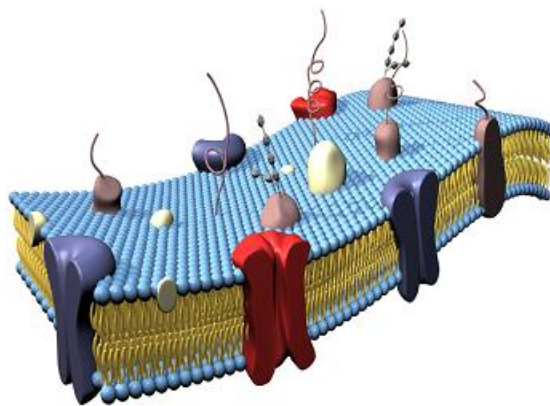


**Figure 2.2.** In a biomembrane the lipids form a bilayer, in which membrane proteins are embedded.

Cell membrane surfaces usually exhibit a negative charge which arises from the presence of negatively charged phospholipids. About 10-20% of the lipids in a biomembrane are anionic and, apart from these, proteins and sugar polymers (see section 2.2.1) also contribute to this overall charge [3]. Biomembranes are not homogeneous, instead they differ in lipid, protein and sugar composition between cell types and organelles but also within the individual membranes. For instance, the lipid composition of the plasma membrane differs from the membrane enclosing the mitochondria but it is also true for the two sides, the *inner* and *outer leaflets*, of a membrane. This can be due to structural reasons, the plasma membrane has a larger sterol content to be more rigid to resist higher mechanical stress [6] compared to organelle membranes, or for recognition reasons, where a certain lipid composition is the characteristic for a specific membrane and leaflet. The composition can also change upon

certain events, a cell dying by *apoptosis* (programmed cell death) increases the amount of cytosolic lipids in the outer leaflet of the plasma membrane [1]. Moreover, the membrane surfaces have highly dynamic microdomains enriched with specific lipids, like sphingolipids and cholesterol, and specialized proteins. These microdomains have been subjected to extensive debates due to the difficulties to prove their existence by visualization [7]. New, powerful microscopy techniques with higher resolution have been able to further strengthen the idea of their presence in biomembranes [8,9]. Signal transduction, membrane trafficking, organization of the cytoskeleton, viral infection and cellular entry are different suggested functions for these microdomains, which show that the diversity of lipids has additional biological roles other than structural reasons [6,8,9].

### 2.2.1 Proteoglycans

On the extracellular surface of the plasma membrane there are, in addition to the proteins, sugar polymers that are anchored to the bilayer by attachment to proteins or lipids. Most of these *glycoproteins* or *glycolipids* carry short branched oligosaccharides with varying composition. *Proteoglycans*, however, differ from the majority of glycoproteins because of their high glycosylation (up to 95 mass%) [1]. They consist of a protein core, varying between the different proteoglycan types, with at least one *glycosaminoglycan* (GAG) chain attached. GAGs are long unbranched polysaccharide chains, usually repeated disaccharides with derivatives of sulfated aminosugars and uronic acid [1]. Uronic acids have carboxylic acids, and together with the sulfate groups, they give the highly negative charge of GAGs at physiological pH. The proteoglycans are associated to the membrane either by an anchor, a transmembrane moiety of the protein or by attachment to a lipid, or they are found freely in the extracellular space.

One category of proteoglycans that has caught interest because of their interaction with peptides and proteins is the *heparan sulfate proteoglycans* [10–12]. The GAG heparan sulfate is composed by disaccharides of the uronic acid derivatives, glucuronic or iduronic acid, and a glucosamine with different degrees of substitution with sulfate or acetyl groups (Figure 2.3). The heparan sulfate chains have about 40-300 sugar residues and the sulfation and acetylation are not uniformly distributed over the molecules but rather arranged in a pattern with high density of these functional groups in some regions and low in others [10,13]. Heparan sulfate proteoglycans are important for the structure of the extracellular matrix as well as for encapsulating molecules to prevent proteolysis and the membrane bound heparan sulfate proteoglycans have also functions as receptors or co-receptors [10].

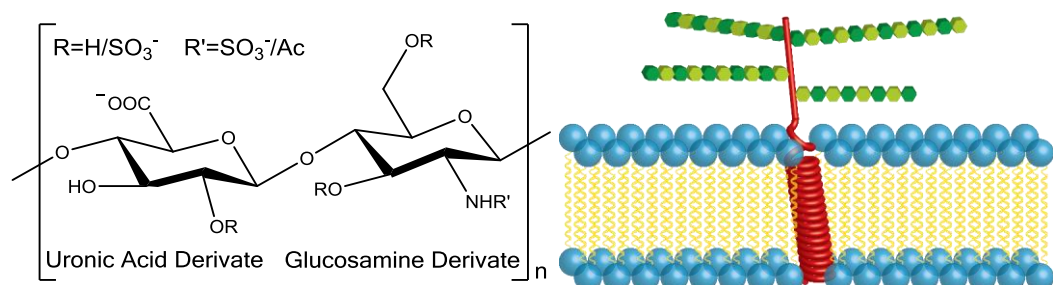


**Figure 2.3.** Proteoglycans are proteins with one or several GAGs. The GAGs are polymers of disaccharide units, usually derivatives of uronic acid and glucosamine which often are highly sulfated (left). The core protein varies between the proteoglycan types, some of them have a transmembrane part, which anchors the proteoglycan in the membrane (right).

## 2.2.2 Transport through the Cell Membrane

The transport of molecules through the membrane can occur in different ways. Many small, uncharged molecules are able to directly translocate the lipid bilayer whereas larger and charged molecules that are essential for the cell are dependent on transport processes through proteins. Some macromolecules enter cells by *endocytosis*, a term used for cellular uptake where the molecules are encapsulated in membrane vesicles, which then are pinched-off into the cytoplasm. Endocytosis can be divided into the two categories *phagocytosis*, “cell eating”, of big particles performed by specialized cells and *pinocytosis*, “cell drinking”, of liquid, solutes, and membrane bound molecules by almost all cell types [14–16]. Pinocytosis can be further classified into the sub-categories: macropinocytosis, clathrin-mediated endocytosis, caveolin-mediated endocytosis, and clathrin- and caveolin-independent endocytosis, depending on the mechanism of vesicle formation [15,16], see Figure 2.4. *Macropinocytosis* is different from the other mechanisms and occurs from areas where the cell membrane is highly ruffled [16]. A bulge collapses and fuses with the plasma membrane into a vesicle, a process dependent on intracellular polymerization of the protein actin [15]. *Clathrin-mediated endocytosis* is a receptor mediated process where pits are formed by membrane coating of proteins, mainly clathrin, on the cytosolic leaflet [15–17]. *Caveolae-mediated endocytosis* is dependent on the flask-shaped pits, caveolae, which are found in the cholesterol and sphingolipid-rich microdomains. The caveolae are shaped by oligomerized caveolin, a cholesterol-binding protein, and are budded off into the cell upon endocytosis [15,16]. The diffuse sub-class of *clathrin- and caveolae-independent endocytosis* includes mechanisms where pits are formed in other ways. These processes occur also frequently in cells but much is still unknown about them [15,18]. Besides proteins like actin, clathrin and caveolin, many different actors in the pinocytotic uptake mechanisms have been identified, including a number of specific proteins and lipids, plasma membrane microdomains, and glycosaminoglycans [9,10,13,15–19].

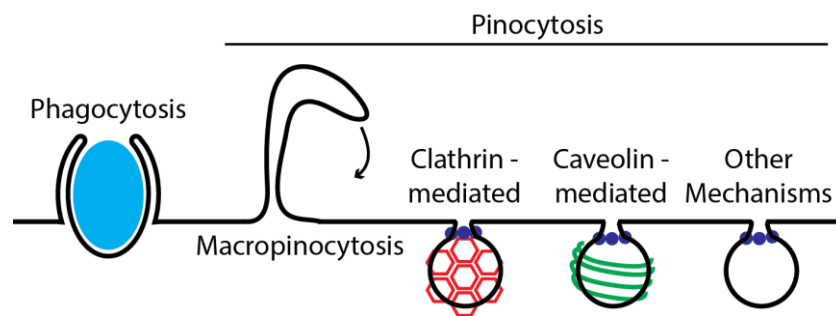


**Figure 2.4.** Endocytosis can be divided into *phagocytosis* and *pinocytosis*, of which the latter can further be classified depending on the uptake mechanism.

Once in the cytoplasm, the vesicles fuse and form larger vesicles, *endosomes*, which undergo a maturation process from early to late endosomes, see Figure 2.5. During that process, the endosomes alter in size, shape and lipid composition as well as internal ion concentration and pH (from physiological pH of 7.4 to pH 4.9-6) [20]. Material in the endosomal interior or membrane is transported to the Golgi apparatus for further transport within the cell or recycled back to the plasma membrane by smaller vesicles that pinch-off from the endosomes during the entire maturation process. Reverse transport, vesicles fusing with the endosomes carrying cargo from the Golgi apparatus, is also occurring simultaneously. In the final state of the late endosomes, they fuse with the lysosomes where the remaining material is degraded [15,19,20]. The cellular uptake by endocytotic pathways consumes energy [14,21] as do the processes during endosomal maturation [20].

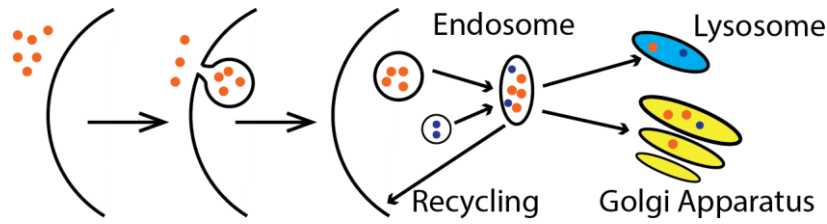


**Figure 2.5.** The cellular uptake by endocytotic processes involves encapsulation of molecules or particles in vesicles. The vesicles fuse and form endosomes which undergo a maturation process. During this process, the cargo can be transported to the Golgi apparatus for transport within the cell, to the lysosomes for degradation or recycled back to the cell membrane and the extracellular space.

### 2.2.3 Membrane Potential

All cells have a transmembrane potential over the plasma membrane which is established by a difference in ion concentrations. The most important ion for this potential in animal cells is  $K^+$ , which has a high intracellular concentration to balance the many anions found on nucleic acids and proteins. Transport of this ion over the membrane is performed by the  $Na^+/K^+$ -pump, that transports actively  $Na^+$  out of and  $K^+$  into the cell, and also by the  $K^+$  leak channels, that make it possible for  $K^+$  to passively diffuse out from the cell, see Figure 2.6. The  $K^+$  ions diffuse out to the extracellular space with the chemical gradient until this chemical potential is balanced by the electrostatic force from the negatively charged macromolecules found intracellularly. The electric membrane potential in the equilibrium state is called *resting potential*, and in mammalian cells this is about  $-70$  mV [1] intracellularly with respect to the exterior. This potential is crucial for the processes carried out by the membrane for all cell types but for some specialized cells a variation of the potential is also important for their functions. For example neurons and muscles vary their membrane potential in order to generate nerve signals and contract. A membrane potential is also found over the membrane of the mitochondria, which is important for its production of energy in form of ATP.

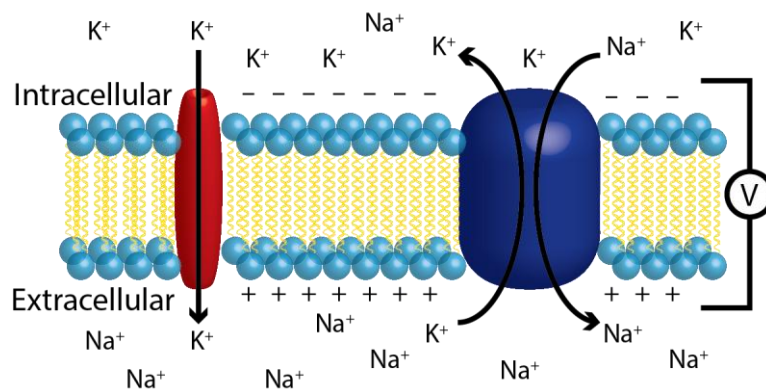


**Figure 2.6.** In animal cells the membrane potential is established by active transport of  $K^+$  to the intracellular space by the  $Na^+/K^+$ -pump and diffusion out from the cell through  $K^+$  leakage channels. The magnitude of the resting potential is determined by the equilibrium between the  $K^+$  diffusion with the concentration gradient and the opposing electrical force by negatively charged molecules intracellularly.

## 2.2.4 Membrane Models

Biological membranes are indeed composed of several different components and provide hence various types of environments that allow interactions with different types of molecules. Polar molecules can interact with the membrane surface, positively charged molecules are attracted to the negatively charged lipids, proteins, and sugar residues, and hydrophobic molecules can be embedded in the lipid bilayer interior. The lipid bilayer is also an ideal site for amphiphilic molecules which can anchor in the membrane with the hydrophobic part close to the fatty acids of the lipids and the polar moiety interacting with the lipid heads. The complex nature of cell membranes makes them thus hard to study and therefore simplified membrane models are often used in biophysical studies. There is a large variety of lipid systems that can be used as models. The amphiphilic nature of lipids and their geometry make them to spontaneously form different structures for instance micelles, inverted micelles, lipid bilayers, and hexagonal structures in water environment [3]. The choice of lipid does not exclusively alter the shape of the model but also the fluidity of the membrane. Many lipids form lipid crystalline phases, in which the membrane behaves as a two-dimensional liquid allowing molecular diffusion and below a certain temperature the membrane undergoes a transition to the less fluid gel phase [3,22]. This transition temperature depends highly on the degree of saturation of the fatty acid. By mixing different lipids, it is possible to obtain membrane models with different properties, for instance membrane rigidity can be increased by introduction of cholesterol.

The most relevant models for cell membranes are the bilayer models, for instance a single bilayer on a support, a liquid crystal with a number of stacked bilayers or liposomes [3]. *Liposomes* are lipid bilayer structures which enclose a volume, see Figure 2.7. Generally liposomes can be characterized as unilamellar or multilamellar, meaning that they consist of a single bilayer or several bilayers, respectively. In addition to this classification they are also divided into different groups depending on size [3]. *Small unilamellar vesicles* (SUV) are 20-50 nm in diameter, *large unilamellar vesicles* (LUV) have sizes of 50-500 nm in diameter and *giant unilamellar vesicles* (GUV) have a diameter of 500 nm or larger. LUVs have the advantage of being more stable than SUVs and GUVs and, additionally, they do not have a high membrane curvature as the smaller SUVs [3]. High curvature makes the SUVs less stable since they are more prone to fuse but gives also a very high surface area difference between inner and outer leaflet which can lead to asymmetry if different lipids are used. Additionally, the high curvature can affect the interaction of the vesicles with other molecules.



**Figure 2.7.** A liposome is a spherical lipid bilayer that enclose a volume and can be used as a model of the lipid bilayer.

As said before, the properties of the membrane models can be varied by the lipid composition. To mimic the lipid bilayer of a mammalian cell I have mainly used LUVs of the synthetic phospholipids *DOPC*<sup>3</sup> (zwitterionic) and *DOPG*<sup>4</sup> (anionic), see Figure 2.8. These lipids are unsaturated and form fluid phase bilayers at room temperature (well above the phase transition temperature of -17°C for *DOPC* and -18°C for *DOPG*). I have used them to study membrane interaction, in terms of affinity and geometry, of cellular dyes and bioactive peptides.

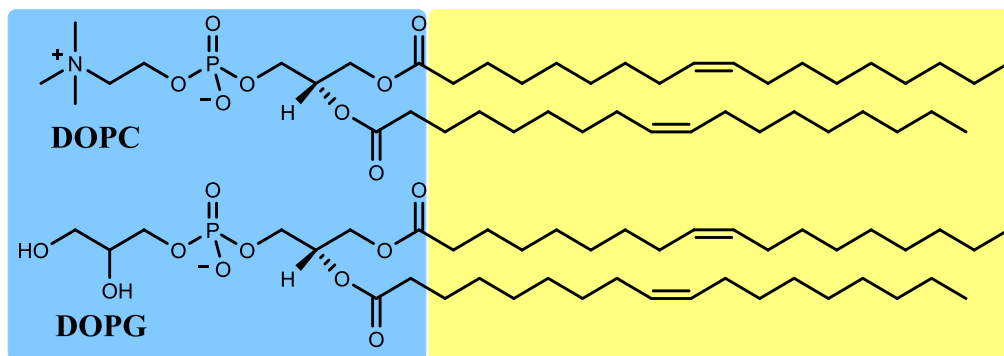


**Figure 2.8.** The structures of the synthetic phospholipids *DOPC* (zwitterionic) and *DOPG* (negatively charged). Lipids are composed of a hydrophilic head (blue background) and hydrophobic tails (yellow background).

As a model for proteoglycans, *heparin* is often used in biophysical experiments as it is structurally related to heparan sulfate. Unlike heparan sulfate, the polymer is mostly composed of one disaccharide, 2-O-sulfated iduronic acid and 6-O-sulfated, N-sulfated glucosamine, to make up its right-handed helical structure [13] (see Figure 2.9). Heparin also differs from heparan sulfate by its higher degree of sulfation, about 2.3 sulfate groups per disaccharide compared to 0.8 for the average heparan sulfate molecule [10]. Heparan sulfate has, however, areas of higher sulfation degree and heparin can therefore be used as a model for these regions.

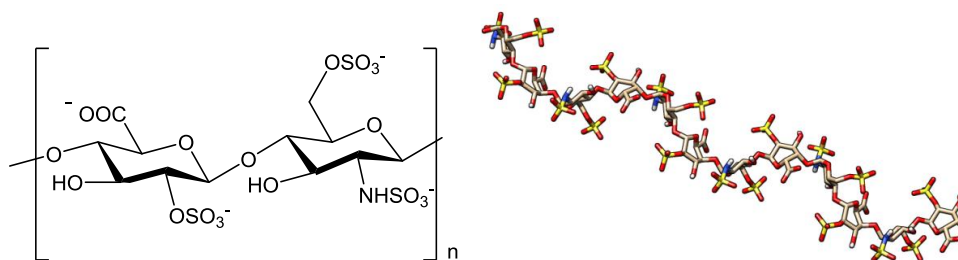


**Figure 2.9.** The structure of the major disaccharide of heparin and the three-dimensional conformation of a heparin molecule with 12 disaccharide units.<sup>5</sup>

<sup>3</sup> 1,2-dioleoyl-sn-glycero-3-phosphocholine

<sup>4</sup> 1,2-dioleoyl-sn-glycero-3-phospho-(1'-rac-glycerol)

<sup>5</sup> PDB-ID: 1HPN

## 2.3 Nucleic Acids

*Deoxyribonucleic acid*, DNA, is the nucleic acid that contains our genetic information. The smallest unit of DNA is the *nucleotide*, which is composed of a phosphate group, a *deoxyribose* sugar unit and a *nucleobase*. The nucleotides are attached by covalent bonds between the phosphate and sugar groups, forming a DNA strand. There are four different nucleobases, *adenine* (A), *thymine* (T), *cytosine* (C) and *guanine* (G) which are able to base pair by hydrogen bonding in the specific pairs A-T and C-G, see Figure 2.10. This feature allows two strands with complementary sequence to self-assemble to the B-form double helix (Figure 2.10), which is the most commonly found form of DNA in nature [4]. In this form, the highly negatively charged DNA backbone faces the water surrounding whereas the nucleobases are screened from the aqueous solution and provide a hydrophobic environment. The helix is twisted in a way that *minor* and *major grooves*, differing in their geometries, are formed.

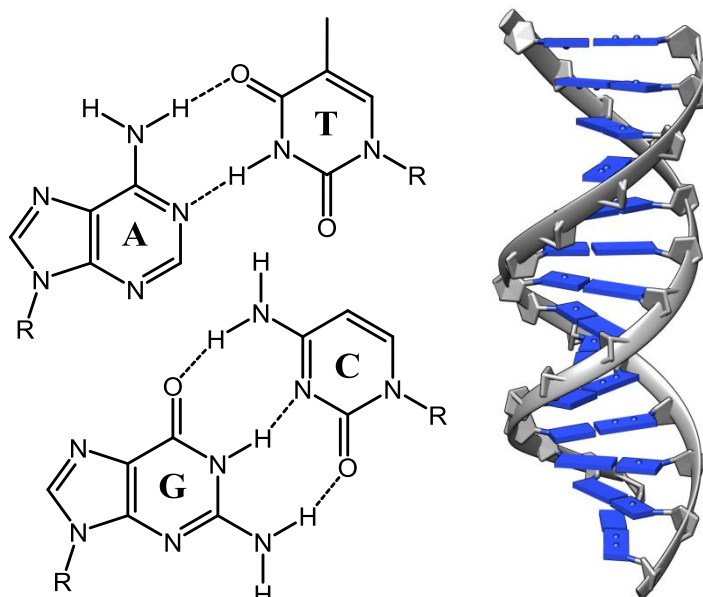


**Figure 2.10.** Adenine (A), thymine (T), guanine (G) and cytosine (C) are the four nucleobases in DNA. The bases are connected with the phosphate-sugar backbone (R) and they base pair A-T and G-C (left) to build up the double stranded DNA helix<sup>6</sup> (right).

The particular structure and properties of the DNA molecule make interaction with other molecules possible in different ways [4]. Positively charged molecules can bind through electrostatic interaction to the highly negatively charged phosphates of the backbone and hydrophobic molecules can interact with the nucleobases. The geometry of the grooves makes some molecules more prone to interact with one of the grooves compared to the other groove. Planar, hydrophobic molecules are also able to insert in between the base pairs, a binding mode called *intercalation*.

*Ribonucleic acid*, RNA, is like DNA composed of nucleotides but is differing by having a *ribose* sugar unit with an additional hydroxyl group and the nucleobase *uracil* (U) instead of thymine (Figure 2.12). In addition, RNA is usually found as a single stranded molecule that can be folded in various ways for instance to A-form double-helical sections, which are more compressed helices compared to the B-form, and single-strand loops [4]. There are several types of RNA present in the cell of which the major types are *messenger RNA* (mRNA), *transport RNA* (tRNA) and *ribosomal RNA* (rRNA). These three categories of RNA are all

<sup>6</sup> DNA strand with an unspecific sequence

important part of the expression of proteins. The DNA sequence for the protein that will be expressed is transcribed into a mRNA sequence which, unlike DNA, is able to translocate from the nucleus into the cytoplasm where it is translated into a protein by the ribosome (Figure 2.11). Three nucleotides make up the code (codon) for an specific amino acid, which is brought to the ribosome by a tRNA, functioning as an adaptor between the mRNA and the amino acid. The amino acid is incorporated and the protein is elongated. The rRNA has the role of being structural material, together with proteins, for the ribosome organelle itself and has some catalytic functions.

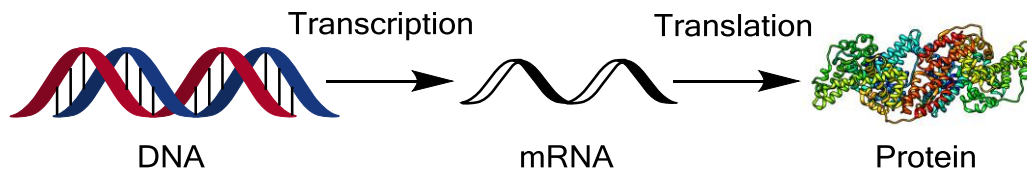


**Figure 2.11.** DNA and RNA are involved in the production of proteins. DNA carries the information in the form of a gene, which is transcribed into a mRNA molecule that later is translated to the protein.<sup>7</sup> tRNA and rRNA molecules are important in the translation process.

There are differences in structure between these RNA molecules. mRNA is found in a linear single stranded form supported by proteins whereas tRNA has a L-shaped three-dimensional structure (Figure 2.12) made up from a single strand folded into loops and short base paired sequences [4] and rRNA is forming an even larger structure of loops and base paired regions. Even if DNA and RNA molecules are similar in their basic primary structure, the higher order structures are different, providing various types of binding sites, which could be important for interacting with molecules.

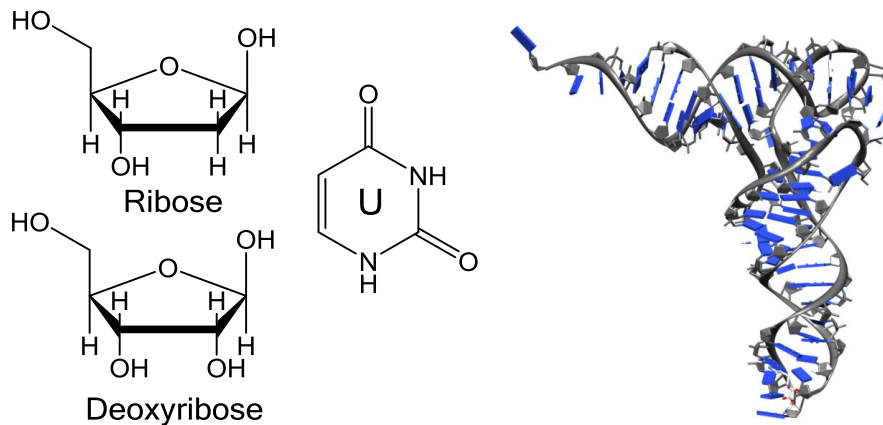


**Figure 2.12.** The major differences between RNA and DNA are the sugar residue, ribose instead of deoxyribose, and the base uracil (U) that replaces T in DNA. In addition, the conformation of RNA is more varied in nature, with single strands folded into helices and loops. In the tRNA molecule the single strand has base paired areas and loops and it is folded into its characteristic L-shape.<sup>8</sup>

<sup>7</sup> The protein in this figure is bovine serum albumin PDB-ID: 4F5S.

<sup>8</sup> PDB-ID: 1TN2



# 3. Enhancing the Visualization of Cells – Cellular Dyes

Biological samples are usually rather transparent and it can be hard to distinguish details of the cell by microscopy. To enhance the contrast between a region, an organelle, or a molecule and the background, fluorescent dyes can be used. There are a number of important properties for cellular dyes, for example specificity for the target and stability without showing any photobleaching or photodamage to the studied sample. There are also a number of desired photophysical properties for cellular dyes which will be discussed later. This section focus on the molecular interactions of ruthenium polypyridyl complexes and voltage-sensitive styryl dyes.

## 3.1 Ruthenium Polypyridyl Complexes in Biological Systems

Ruthenium complexes with polypyridyl ligands have been studied during decades in a number of different fields with potential applications such as solar cells, molecular motors, electrochemical displays, molecular electronics, optical sensing of oxygen, and DNA-binding therapeutics [23]. In this thesis, mononuclear ruthenium complexes of this type are investigated as cellular dyes and this section will focus interactions with biomolecules and cells of these complexes. A brief description of their photophysical properties is found in section 5.1.3.

Ruthenium(II) complexes have six coordination bonds and form octahedral complexes. This geometry in combination with *bidentate* ligands, which coordinate to the ruthenium ion through two electron donors per ligand, results in propeller shaped complexes which are either turned in a left handed ( $\Lambda$ ) or right handed ( $\Delta$ ) manner, see Figure 3.1. The bidentate polypyridyl ligands *bipyridine* (bpy), *phenantroline* (phen), and *dipyridophenazine* (dppz), see Figure 3.2, forms thus chiral complexes with two stereoisomers that are mirror images of each other, i.e. enantiomers<sup>9</sup>.

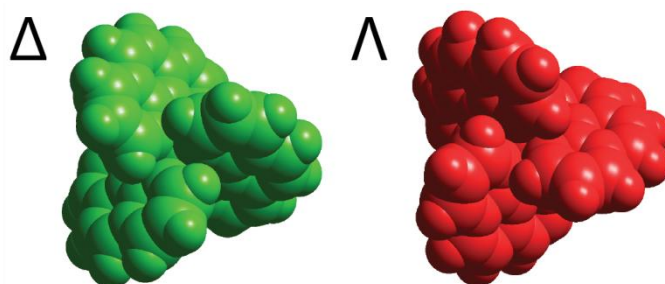


**Figure 3.1.** Ruthenium complexes with bidentate ligands and octahedral geometry have the appearance of propellers. The two enantiomers of  $[\text{Ru}(\text{phen})_3]^{2+}$  are shown here.

Since 1984, when  $[\text{Ru}(\text{phen})_3]^{2+}$  was found to interact with DNA [24], the DNA binding of ruthenium polypyridyl complexes has been intensively explored [23–34]. These studies include investigations of DNA binding properties such as affinity, binding mode, and the effect of stereochemistry but also the photophysical properties upon binding. A well-studied complex is  $[\text{Ru}(\text{phen})_2\text{dppz}]^{2+}$ , which binds to DNA by intercalation [28,29], a binding mode in which the dppz ligand is inserted in between the DNA nucleobases. In addition, the dppz complex shows interesting photophysical properties with bright luminescence when bound to DNA but no luminescence in aqueous solution [27,33].

<sup>9</sup> An equal mixture of both enantiomers is referred to as a racemic mixture or racemate.

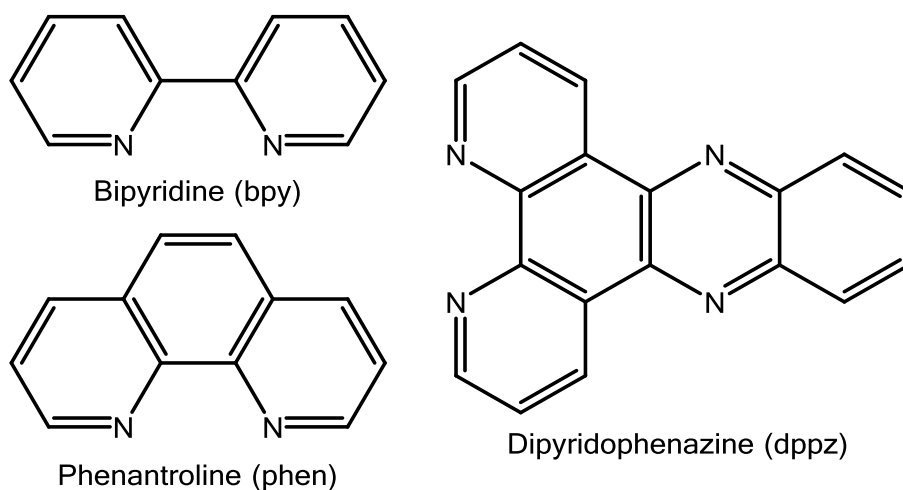


**Figure 3.2.** The polypyridyl ligands of the ruthenium complexes used in this thesis.

The chemical structure of the complexes can relatively easily be varied and a large number of mononuclear polypyridyl complexes have been developed [23,25,26,34–36]. Alterations have also resulted in dinuclear ruthenium complexes like  $[\mu-(11,11'-bidppz)(phen)_4Ru_2]^{4+}$  which is known to intercalate DNA by threading intercalation where the bridging ligand is inserted between the DNA base pairs [37]. Prior to this binding mode, one of the ruthenium cores with its bulky ligands passes through the DNA double strand, a process that requires large conformational changes of the DNA and hence the binding occurs with very slow association rate. Structural changes also alter the complexes ability to interact with other cellular targets. For instance the dppz ligand has been modified with several different substituents which were shown to affect the membrane binding geometry [38,39]. Complexes with unsubstituted or alkyl ether modified dppz ligands bind by insertion of the dppz moiety between the lipid chains whereas nitrile and amide substituted dppz ligands prefer to bind parallel to the membrane surface. Further, only a few studies have been focusing on the RNA binding of ruthenium complexes [30,40–45], an interaction which seem to be highly affected by the ligand structure and complex stereochemistry [30,40,41].

The light-switch effect in combination with the possibility to tune the molecular affinities of the complexes by structural changes makes derivatives of ruthenium dppz complexes interesting for cell imaging. Mono- and dinuclear complexes have been shown to be useful as probes for the nucleus [46–48], plasma membrane [49], endoplasmic reticulum [50], and cellular viability [51]. In *Paper I* and *II*, a series of three lipophilic ruthenium complexes with dppz ligands substituted with alkyl ether chains of varied lengths are investigated as cellular dyes. The effect of slight structural changes on the binding preferences, comparing lipid membranes, DNA, and RNA, *in vitro* and the cellular localization and uptake of the complexes are investigated.

## 3.2 Voltage-Sensitive Dyes

It is common to use microelectrodes to monitor the membrane potential but for some applications this method is not feasible. For instance, some cell types and intracellular compartments are too small for it to be practical. Instead, *voltage-sensitive dyes* can be used to indirectly measure the variation in membrane potential. The dyes respond by changing their characteristics of the absorption and/or fluorescence, therefore examination of their spectral properties can be done to study and visualize the variation in the membrane potential [52–55]. Common applications of these dyes are imaging the change of voltage in neurons [56–58] or to study the reaction mechanisms of ion pumps like the  $\text{Na}^+/\text{K}^+-\text{ATPase}$  [59–62].

Although these probes are today used for membrane potential detection, the mechanism behind the voltage sensing is not fully understood. There are several suggestions of their function, including mechanisms that involve direct sensing of the electric field or indirect mechanisms that are caused by shifts in the environment, see Section 5.1.4. Since the voltage sensing ought to be most efficient when the probe is well aligned with respect to the membrane normal, irrespective of the type of mechanism, the orientation of the probe is important. A poor orientation can be expected to provide a wide orientation distribution, each molecule being differently affected by the field, and hence a less distinct response to the electric field. The probes were first assumed to align perfectly with the membrane normal [63–65] but several studies have shown results differing from this orientation and various binding angles have been suggested [66–69].

In *Paper III*, three styryl dyes are investigated, di-4-ANEPPS, di-8-ANEPPS and RH421, see Figure 3.3. Their shift in wavelength of absorption and emission and change in fluorescence intensity due to polarity and viscosity of the solvent is studied. The binding geometry of the dyes in liposomes and octanoate-decanol based liquid crystals as well as their binding kinetics to liposomes are also examined in order to compare the different probes.

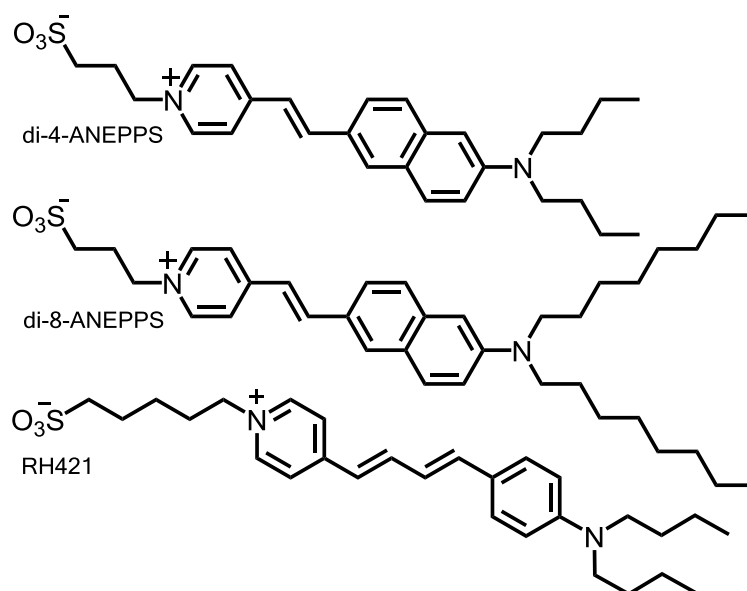


**Figure 3.3.** The three studied voltage-sensitive styryl dyes.



# 4. Bioactive Peptides for Therapeutic Applications

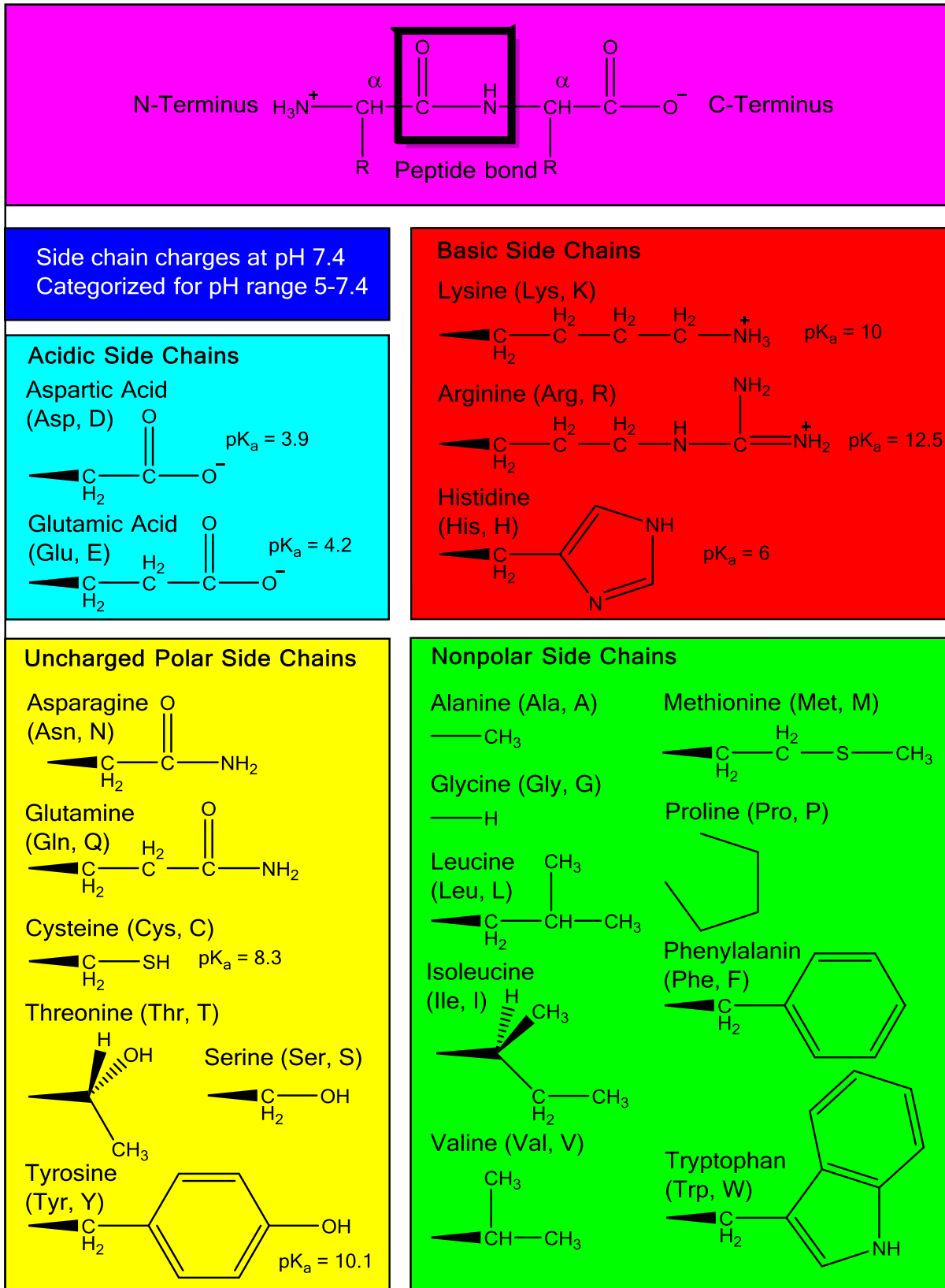
---

*There is an ever increasing interest in peptides and proteins as drugs. Currently there are several protein-based pharmaceuticals on the market for instance for the treatment of cancer, autoimmune diseases, hepatitis A and B, and diabetes [70]. Further, bioactive peptides are also promising as drugs such as antibiotic, antimicrobial, immunopromoting and antioxidative agents as well as drugs against cancer and metabolic disorders [71]. The peptide AF-16 has remarkable properties, making it a potential drug for secretory and inflammatory diseases, see section 4.2. Bioactive peptides are thus important to study for therapeutic applications but peptides show generally low cellular uptake, which is one of the main problems for peptide-based drugs [70]. There is however a specific class of peptides, cell-penetrating peptides, that has the ability to transverse the cell membrane together with a cargo and therefore can be used as drug delivery vectors for biomolecular-based drugs, see section 4.2. Peptides can thus both have therapeutic properties themselves or serve as drug-delivery systems. In both cases, the specific structure of the peptide is crucial therefore I will briefly describe the general structure of peptides before focusing on the specific peptides. Further reading about the peptides can be done in the referred textbook about CPPs [72] and reviews about AF-16 and its parent protein, antiseecretory factor [73,74].*

## 4.1 Structure of Peptides

Peptides are composed of amino acids. There are 20 different natural amino acids, which all have an amino group, a carboxyl group, and a side chain covalently bound to the  $\alpha$ -carbon. The side chain structure varies between the amino acids and gives rise to their different properties. Further, the amino acids are linked together by a bond between the amino group and the carboxylic group of another amino acid, the *peptide bond*, and in a peptide sequence the amino end is referred to as the *N-terminus* and the carboxylic end as the *C-terminus*, see Box 1. An amino acid sequence shorter than 50 residues is generally defined as a peptide whereas longer polypeptides usually are referred to as proteins. The synthesis of peptides and proteins is made by the ribosome in the translation processes but in addition, peptides can also be formed due to proteolytic degradation of proteins in the regeneration process of the cells. The properties of the specific amino acid sequence give sometimes rise to various secondary structures as  $\alpha$ -helices,  $\beta$ -sheets or random coils.

**Box 1.** The twenty amino acids which are the building blocks of natural proteins and peptides, presented with their three and one letter abbreviation and classified for the pH range 5-7.4. The charge of the amino acid side chain is shown as at pH 7.4 and the pK<sub>a</sub> are approximate values for free amino acids [2].



## 4.2 Cell-Penetrating Peptides

*Cell-penetrating peptides* (CPPs) are 5-40 amino acid long peptides that have the ability to enter cells [72]. Furthermore, CPPs are interesting as drug delivery systems since they have been shown to assist the cellular uptake of bioactive cargoes, including DNA, nanoparticles, peptides, proteins, drugs, or liposomes enclosing any biologically active molecule.

The interest in CPPs started in the late 1980's, when it was discovered that some proteins could enter cells. The first observation was the Trans-Activator of Transcription (Tat) protein of the Human Immunodeficiency Virus (HIV), [75] followed by the transcription factor Antennapedia homeodomain from the fruit fly *Drosophila melanogaster* [76]. The search for the shortest amino acid sequence from these proteins that could transverse the cell membrane resulted in the two CPPs: HIV-TAT peptide [77,78] (YGRKKRRQRRR) and the peptide penetratin [79] (RQIKIWFQNRRMKWKK). Since then, various sequences from proteins have been found to have cell-penetrating properties and, additionally, CPPs have also been designed according to results from sequence-cellular uptake relationship studies. CPPs can be classified based on their origin: CPPs derived from proteins, chimeric CPPs (which are a combination of two or several natural sequences), and synthetic designed CPPs [80,81]. Another important way of classifying the peptides is according to their physical-chemical properties [80]. A large group is the *cationic CPPs*, which includes for instance the HIV-Tat peptide and nuclear localization signals. The class of *amphipathic CPPs* consist of peptides with defined hydrophobic and hydrophilic parts, which further can be divided into the sub-classes of primary and secondary amphipathic peptides. The primary amphipathic peptides have defined hydrophilic and hydrophobic regions directly in the amino acid sequence, as for instance the peptide Pep-1 [82] which is a chimeric CPP based on a hydrophilic nuclear localization signal fused with a tryptophan rich hydrophobic region. Secondary amphipathic peptides do not have the amphipathic character in their primary structure but upon formation of secondary structures the peptides form hydrophobic and hydrophilic regions. An example of peptide in this category is penetratin [79]. The last category is the smaller sub-class of *hydrophobic CPPs*. There are a few examples of anionic peptides but they have no own category since they often also have amphipathic or hydrophobic properties [80]. The CPPs are, as seen, a category that includes peptides with a large diversity in their properties.

Although the cellular uptake of CPPs has been extensively studied, the cell internalization mechanism is still not clear and has been subjected to a lot of debates. The predominant pathway seems nowadays to be considered as endocytosis [81,83,84] but some peptides, especially rich in arginine residues, have been shown to utilize *direct translocation* [83,85] or combination of these mechanisms [81,83,86]. Direct translocation pathways include energy-independent mechanisms and generally depend on the destabilization of the cell membrane followed by cell entry [81]. The mechanism of internalization seems to be correlated to the peptide properties as the amino acid composition, sequence, length and secondary structure but also on the experimental conditions such as extracellular peptide concentration, incubation time, cell line, and type of cargo [81,87–89].

Binding to negatively charged molecules at the membrane surface seems to be the first step in direct translocation mechanisms and indeed highly cationic peptides with hydrophobic residues, have been suggested to be the main category using these mechanisms [81]. However, interactions with the negatively charged membrane components have also been shown to be important for endocytotic pathways [11]. Many studies have therefore been

focusing on interaction of CPPs and lipid bilayers for investigations of binding characteristics such as affinity, peptide conformation, and binding geometry but also the effect of peptide binding on the membrane integrity [11,90–95]. The affinity of CPPs to membranes depends highly on the peptide properties and is generally increased with the number of positive charges and hydrophobic residues [11,91] but the composition of the membrane models is also important [90,92,95]. In addition to lipid bilayers, proteoglycan binding is well-studied for CPPs [11]. Various peptides do not only bind to the proteoglycans but also cluster them [11,89,96–98]. This is possible if the positive charges of the peptides neutralize the negative charges of the proteoglycans. The clustering seems to promote direct penetration whereas binding without clustering often is followed by endocytotic internalization [99]. The presence of tryptophan residues in these peptides has been shown to both increase their binding affinity to GAG's as well as enhance their cellular uptake by both direct translocation and endocytotic pathways [96].

Interestingly, increased affinity to negatively charged membrane components gained by positive amino acids residues does not necessary lead to enhanced cellular uptake, instead it is in particular arginine residues that increase the cellular uptake [97,100,101]. In fact, a penetratin analogue in which the lysine residues were substituted with arginines showed a higher cellular uptake compared with penetratin whereas an analogue with lysines instead of arginines gave the opposite result [97]. The uptake is thus not only dependent on the charge but rather on the specific guanidine structure provided by the arginine. The internalization efficiency of peptides is known to increase with the number of arginine residues and an optimal length has been suggested to be 8-15 arginine residues [83,101]. Additionally, the uptake of arginine-rich peptides seems to be further increased by the presence of a tryptophan residue [102]. Furthermore, the backbone spacing of arginine peptides is important for the cellular uptake, since the insertion of aminocaproic acid as a spacer between the arginine residues was found to enhance the internalization efficiency [103]. The effect of backbone spacing using ordinary amino acids has, however, not been investigated. In *Paper IV*, six short arginine- and tryptophan-rich peptides, differing in number and position of tryptophan residues, were studied to deduce if these factors influence the membrane interaction as well as cellular uptake and toxicity of CPPs.

### 4.3 The Antisecretory Peptide AF-16

*Antisecretory Factor*, AF,<sup>10</sup> a 41 kDa protein, is natively found in most mammalian tissues, neurons and blood [73,104,105]. It has remarkable properties being able to prevent hypersecretion of body fluids [106,107] (so called antisecretory effect) and having anti-inflammatory properties [107–109]. The protein was discovered by Lange and Lönnroth in 1984 [110,111] when searching for natural anti-diarrheal factors in rats that could explain the fact that the diarrheal response induced by cholera toxin decreased each time the animals were exposed. AF is found in the body in an inactive form [104] but upon exposure to bacterial toxins it converts into an active form [112,113] and, in addition, the toxins also induce an increased expression of the protein [113,114]. The details of the activation process and the difference between active and inactive form is, however, still not known.

---

<sup>10</sup> Abbreviation in older literature: ASF

The sequence responsible for the antisecretory and anti-inflammatory effect has been identified as a minimum of 7 amino acids in the N-terminal region of the protein [115]. A 16 amino acid long peptide, AF-16,<sup>11</sup> has been developed, see Figure 4.1, containing the active site and additional amino acids to ensure its stability in blood. Both AF and AF-16 have shown to be promising drug candidates to treat diseases where imbalances in secretion and/or inflammation are important conditions. For instance, AF therapy can reduce diarrheal responses induced by bacterial toxins in humans and animals [107,116] but is also effective in reducing high intra-cranial pressure [117] and high tumor pressure [118]. Additionally, positive effects on inflammatory bowel diseases [109], mastitis [119], and Ménière's disease [120] have also been established. Brief descriptions of the different conditions are found in Box 2.

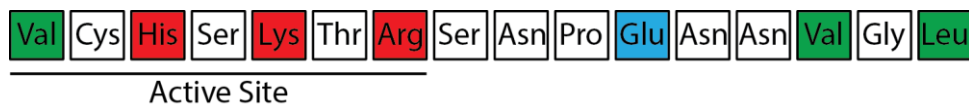


**Figure 4.1.** The sequence of AF-16 presented with the three letter amino acid abbreviations and a color code according to the amino acid properties, where green is hydrophobic, red basic, and blue acidic. The majority of the amino acids is polar and the active site of the AF protein is indicated by the line.

Two different medical foods have been developed [73,74], special processed cereals (SPC), which induce the expression of AF by the body, and the egg yolk drink Salovum, made from eggs by hens fed with SPC which therefore has high AF levels in the yolk. Both types of medical foods have been used in clinical trials with positive results. For instance, a trial on children with diarrhea resulted in an increased restoration of hydration after intake of Salovum [116]. In addition to the health promoting effects in humans, AF and AF-16 can be used in rising of livestock [73]. Many countries use antibiotics for preventing diarrhea of the livestock, in Sweden this is prohibited since 1984. Instead, AF treatment can be used as the preventive agent, reducing the problems with livestock diarrhea without increasing the antibiotic resistance.

A peptide-based drug would be beneficial compared to inducement of the AF levels of the body, since there is no need for upregulation of the protein expression, the peptide is already in the active state and, in addition, it is possible to do modifications to improve the efficiency of the peptide. In order to develop this peptide-based drug, the underlying mechanism behind the antisecretory and anti-inflammatory effect of AF and AF-16 has to be understood. To this date there is still no identified receptor for AF [73,74]. The main focus of the research has been on the physiological effects and the experiments have mainly been performed on organism level. Only a few studies of the molecular interactions have been published. The C-terminus of AF has been found to have binding sites for polyubiquitin [121] whereas the N-terminus of AF interacts with the membrane protein flotillin-1 [122]. Furthermore, AF-16 has been found intracellularly as well as co-localized with cholesterol and the glycosphingolipid galactosylceramide in the cell membrane of the pancreas from rats after intake of the peptide [123]. In *Paper V*, the membrane interaction and cell internalization of AF-16 are investigated in order to understand the its cellular uptake mechanism.

<sup>11</sup> Abbreviation in older literature: AF10

**Box 2.** Potential Applications of AF-16. These diseases or conditions, all related to imbalances of body fluids and/ or inflammation, have been shown to be reduced by AF therapy.

### Diarrheal Diseases

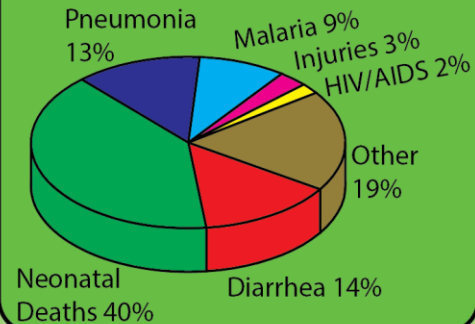
Loss of body fluids with the stool. There are several types of diharreal diseases with different causes:

**Acute:** Caused by bacterial toxins and bacterial or virus infection.

**Chronic:** Caused by chonical disease in the intestinal region.

**Endocrine:** Caused by unbalanced hormone levels.

### Cause of Death for Children up to 5 years of age



### High Intra Cranial Pressure



Increase in fluid pressure outside or within the brain, swelling of tissue, which leads additional pressure on areas of the brain or spinal cord. Can lead to shut down of life supporting body functions.

Cause: brain tumor, stroke, cebral infarction, or head injury.

### High Tumor Pressure

The tumor is swollen and blood flow reduced. Cancer medications are not effective since it cannot reach the tumor.

Cause: Tumor growth.

### Mastitis

Inflammation in breast tissue . Can afflict breast feeding women.

Cause: Bacterial infection.

### Ménière's Disease



Disorder in inner ear, affects hearing and balance.

Cause: The origin is not known but may be due to increased fluid volume in the ear.

### Inflammatory Bowel Diseases

Group of chronic diseases in the gastrointestinal tract. Abdominal pain, movement of bowels, and diarrhea. The most common types are ulcerative colitis and Crohn's disease.

Cause: Inflammation.

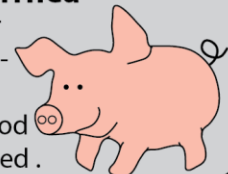
### Short Bowel Syndrome

Abdominal pain, diarrhea, fluid depletion, weight loss, fatigue.

Cause: Surgical removal of parts of small intestine or dysfunction in bowel.

### Livestock Diarrhea

Antibiotics are often used for prevention of diarrhea in live-stock. In Sweden this is not allowed anymore. Instead, food supplemented with SPC is used .



*Child mortality statistics from [124]. The descriptions of the conditions are based on facts from [74,125].*

# 5. Methodology and Fundamental Concepts

---

In this chapter the main methods to study the interactions with membrane models and cells are briefly described with the aim of introducing the concept of the techniques and their usage. Many of the methods are based on the interaction between light and matter therefore some theory about photophysics is included in the spectroscopy section. I also intend to give some experimental considerations that are important for the context of this thesis. Further reading can be done in the referenced textbooks about optical spectroscopy and photophysics [126–128], polarized spectroscopy [129], confocal laser scanning microscopy [130], flow cytometry [131], and reviews of isothermal titration calorimetry [132–134].

## 5.1 Spectroscopy and Photophysics

*Spectroscopy* methods are based on the interaction of electromagnetic radiation with matter. Electromagnetic radiation can be described both as a propagating wave with magnetic and electric components and as an energy package, a *photon*, with particle-like properties. This phenomenon is referred to as the *wave-particle duality*. The interaction of electromagnetic radiation and matter can result in different events such as absorption or emission of a photon as well as light scattering. The later is an important concept and will be briefly mentioned in this thesis but the theory behind it will not be described here.

### 5.1.1 Absorption Spectroscopy

Upon exposure to electromagnetic radiation some molecules are able to absorb photons and become excited as a result of the increase of the molecule's energy. This is only possible if two main conditions are fulfilled. First, the energy of the photon has to correspond to the energy gap,  $\Delta E$ , between the ground and excited states,  $E_1$  and  $E_2$ . The energy is inversely proportional to the wavelength,  $\lambda$ , of the electromagnetic radiation and hence it needs to have the right wavelength to be absorbed.

$$\Delta E = E_2 - E_1 = h\nu = \frac{hc_0}{\lambda} \quad (1)$$

where  $h$  is the Planck's constant,  $\nu$  is the frequency of the light, and  $c_0$  the speed of light in vacuum. The energy gaps for electronic excitations of molecules correspond to electromagnetic radiation of wavelengths in the ultraviolet and visible light region. Only these wavelengths are relevant for this thesis and therefore I will further only describe in terms of molecular interactions with light.

When absorption of light occur the charge distribution in the molecule interferes with the oscillating electric field of the light. This gives rise to a distortion of the charge distribution, when the molecule passes from the ground state to the excited state, which mainly occurs in direction of the *transition dipole moment*. The probability for the light to be absorbed is proportional to the magnitude and relative orientation of the transition dipole moment.

$$A \propto \mu^2 \cos^2\theta \quad (2)$$

where  $A$  is the absorption,  $\mu$  the magnitude of the transition dipole moment and  $\theta$  the angle between the transition dipole moment and the direction of the oscillating electric field of the light. The second condition that needs to be fulfilled is hence that the direction of the

electric component of the light is oriented in a suitable direction compared to the transition dipole moment. An angle of  $90^\circ$  results in no absorption whereas maximal absorption occurs when the light is perfectly aligned with the transition dipole moment. In an *isotropic*, randomly oriented, sample illuminated with isotropic light, this feature is not seen whereas this fact is the basis of the signals in linear dichroism spectroscopy (see section 5.1.).

Absorption measurements are done with a spectrophotometer, consisting of a light source, a monochromator and a detector. The monochromator selects a specific wavelength from the light source which then hits the sample with intensity  $I_0$ . If the sample absorbs light of this wavelength, the intensity that hits the detector,  $I$ , will be reduced compared to  $I_0$ , see Figure 5.1. The absorption can be calculated from the intensity difference (transmission).

$$A = \log \left( \frac{I_0}{I} \right) \quad (3)$$

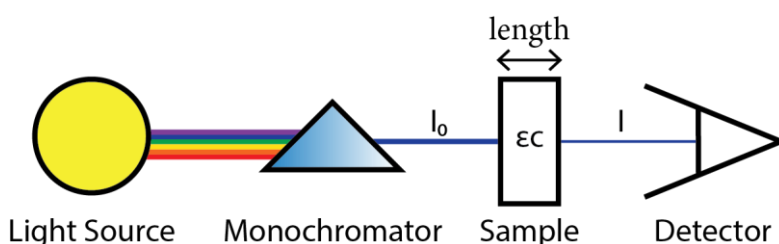


**Figure 5.1.** The principle of a spectrophotometer which can be used for absorbance measurements.

The absorption is also dependent on the number of molecules (concentration),  $c$ , the pathlength that the light travels in the sample,  $l$ , and the extinction coefficient of the molecules,  $\epsilon$ , which is a factor that expresses the molecules ability to absorb light of a certain wavelength. This relationship is called the *Lambert-Beer law*.

$$A(\lambda) = \epsilon(\lambda)cl \quad (4)$$

Because this proportionality exists, absorption spectroscopy is a great tool for concentration determinations, which have been a major and important use of this technique in this thesis. The absorption wavelength, the extinction coefficient and the shape of the spectrum can depend on the local environment. For instance some molecules are sensitive to the polarity of the solvent which is referred to as a solvatochromic effect [135]. Absorption spectra are usually less sensitive to variations in the local polarity compared to emission spectra [128,135]. but are still detectable for many molecules. The changes in the absorption spectra were studied for the voltage-sensitive membrane dyes, see section 6.2 and *Paper III*.

### 5.1.2 Emission Spectroscopy

It is thermodynamically unfavorable for a molecule to be in the excited state and it will therefore release the extra energy and go back to the ground state,  $S_0$ , by radiative or non-radiative pathways. The different processes are usually displayed with a *Jabloński diagram*, see Figure 5.2. To go back to the ground state most molecules undergo *internal conversion*, an isoenergetic non-radiative process, followed by *vibrational relaxation*, in which heat is released to the environment. For some molecules, called *fluorophores*, emission in the form of fluorescence is used as a relaxation pathway (often in combination with internal conversion). Absorption can occur to any electronic and vibrational state and since the internal conversion from the higher excited states and vibrational relaxation within an electronic state are very fast processes, the fluorescence is almost exclusively occurring from the lowest vibrational level of  $S_1$ . Because of this loss in energy and also the possibility for the molecule

to relax to any of the vibrational levels of  $S_0$ , the energy gap between the levels for the fluorescence is lower in comparison to the one for the absorption. This is the reason why the fluorescence spectra are usually found somewhat red-shifted (towards longer wavelengths) compared to the absorption spectra. The difference between the absorption and fluorescence maximum wavelength is usually referred to as the *Stoke's shift*.

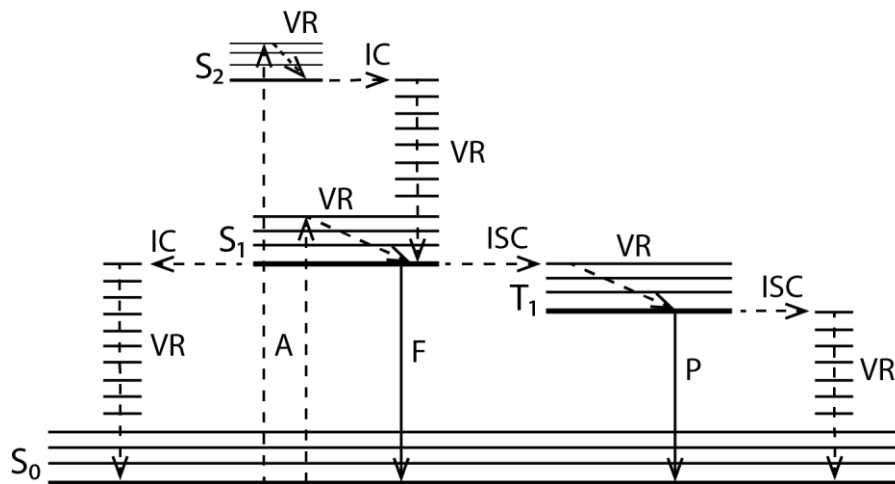


**Figure 5.2.** A Jablonski diagram. Upon absorption (A) the molecule becomes excited and can relax back to the ground state via fluorescence (F) or internal conversion (IC) followed by vibrational relaxation (VR). In some cases the molecule undergoes inter system crossing (ISC) from a singlet state (S) to a triplet state (T) from which phosphorescence (P) is possible.

Apart from the wavelength, the intensity of the fluorescence is an important characteristic. The intensity is dependent on the extinction coefficient of the molecule and on its *fluorescence quantum yield*,  $\Phi_F$ , which in principle is the ratio between the photons emitted and absorbed which can be calculated from the magnitude of the *fluorescence rate constant*,  $k_F$ , in comparison to the sum of all the rate constants for the system.

$$\Phi_F = \frac{\text{Photons emitted}}{\text{Photons absorbed}} = \frac{k_F}{\sum_i k_i} \quad (5)$$

Another important characteristic is the *fluorescence lifetime*,  $\tau_F$ , which describes the average time the molecule is spending in the excited state.

$$\tau_F = \frac{1}{\sum_i k_i} \quad (6)$$

Emission is recorded by a fluorometer. Just as in the spectrophotometer, the fluorometer contains an excitation monochromator that selects a specific wavelength from the light source. The sample is excited by the light and the emission then collected at an angle of  $90^\circ$ , to eliminate the influence of stray light from the excitation, and through a second monochromator, see Figure 5.3.

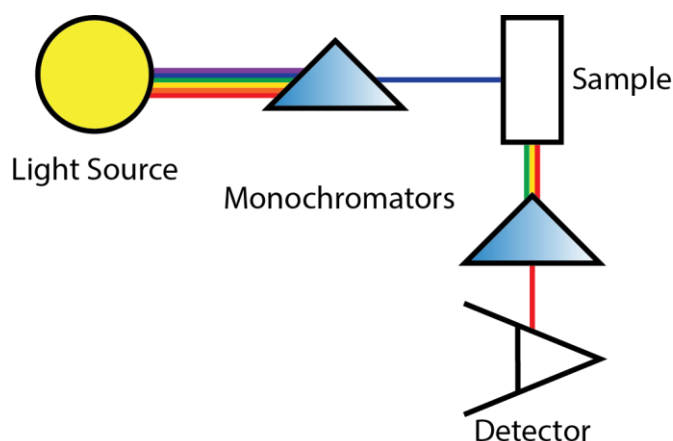


**Figure 5.3.** The fluorometer has two monochromators, one for the excitation light from the light source and one to distinguish emitted light of a specific wavelength. The detection of the luminescence is done at an angle of  $90^\circ$  to minimize detection of excitation light.

In some cases the system relaxes via *inter-system crossing* to a triplet state, see Figure 5.2. This crossing is not favorable under normal circumstances since it involves a change of the electron spin but can for instance occur in the presence of heavy atoms. Emission from this state is called phosphorescence. Phosphorescence is generally more red-shifted because the triplet state is lower in energy compared to its corresponding singlet state. In addition, phosphorescence generally shows longer lifetimes in the range of milliseconds to seconds whereas fluorescence commonly has lifetimes of about 10 ns. It is not always easy to distinguish between fluorescence and phosphorescence. Due to spin-orbit coupling, transition metal complexes with organic ligands frequently exhibit mixed singlet-triplet excited states and display lifetimes from 100 ns to microseconds. For this reason the terms emission or luminescence will be used in the sections about the ruthenium complexes.

As for absorption, the characteristics of the emission from a molecule can be sensitive to the local environment. By studying the emission wavelength, intensity or lifetime, interactions can be studied for molecules that change any of these parameters upon variations in the surroundings. This fact has been used in *Paper I, II, III and IV*. As mentioned before, solvent polarity can affect the spectral properties. Generally, molecules with a larger dipole moment in the excited state compared to the ground state exhibit this effect [128]. The fact that the emission is usually more sensitive to the polarity than absorption has to do with the smaller rate constants of emission that makes it possible for solvent relaxation during the luminescence whereas absorption is a much faster process. Other parameters that may influence the emission properties are for instance temperature, viscosity and interactions with the solvent.

### 5.1.3 Absorption and Emission of Ruthenium dppz Complexes

Ruthenium polypyridyl complexes have interesting photophysical properties which are useful in their application as cellular dyes. Upon absorption of visible light, excitation from a d-orbital of the ruthenium ion to anti-bonding  $\pi$ -orbital of the ligands occurs, so called metal-to-ligand charge transfer (MLCT) state [136]. MLCT transitions absorb with a broad band around 440 nm, resulting in the characteristic orange color of the complexes, see Figure 5.4. Ligand centered (LC) transitions from a bonding to an anti-bonding  $\pi$ -orbital occurs at shorter wavelengths. After excitation, LC and MLCT states rapidly relaxes to the lowest MLCT state, which has the charge localized on the ligand with the lowest anti-bonding  $\pi$ -orbital (dppz in our case). For interaction studies, ruthenium dppz complexes are

advantageous, compared to the similar complexes  $[\text{Ru}(\text{bpy})_3]^{2+}$  and  $[\text{Ru}(\text{phen})_3]^{2+}$ , since they possess the so-called *light-switch effect* [27,33,137–139]. This phenomenon makes the complexes very sensitive to their microenvironment, being highly luminescent in hydrophobic environments as in organic solvents or when bound to hydrophobic molecules whereas in aqueous solution the emission is quenched, see Figure 5.4. The quenching effect is due to water which is efficiently hydrogen bonding to the aza-nitrogens on the dppz ligand in the lowest MLCT state, therefore interactions of the complex with molecules that somehow shield water from the dppz ligand may result in a increased luminescence. This light-switch effect is also useful for cellular imaging since they will brightly stain areas where interaction with biomolecules occur with very low background emission. In addition to the light-switch effect, these ruthenium complexes also possess other photophysical properties that generally are beneficial for cellular imaging [35]. For instance, the relatively high photostability and low photobleaching enables imaging during longer times by microscopy. Moreover, the large Stoke's shift prevents self-quenching due to re-absorption of the emitted light and the red emission is able to more efficiently penetrate tissue compared to emission of shorter wavelengths. Furthermore, the long-lived emission lifetime is easily distinguished from the lifetime of the auto-fluorescence and can be used for detection by lifetime techniques. The stereochemistry of the complex is also important to consider. For instance, the emission quantum yield of DNA bound  $[\text{Ru}(\text{phen})_2\text{dppz}]^{2+}$  is highly dependent on the stereochemistry although the binding mode and affinity seems to be similar for the two enantiomers [27]. This effect is probably due to a small difference in binding position of the two enantiomers in the intercalation pocket. The ruthenium complexes thus possess a variety of properties making them interesting as cellular dyes and in addition the photophysical properties and affinity to biomolecules of the complexes can easily be tuned by modification of the ligands [36] and therefore different probes for different cellular areas can be developed.

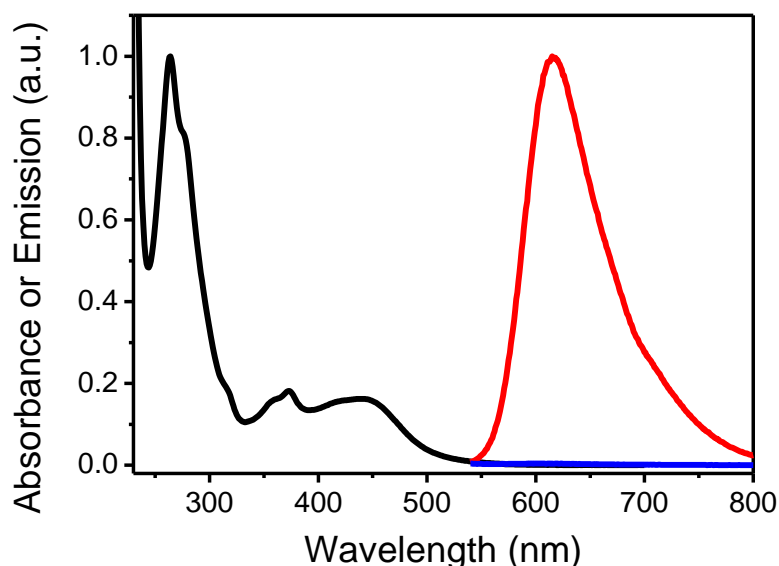


**Figure 5.4.** Absorption (black) and emission (blue) spectra in buffer and emission spectra when bound to DNA (red) of the complex  $\text{rac-}[\text{Ru}(\text{phen})_2\text{dppz}]^{2+}$ .

### 5.1.4 Spectral Properties of Voltage-Sensitive Dyes

Voltage-sensitive dyes have been shown to change their spectral properties upon variation of the transmembrane voltage (Figure 5.5). These changes include wavelength shifts of the absorption and fluorescence, as well as variation of the fluorescence quantum yield. The mechanism of the voltage-sensing is still not fully understood but has been suggested to be a charge-shift *electrochromic mechanism* [64,65,140–142] or *solvatochromism* [66,142–144]. In the first mechanism the electric field is directly affecting the energies and transition probabilities of the molecular chromophore, whereas in the latter the effect is believed to involve the positioning and orientation of the probe and hence the microenvironment is changed. The response has also been suggested to depend on more than one mechanism [64,145].

The spectral properties of the dyes have been shown to be sensitive to the local environment [17-18, 24, 63-73] where solvent polarity [146–149], pH [150,151] and ionic strength [150,151] have been found to cause shifts in wavelength for the absorbance and emission but also changing the fluorescence quantum yield and fluorescence lifetime [66,149,152–155]. Also lipid membrane interactions of voltage-sensitive dyes have been shown to change the spectral properties of the probes [63,140,143,147,155] as well as the application of an external electric field over the membrane [64,65,140,141,145,156,157].

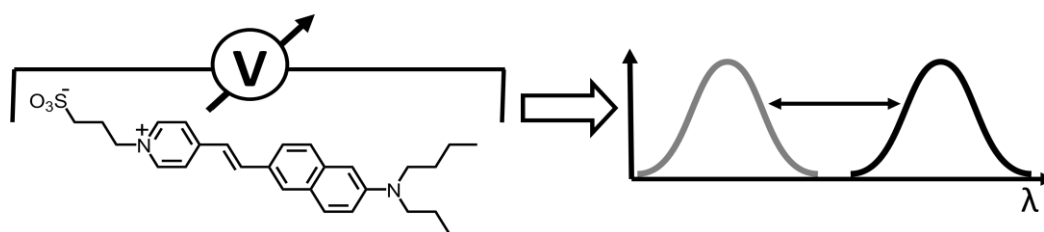


**Figure 5.5.** A variation of the membrane potential causes spectral shifts of the voltage-sensitive dyes. The mechanism behind this effect is still not fully understood.

### 5.1.5 Photophysical Properties of Peptides

There are three different amino acids which show photophysical properties, phenylalanine, tyrosine and tryptophan. Of these tyrosine and tryptophan are more useful in spectroscopy measurements since they display higher extinction coefficients and fluorescence quantum yields compared to phenylalanine. Both amino acids have absorption maxima at about 280 nm and the fluorescence maximum is at around 340 nm for tryptophan and 303 nm for tyrosine in water solution. Unlike tyrosine, tryptophan displays an emission which is very sensitive to solvent polarity. It is the possibility of hydrogen bonding to the imino nitrogen of the indole group that makes the fluorescence to blue-shift and the quantum yield to increase with decreased polarity [128], see Figure 5.6. This feature can be used to determine if a protein is folded or denatured or in studies of peptide-membrane interactions by measuring the emission spectra (see *Paper IV*).

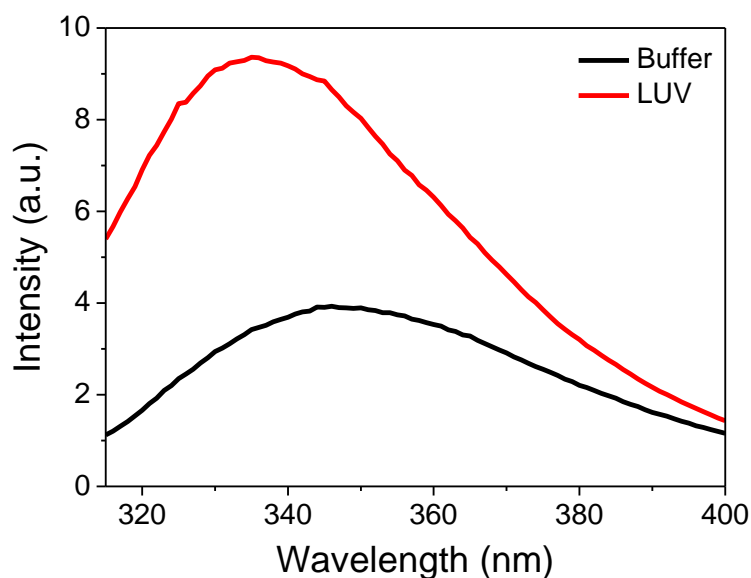


**Figure 5.6.** The tryptophan fluorescence is blue-shifting and increasing in intensity when going from buffer solution to lipid membrane binding.

In addition to the side chain absorption in the region of 200-300 nm, peptides also display absorption due to the peptide bond at 180-230 nm and, in the case of disulfide bonds between two cysteine side chains, also around 260 nm [129,158]. The concentration of peptides are often determined using the intrinsic chromophores tryptophan ( $\epsilon_{280\text{nm}}=5500$  in buffer neutral pH) [159] or tyrosine ( $\epsilon_{280\text{nm}}=1490$  in buffer neutral pH) [159] residues. For peptides lacking these two amino acids could in principle the peptide bond absorption at around 200 nm be used for concentration measurements but since buffer salts also strongly absorb at this wavelength the absorption from the peptide bond is hard to accurately measure. Instead colorimetric assays like the bicinchoninic acid (BCA) [160] assay could be used. In this assay the peptide sample is mixed with an alkaline reagent solution containing BCA and  $\text{Cu}^{2+}$ . The  $\text{Cu}^{2+}$  is reduced to  $\text{Cu}^+$  by the amino acids cysteine, tryptophan and tyrosine as well as the peptide bond in the alkaline environment [160,161]. Further, the  $\text{Cu}^+$  ion forms a complex with the BCA molecule which has a strong absorption at 562 nm. The absorption of the sample is compared to a standard curve of reference solutions with known peptide concentrations, preferable with the same peptide, for determination of the sample with unknown concentration. This assay was used to determine the concentration of the peptide AF-16 in *Paper V*.

## 5.1.6 Polarized Spectroscopy

The interaction with matter and polarized light can give further information about molecular structure and interactions. Below the principles of linear dichroism and circular dichroism spectroscopy and their use in this thesis are described.

### 5.1.6.1 Linear Dichroism Spectroscopy

*Linear dichroism*, LD, spectroscopy is a great tool to investigate the binding geometry of molecules to DNA or lipid bilayers (see *Paper II* and *III*). The definition of LD is the difference in absorption between parallel and perpendicular linearly polarized light.

$$LD = A_{\parallel} - A_{\perp} \quad (7)$$

To obtain an LD signal the molecules of the sample have to be oriented. Orientation can be achieved by subjecting the sample to a shear flow, electric field, magnetic field or to stretch a film but there are also samples that have an intrinsic orientation. A *Couette flow cell*, consisting of two concentric cylinders where the sample is applied in the gap between them, can be used to create a shear flow by rotation of one of the cylinders. Long DNA molecules are able to align in the flow direction, with the helix direction as the *macroscopic orientation axis* and gain a negative LD signal at 260 nm corresponding to the absorption of the bases approximately perpendicular to the helix axis. Small molecules which are not oriented by the shear flow themselves can gain orientation, and hence show LD, upon non-random binding to the DNA. Liposome interaction of molecules can also be studied in the Couette cell since the shear flow deforms the liposomes into a more elliptical shape, with the long axis parallel to the flow. By adding sucrose to the buffer, this effect can be enhanced and, additionally, the refractive index is closer to that of the liposomes which reduces their light scattering [162].

To make the LD independent of the concentration and pathlength of the sample cell, the signal can be normalized with respect to the isotropic absorption,  $A_{iso}$ , and the *reduced LD*,  $LD^r$ , is obtained. Already from the LD signal it is possible to determine qualitatively which direction the transition dipole moment is compared to the macroscopic orientation axis but even more information can be obtained from  $LD^r$  since the binding angle can be determined if the *orientation factor*,  $S$ , of the system is known. For measurements of DNA binding agents the absorption of the nucleobases can be used to calculate the  $S$  factor whereas for lipid membranes the use of membrane dyes with known orientation is required.

$$LD^r = \frac{LD}{A_{iso}} = 3S \left( \frac{3\cos^2\alpha - 1}{2} \right) \left( \frac{3\langle \cos^2\beta \rangle - 1}{2} \right) \quad (8)$$

where the angle  $\alpha$  is found between the transition dipole moment of the chromophore and the *system director*, which for DNA is the helix direction and for lipid bilayers the membrane normal, see Figure 5.7. The orientation factor  $S$  describes how well the system is oriented compared to the reference axis ( $S=1$  for perfectly aligned systems whereas  $S=0$  for random samples). For LUVs the orientation factor is dependent on both the macroscopic orientation of the lipid chains but also the deformation of the LUVs in the flow. The angle between the reference axis and the system director is described by  $\beta$ , which is defined as  $90^\circ$  for LUVs and hence the following expression can be used.

$$LD^r = \frac{3}{4}S(1 - 3\cos^2\alpha) \quad (9)$$

The angle  $\beta$  for DNA is, however, defined as  $0^\circ$  and thus the  $LD^r$  can be calculated by

$$LD^r = \frac{3}{2}S(3\cos^2\alpha - 1) \quad (10)$$

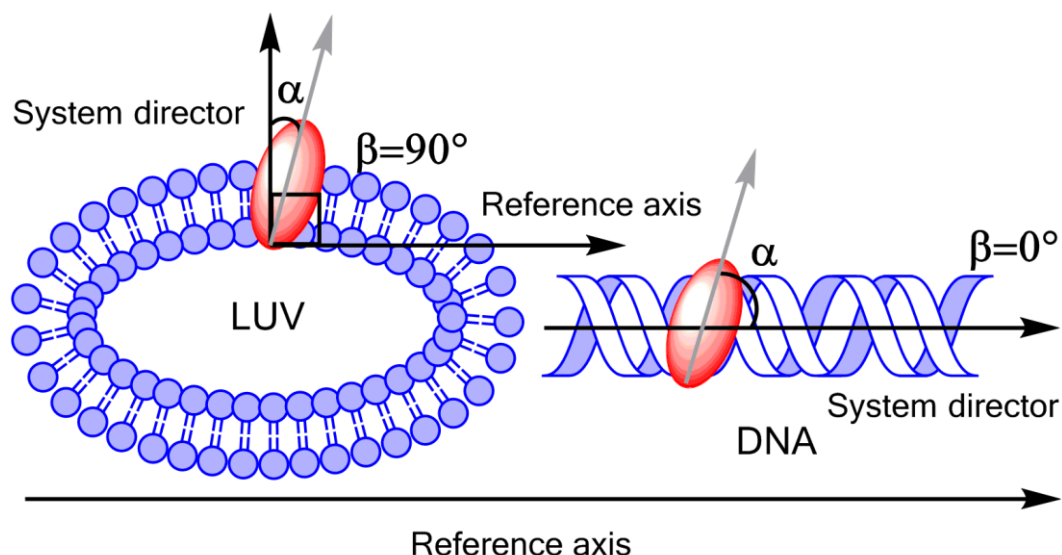


**Figure 5.7.** The ideal orientation of flow-aligned LUVs and DNA. Indicated are the orientation of the system directors compared to the reference axis (described by angle  $\beta$ ) as well as the relative orientation of the transition dipole of the red molecules (grey arrow) to the system director (described by angle  $\alpha$ ).

### 5.1.6.2 Circular Dichroism Spectroscopy

Circular Dichroism, CD, is the difference in absorption of right and left circularly polarized light.

$$CD = A_l - A_r \quad (11)$$

To obtain a CD signal the molecule needs to be chiral, be folded into a chiral structure (e.g. the DNA double helix or protein secondary structures) or the signal can be induced by binding to a chiral molecule (e.g. ligand binding to DNA).

CD can be used to analyze the purity of enantiomers of synthesized molecules but is also commonly used to study biological molecules. It is a great tool to employ for secondary structure investigations of protein and peptides, for this purpose the backbone absorption in the region 180-250 nm is useful. CD spectrum of a pure secondary structure has very distinctive shapes, see Figure 5.8.  $\alpha$ -helices are giving rise to two negative peaks at 222 nm and 208 nm and a larger positive peak around 195 nm whereas  $\beta$ -sheets generally generate a negative peak around 217 nm and a positive peak at 195 nm and random coil often give rise to a large negative peak around 200 nm and a smaller negative band at around 218 nm. The CD spectrum of a protein or peptide with a mixture of secondary structures displays hence a spectrum that corresponds to the contribution of the different structures. It is possible to calculate the secondary composition from a CD spectrum through databases of proteins with known composition but these results are, however, not so accurate for short peptides since there are not so many short polypeptide sequences in the databases. Furthermore, when performing CD measurements below 200 nm it is important to notice that most buffer salts are strongly absorbing in this region. The accuracy of the measurement is questionable when too strongly absorbing buffer components are used since too little light reaches the detector and the influence of for instance stray light is very high. To avoid these artifacts, buffer should be carefully chosen for instance highly absorbing chlorine salts should be substituted with fluorine salts. In this thesis the secondary structure of the AF-16 peptide was studied by CD (*Paper V*).

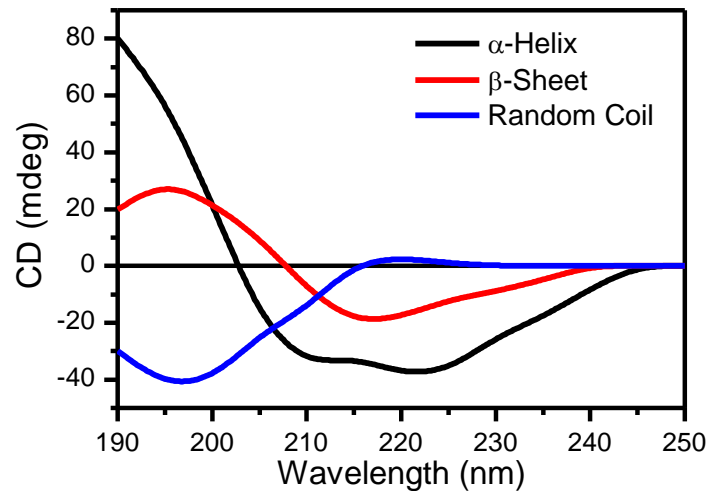


**Figure 5.8.** Predicted CD spectra for peptides or proteins in different conformations.

## 5.2 Isothermal Titration Calorimetry

*Isothermal titration calorimetry* (ITC) is a method widely used for studies of biomolecular interactions. The technique is based on detection of heat released or consumed by the system upon the interaction which is done, as the name implies, as a titration at constant temperature. The experimental procedure will further be discussed in terms of an interaction of a ligand and a macromolecule. The calorimeter is composed of two identical highly isolated chambers, in one of them a sample with the macromolecule is applied and the other one is used as a reference (usually containing the buffer or water), see Figure 5.9A. Titration of the ligand is done with a titration pipette under high stirring. When the interaction occurs heat is released or consumed with a magnitude that is proportional to the amount binding ligand and the instrument records the power needed to maintain an unchanged temperature difference between the sample and reference chambers during the titration time. This compensatory power is either negative or positive compared to a reference power depending on the nature of the interaction which results in negative peaks for *exothermic* interactions and positive peaks for *endothermic* interactions. By integrating these peaks, the enthalpy difference for each titration is obtained which usually is normalized to the moles of titrant and plotted against the molar ratio. By fitting this graph with a suitable binding model, the ITC experiment can provide information about binding constants, binding enthalpy and entropy as well as the stoichiometry. In Figure 5.9B an example of an ideal experiment of a macromolecule with a number of identical binding sites for the ligand is shown. The integrated heats build up a *sigmoidal* curve showing tendency to have a plateau both in the beginning and in the end of the titration. The value of the initial plateau is the *binding enthalpy*,  $\Delta H_b$ , of this interaction (if a plateau is seen this means that all ligand is binding for these titrations). The peak magnitude decreases and gains the constant value corresponding to the dilution heat of the ligand in the end of the titration. From the middle of the sigmoidal curve it is easy to estimate the *binding constant*,  $K$ , from the slope as well as the stoichiometry,  $n$ , from the value of the molar ratio.

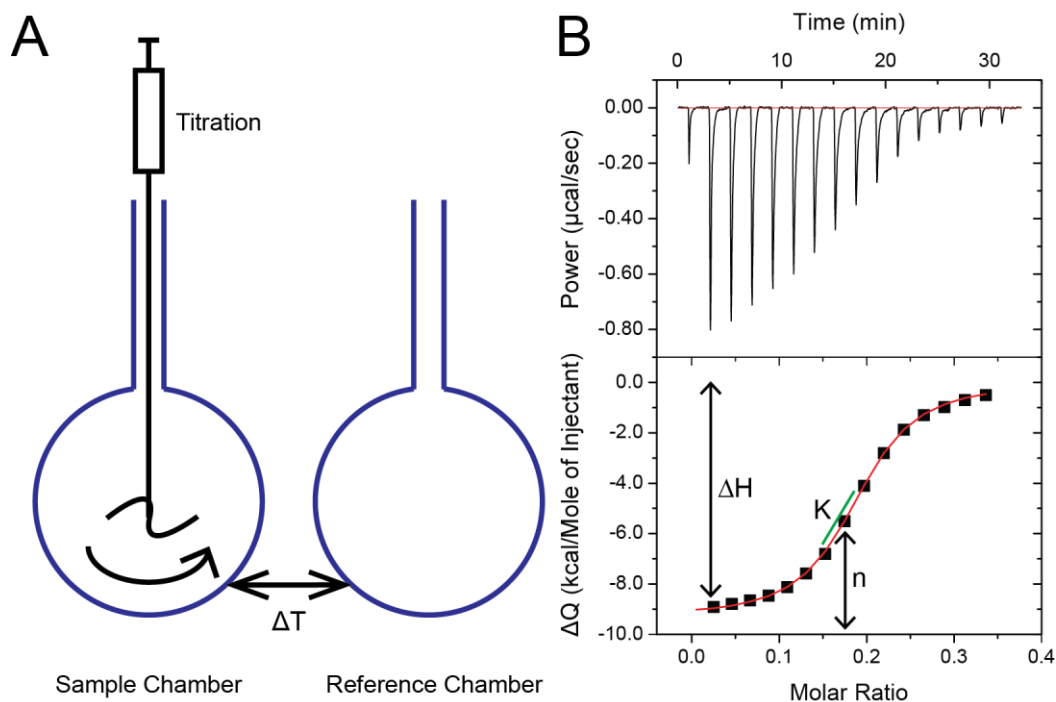


**Figure 5.9.** An interaction between two molecules can be studied with ITC, for instance the macromolecule  $M$  and the ligand  $L$ . (A) The calorimeter has two chambers, one where a titration of  $L$  into  $M$  is done and one as a reference. Heat is produced or consumed upon the interaction and the calorimeter registers the energy that is needed to cool or heat the chamber in order to maintain the same temperature as the reference chamber. (B) Top: the graph shows the compensating power with the time. Bottom: The integrated peak area from the power plot gives the change in heat for each titration, here displayed normalized with the mole of injectant and as a function of the molar ratio ( $L:M$ ). From this graph parameters as the enthalpy change upon binding ( $\Delta H_b$ ), binding constant ( $K$ ) and stoichiometry ( $n$ ) can be estimated directly or determined by fitting the curve with a suitable binding model.

ITC is hence a powerful tool to study binding affinities but also the characteristic thermodynamics of the interactions. Furthermore, it is possible to assign the nature of the binding by changing the experimental conditions, commonly by performing the same experiment at different temperatures. By determining the binding enthalpy,  $\Delta H_b$ , at different temperatures (assuming a constant pressure) the change in *heat capacity* associated with the binding,  $\Delta c_p$ , can be obtained.

$$\Delta H_b = \Delta c_p \Delta T \quad (12)$$

Generally,  $\Delta c_p$  is negative for interactions of hydrophobic character whereas electrostatic interactions generate a positive sign or only small variations of the change in heat capacity. Other methods can be used for determination of the binding constants but only calorimetric methods are able to directly measure the binding enthalpy. In addition, ITC does not rely on any specific characteristics of the molecules (e.g. being fluorescent). Instead molecular interactions can be studied of, in principle, any molecule as long as the heat change is within the detection limits of the instrument. The gained signals can, however, also arise from other effects rather than the interaction of interest. Dialysis of the samples is highly recommended to avoid heat changes due to differences in the solvents. The dilution of the titrant is also giving some contribution for the heat change and therefore its enthalpy is usually subtracted from the raw data (the dilution of the molecule in the sample chamber gives usually a negligible effect but should be corrected for if significant). Additionally, events like

aggregation and disaggregation processes, and for liposomes fusion and leakage, can also contribute to the heat changes. Although there are some important factors that need to be considered, the method can obtain thermodynamic parameters directly from the system and is therefore a very important technique in the field of molecular interactions. In this work ITC measurements were performed to investigate the interaction between the peptide AF-16 and heparin (see *Paper V*) or LUVs.

### 5.3 Confocal Laser Scanning Microscopy

There are various microscopy methods, which all are used to visualize objects that are too small to be seen by the naked eye. Optical microscopy techniques are based on the diffraction of light by the sample. The *limit of the image resolution*,  $d$ , i.e. smallest separation between two objects which still can be distinctly visualized, is dependent on the wavelength of the radiation used for the visualization and the so called *numerical aperture* of the objective,  $NA$ . This limitation of the resolution is described by the *Rayleigh criterion* [130].

$$d = 0.61 \frac{\lambda}{NA} \quad (13)$$

$NA$  is a measurement of the capacity of the objective to collect light which is dependent on the refractive index,  $n$ , of the medium applied between the objective and sample as well as the half-angle,  $\theta$ , of the cone of light to objective lens.

$$NA = n \sin \theta \quad (14)$$

In a conventional bright-field microscope the sample is illuminated and the detection of transmitted light is used for visualization. This is a fast and simple fashion to obtain images of objects with high contrast to the background. Most biological samples are, however, more or less transparent and is preferably labeled with fluorescent dyes and studied by fluorescence microscopy. If a wide field fluorescence microscope is used, the fluorescence from the entire sample is collected which can be useful for many applications but if more detailed information for instance about intracellular localization, confocal microscopy is generally preferred.

In *confocal laser scanning microscopy* (CLSM) the sample is, as in the case of wide field microscopy, illuminated and the fluorescence collected but in addition the confocal microscope also is equipped to perform excitation and detection at a certain focal point. This is achieved by two *pinholes* that allow the light source to focus at a point and exclude the majority of the fluorescence which is not originated from this point (Figure 5.10). The background in the form of out-of-focus emission is hence highly reduced compared to the standard fluorescence microscopy. An image is created by scanning a defined area, detecting emission from a number of focal points at this plane. CLSM is a great tool for visualization of cross-section of cells and it is also possible to create a 3D reconstruction of the sample when several cross-sections of different focal planes are combined. The advantage of CLSM is the great contrast, gained by the pinhole technique but it is also important to notice that detection of photons from the focal points requires an high intensity excitation source which can cause photobleaching of dyes and photodamage on cells that leads to cell death[130,163]. In this thesis, CLSM was used to image intracellular distribution of the ruthenium complexes (*Paper I and II*) and the cellular uptake of peptides (*Paper IV and V*).

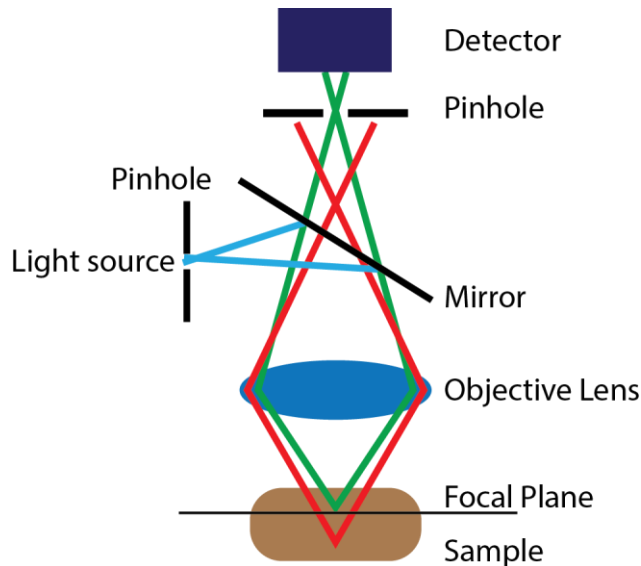


**Figure 5.10.** Principle of confocal laser scanning microscopy. The excitation light is passing through a pinhole to only illuminate the sample at a certain focal plane. The emission is then collected from the same focal plane by the detector (green) whereas out-of-focus light is excluded by a pinhole (red).

## 5. 4 Flow Cytometry

*Flow cytometry* is a technique that makes statistical analysis of size, shape and fluorescence detection of particles and cells possible. It is widely used in the medical field for instance in cancer diagnostics and blood cell analysis but there is an increasing interest for applications in other fields. The flow cytometer consists of five main components: one or several light sources (usually lasers), a flow chamber, optics, detectors (photodiodes or photomultiplier tubes) and a computer with data processing [131], see Figure 5.11. The cells or particles are aligned to pass the laser beam one by one in the *flow chamber*, commonly by the use of a sheath fluid that focuses the cells by hydrodynamic forces. The sample is injected into the flow chamber and since the sheath fluid has higher velocity (but still laminar) the cross-sectional area of the sample stream is reduced so the cells will only pass one by one. Another alternative is to use a microcapillary which by its geometry focuses the cells or particles [164]. The latter technique was used during the experiments presented in this thesis.

When exposed to the laser beam the cells or particles are scattering light in different directions. The *forward scattering* is proportional to the size of the object and can be used to discriminate between different sizes [131], e.g. live and dead cells since dead cells are smaller in size. The *side scattered* light, on the other hand, is dependent on the granularity (the complexity of the internal of the cell), which for example can be used for distinguishing different types of blood cells. Besides light scattering, fluorescence of different wavelength can be detected in flow cytometry measurements. Commonly, dyes or labeled antibodies are used to distinguish different types of cells, cells expressing a certain receptor or antigen, enzyme activity, membrane potential or DNA content [131]. Depending on the filters of the detectors as well as the spectral characteristics of suitable fluorophores it is possible to do multi-color detection for each cell or particle and hence study several characteristics simultaneously. The scattering and fluorescence from the experiment is further analyzed by either *dot plots*, where the intensity of two parameters are plotted on the two axes, or *histograms*, displaying the number of cells with a certain intensity of one of the parameters, see Figure 5.12.

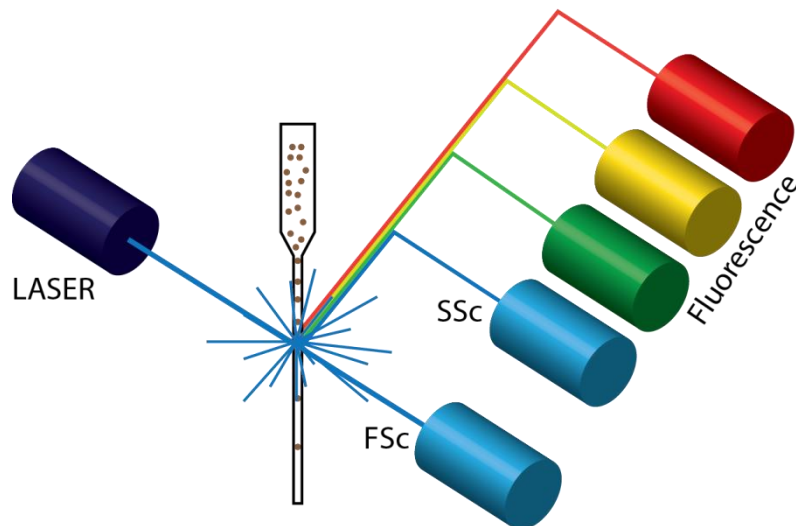


**Figure 5.11.** The flow cytometer uses a capillary, as shown here, or sheath flow to align the cells and exposes them one by one to a laser beam. The intensity of forward scattered (FSc) and side scattered (SSc) light as well as fluorescence of different wavelengths is detected for each cell.

In this thesis flow cytometry has been used to statistically quantify peptide uptake in cells (Paper IV and V) as well as to study the viability of the cells incubated with the peptides (Paper IV). The cell viability can be determined by an assay using Annexin V commonly labeled with phycoerythrin (PE) which show yellow fluorescence and 7-aminoactinomycin D (7-AAD) which fluoresces in the red region [131]. Annexin V is a protein with high affinity to the lipid phosphatidylserine which is externalized on the cell membrane upon apoptosis whereas 7-AAD is a cell impermeable DNA dye which only can access the DNA in the nucleus if the cell membrane is no longer intact, as for late apoptotic and necrotic cells. Thus, with this assay live cells would be non-stained, apoptotic cells would show PE staining and late apoptotic and necrotic cells would show 7-AAD staining and by monitoring the yellow and red fluorescence of the cells the toxicity of the peptide can be obtained.

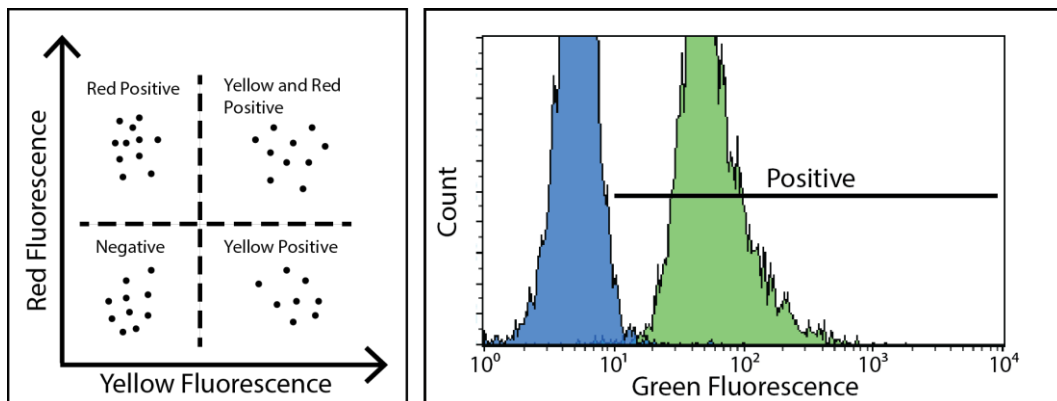


**Figure 5.12.** The flow cytometry data can be displayed as a dot plot (left), where two parameters are plotted against each other, or a histogram (right), where the counts of one parameter is displayed.

## 6. Results

This chapter summarizes the main results from Paper I-V. All papers are focused on molecular interactions with the cell membrane and cells. Some relevant unpublished results are also included.

### 6.1 Tuning the Affinity and Cellular Localization of Dyes based on Ruthenium Complexes

Ruthenium *dppz* complexes show remarkable biomolecular interactions and photophysical properties, including the light-switch effect, that make them interesting as cellular dyes. Since  $[\text{Ru}(\text{II})\text{phen}_2\text{dppz}]^{2+}$  show strong DNA binding, the focus has mainly been to develop nuclear dyes but the possibility to easily structurally alter the complexes gives the opportunity to tune them to target other intracellular sites. In Paper I and II, three ruthenium complexes with *dppz* moieties substituted with alkyl ether chains of different lengths, D2, D4 and D6 (Figure 6.1) were investigated with the aim to study their binding preference comparing lipid membranes, *ct*-DNA and rRNA. Further, the cellular localization in fixed cells and the cellular uptake in live cells were studied to investigate if the binding preferences of the complexes correlate with the cell interactions.

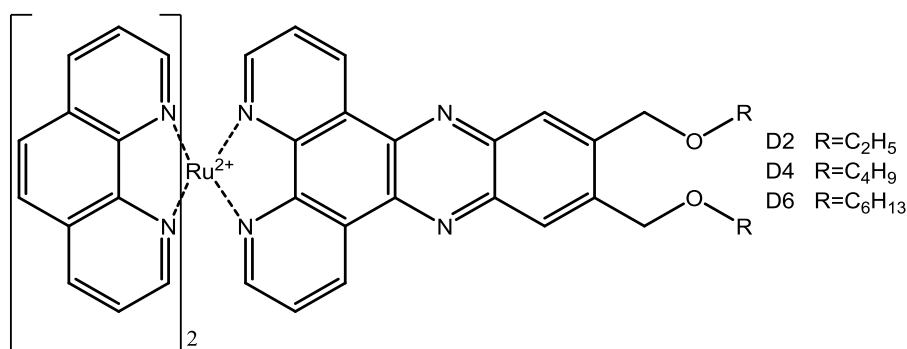
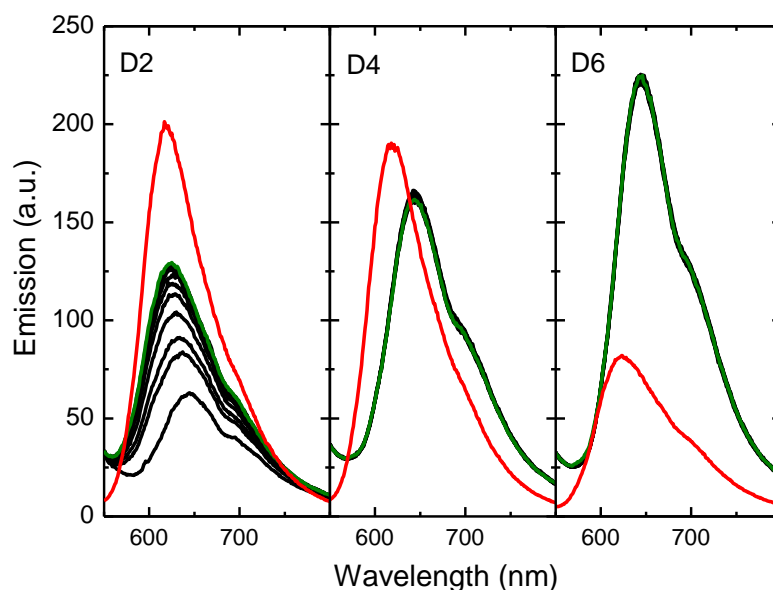


Figure 6.1. Structure of the three ruthenium complexes studied in Paper I and II.

#### 6.1.1 Lipophilicity of the Complexes and Membrane Charge Influence Binding Preferences

The three *dppz* complexes<sup>12</sup> all show environment sensitive emission spectra with significant variations in wavelength and quantum yield. For all complexes, the wavelength in the presence of LUVs is about 645 nm whereas for nucleic acids it is around 620 nm and the intensity in RNA environment is highly reduced compared to DNA. By monitoring spectral properties of the ruthenium complexes during titration experiments with competing components, the binding preference of the complexes were determined. Comparing DNA and negatively charged LUVs (20% negatively charged lipids), the preference was shown to differ between the complexes. The two most lipophilic complexes clearly favored the LUV binding since the emission spectra of membrane bound complexes did not change at all upon titration of DNA, see Figure 6.2, whereas their spectra changed when DNA bound complexes were titrated with LUVs. In contrast, the spectrum of D2 in mixture of DNA and LUVs have an emission maximum wavelength close to DNA bound complex. When negatively charged LUVs and rRNA were compared, all three complexes favored LUV binding.

<sup>12</sup> Here used in the form of racemates.



**Figure 6.2.** Emission spectra of D2, D4, and D6 ( $2 \mu\text{M}$ ) bound to DOPC/DOPG (4:1) LUVs ( $200 \mu\text{M}$ ) titrated with aliquots of ct-DNA (black lines) to a final DNA concentration of  $40 \mu\text{M}$  (green lines). Emission spectra of ct-DNA bound complexes are shown in red.

Although the emission wavelength of ct-DNA and rRNA bound complexes did not differ very much, binding competition studies were still possible to perform because of their significantly different intensities. When samples of DNA bound- and RNA bound complex, respectively, were gradually mixed, see Figure 6.3, the spectra of D2 and D4 changed to intensities in between the intensity of DNA- and RNA bound complex. The affinity for RNA seem to be slightly higher for D4 compared to D2. For the most lipophilic complex the spectra of the fully mixed samples showed an identical spectrum to the one of RNA bound complex, proving a higher affinity for this component.

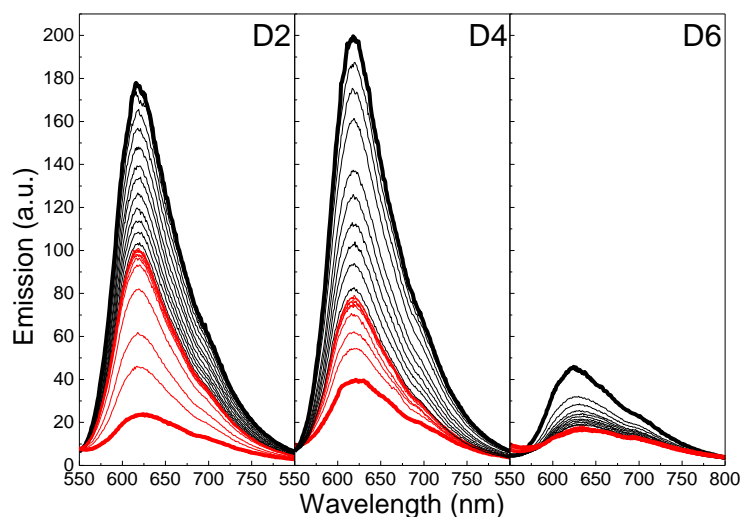


**Figure 6.3.** Emission spectra of D2, D4, and D6 ( $2 \mu\text{M}$ ) in pure ct-DNA ( $40 \mu\text{M}$  bases, thick black line) and in pure rRNA ( $40 \mu\text{M}$  bases, thick red line). When the ct-DNA sample is gradually mixed with the rRNA sample (thin black lines), the intensity of the ct-DNA samples is decreasing, and for D2 and D4, an increase is shown for the rRNA sample upon mixing (thin red lines), whereas the emission of RNA-bound D6 does not change upon addition of ct-DNA.

The plasma membrane of mammalian cells has only up to 20% negatively charged lipids, of which a large fraction is found in the inner leaflet. Therefore also the binding preference of the complexes for zwitterionic LUVs were compared with that to rRNA and ct-DNA, see Figure 6.4. Interestingly, only the middle complex D4 was affected by the LUV charge. With zwitterionic lipids, LUV-bound complex showed a changed emission wavelength upon RNA or DNA titration, proving that the exclusive preference for negatively charged membranes could be perturbed by alterations of the membrane composition. The effect was larger for the experiment with DNA since the spectrum of the mixed sample almost resembled that of the DNA bound spectrum. The more lipophilic complex D6, however, showed still a high preference for membrane environments whereas the least lipophilic complex D2 favors nucleic acid binding (the latter not shown in the graph). This result shows that the electrostatic forces, in addition to the hydrophobic effect, are important for the molecular interactions of the complexes.

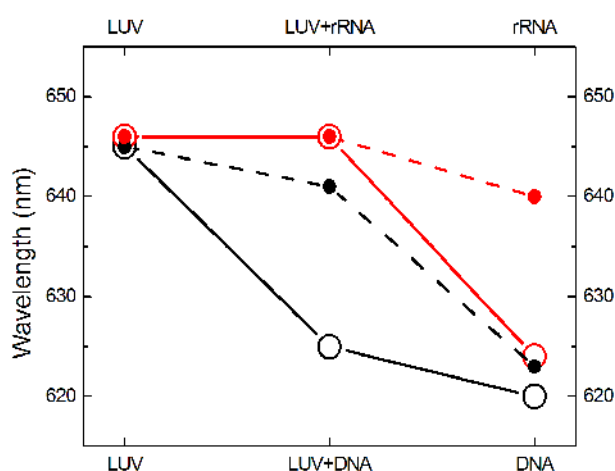


**Figure 6.4.** Emission wavelength maximum of D4 (black) and D6 (red) in DNA, DOPC LUVs, and a mixture thereof (solid lines) and in rRNA, DOPC LUVs, and a mixture thereof (dashed lines).

The complexes relative affinity to lipid membranes, DNA and RNA is thus highly tunable by a small adjustment of their lipophilicity. D2 seems to favor DNA binding whereas D6 prefer lipid membranes. The results from the binding preference studies from *Paper I* and *II* are summarized in Table 6.1.

**Table 6.1.** Binding Preferences of D2, D4 and D6.

Competing Components		Preferred Binding of:		
		D2	D4	D6
DOPC/DOPG	ct-DNA	ct-DNA (eq)	DOPC/DOPG	DOPC/DOPG
DOPC/DOPG	rRNA	rRNA	DOPC/DOPG	DOPC/DOPG
rRNA	ct-DNA	ct-DNA (eq)	eq	rRNA
DOPC	ct-DNA	ct-DNA	ct-DNA (eq)	DOPC
DOPC	rRNA	rRNA	DOPC (eq)	DOPC

*eq = an equilibrium between binding of the two components was found. For some combinations a clear but not exclusive preference was seen, this is indicated with (eq).*

It is also interesting to examine the emission intensity of the complexes. Clear trends are seen when the complexes are bound to lipid membranes or DNA, with increased intensity with increased lipophilicity of the LUV bound complexes whereas the trend is opposite in DNA environment. This correlates with LD measurements of the complexes in different environments. We found that the complexes are interacting with DNA in the same way as the parent complex  $[\text{Ru}(\text{phen})_2\text{dppz}]^{2+}$  but the LD signal is decreased with increased lipophilicity and a previous study showed that LUV binding D6 has higher LD signal compared to D2[39]. Lower LD signals show that the complex is less well oriented which can be both due to a wider distribution of binding orientations but also be an indication of less binding. The very low intensity found for all complexes in RNA environment could be due to that less complex is bound but, since the binding preference experiments show a higher relative affinity of D6 for RNA compared to DNA, this is not very likely. The low intensity is instead probably due to that the dppz ligand is less shielded from water when bound to RNA. The emission intensity can hence be due to both differences in the degree of binding complex but also due to the microenvironment of the complexes. It should also be noted that D6 has a low but significant luminescence in buffer solution suggesting that it forms some kind of aggregates to protect its highly lipophilic dppz ligand from water. This effect is not seen for the other complexes.

There is clearly a difference in relative affinity of the three ruthenium complexes to nucleic acids and membranes. To examine if there is any difference in their interactions with cells we investigated the cellular localization of the complexes in fixed cells, where the plasma membrane has been permeabilized and which hence does not restrict the cellular entry. In Figure 6.5, the staining patterns of the complexes are shown. These are compared with a commercial RNA probe, SYTO RNaselect, which stains the RNA-rich nucleolus and cytoplasm of the cell but not the nucleus. D2 shows a clear nuclear staining which is opposite to the staining pattern of the RNA probe. D4, on the other hand, seems to be very similar to the RNA probe, staining the cytoplasm and the nucleolus intensely but a weaker staining of the nucleus is additionally seen for this complex. The most lipophilic complex, D6, stains mainly the cytoplasm intensely but a weaker staining of the nucleolus is also present. The cellular localization seems thus to correlate with the binding preferences concluded in the *in vitro* experiments. Some results do, however, not clearly correlate with the the *in vitro* experiments. The intensity of D4 in the nucleolus is high compared to the nucleus although the relative intensity of DNA bound complex is very much higher than for RNA bound complex in the *in vitro* measurements indicating a higher affinity to RNA compared to DNA. The exclusive preference for lipid membranes seen for D6 *in vitro* is also not as distinct in the cells, since the nucleolus is stained. The cellular milieu is of course more complex than the *in vitro* experiments, not only because of the large variety of molecules present but also because of the varied accessibility of the molecules. For instance, DNA strands are not free in solution but densely packed into the chromosomes which can affect the possibility for molecules to bind.

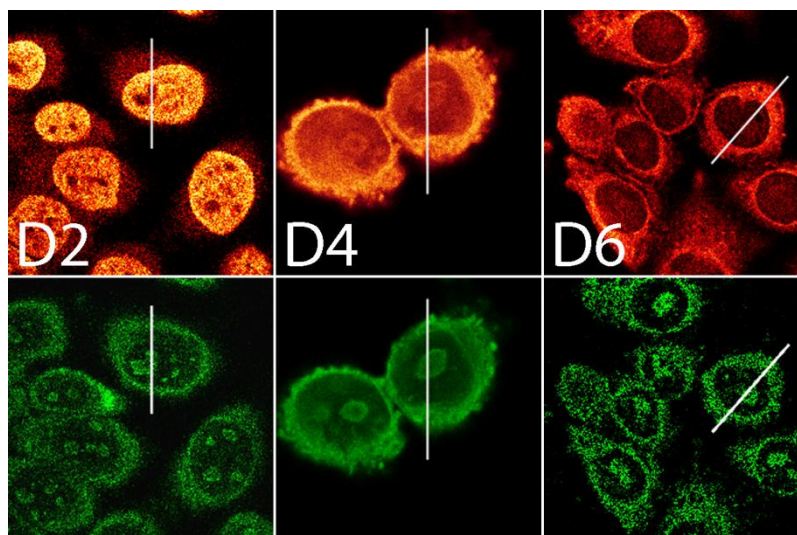


**Figure 6.5.** CLSM images of methanol fixed CHO-K1 cells costained with complex (10  $\mu\text{M}$ , red) and the RNA probe SYTO RNaselect (1  $\mu\text{M}$ , green).

### 6.1.2 Two Different Ways of Cell Internalization

If the ruthenium complexes are added to live cells, D4 and D6 immediately stain the plasma membrane, see Figure 6.6, whereas membrane staining is hard to detect for the least lipophilic complex D2. After 24 hours incubation, the cells show uptake of D4 and D6 with a punctuate staining pattern in the cytoplasm (Figure 6.6). The ability to bind to the plasma membrane seems thus to be important for the cellular uptake of the complexes, which agrees with previous studies where increased lipophilicity of ruthenium polypyridyl complexes were enhanced the cellular uptake [47,165,166]. The punctuate staining pattern seen for D4 and D6 is commonly observed for endocytosed molecules. Other similar mono- and dinuclear complexes seem, however, to facilitate direct penetration of the membrane [167] or non-endocytotic active transport processes [47]. These complexes did, however, not show punctuate staining patterns but rather homogenous staining of the nucleus or cytoplasm.

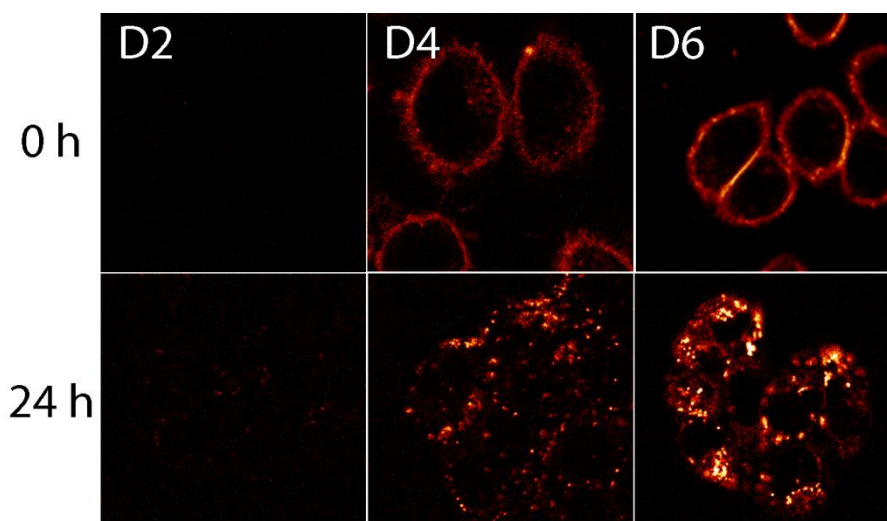


**Figure 6.6.** Live CHO-K1 cells incubated with ruthenium complexes immediately after addition (10  $\mu\text{M}$  complex) and after 24 h incubation (5  $\mu\text{M}$ ). D4 and D6 bind to the plasma membrane instantly. After longer incubation times, these complexes show a punctuate intracellular staining. D2 does not bind to the plasma membrane or internalize cells as efficiently as the more lipophilic complexes.

The membrane barrier of live cells is a hard obstacle for cellular dyes and hence is one of the main considerations in the design of dyes for intracellular targets. The staining of live cells incubated with complexes in dark generates a staining pattern that can be valuable for some studies but it does not show the intracellular localization of membranes or nucleic acids as for the fixed cells. Interestingly, internalization of the more lipophilic complexes was also found to occur upon laser illumination. For instance, the complex D4 is able to transverse the cell membrane only after a few minutes of illumination and translocate from the plasma membrane to intracellular compartments, see Figure 6.7. The intensity of the complex is rapidly increased with time and the staining pattern becomes more similar to the one of the fixed cells, with the highest intensity in the cytoplasm and later on also in the nucleolus. It was also clear that only cells exposed to laser illumination were able to internalize the complex but this photoactivated uptake seems also to perturb the membrane integrity. Similar complexes have also been shown to translocate upon exposure to laser illumination [168]. The mechanism for this has been proposed to be dependent on membrane damage due to development of singlet oxygen species. This hypothesis needs further confirmation.

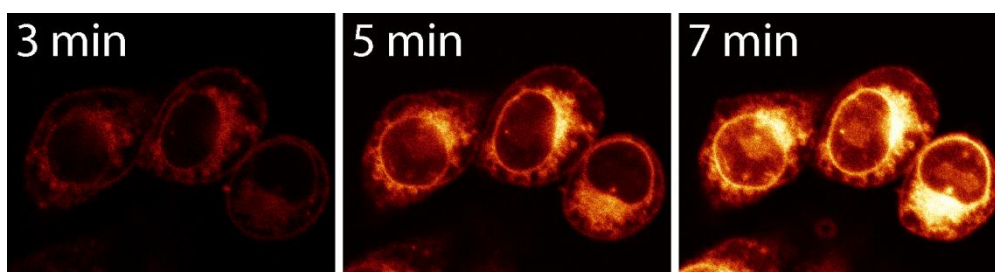


**Figure 6.7.** Photoactivated cellular uptake of D4 ( $10 \mu\text{M}$ ) in CHO-K1 cells and cellular distribution upon illumination for 3, 5, and 7 min.

Ruthenium dppz complexes were thus found to enter cells by presumably endocytotic mechanisms but have also the ability to transverse the membrane by photoactivated uptake. Could the laser illumination also cause endosomal escape? We incubated cells with ruthenium complexes for 24 hours and investigated if the laser illumination affected the staining pattern. The initial punctuate staining did, after a few minutes, decrease in intensity and the staining began to spread out in the cytoplasm indicating that the complex indeed is able to escape the endosomal entrapment (Figure 6.8). The cells did, however, change their morphology indicating that cell death presumably accompanies this treatment.

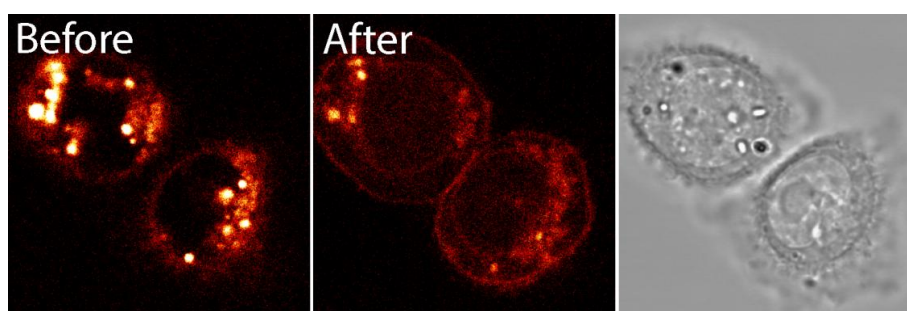


**Figure 6.8.** Emission from D6 ( $5 \mu\text{M}$ ) in CHO-K1 cells incubated at  $37^\circ\text{C}$  for 24 h before and after 10 min of laser illumination and the corresponding transmission image. The complex is entrapped intracellularly in vesicles and upon the illumination D6 is released from the vesicles and spread out in the cytoplasm.

### 6.1.3 Enantioselective Binding Preferences

It is known that some complexes show enantioselectivity when binding to nucleic acids [24,30,31,40,41] and that the emission quantum yield of DNA bound complex can differ between the two enantiomers [27]. A study in our lab showed that the cellular localization and uptake can also be affected by the stereochemistry. The enantiomer  $\Delta$ D4 intensely stains the nucleus whereas  $\Lambda$ D4 shows highest intensities in the cytoplasm and the nucleolus in fixed cells [169]. This was explained by a difference in emission quantum yield, since DNA bound  $\Delta$ D4 has about 9 times higher quantum yield compared to that of  $\Lambda$ D4 whereas in lipid membranes and BSA the quantum yield is about the same for the two enantiomers. Recently, we performed an *in vitro* study of the enantiomers of D4 and the somewhat less lipophilic complex D3 (Figure 6.9) where the binding preference of the complexes for LUVs (20% negatively charged lipids) and DNA was compared as in *Paper I*. We concluded that the  $\Delta$  complexes clearly favored DNA binding whereas  $\Lambda$ -complexes, especially  $\Lambda$ D4, seemed to favor the LUV environment. The difference in staining pattern of the complexes seems thus to be a combination of the difference in emission quantum yield and relative affinity of the two enantiomers. The difference in affinity might be due to that the geometry of the propeller for the  $\Delta$ -complexes might be better suited for interaction with right handed DNA compared to the other enantiomer. The staining pattern of the D3 complexes in fixed cells (Figure 6.10) is very similar to the corresponding D4 complex. Furthermore, also the parent complex  $[\text{Ru}(\text{phen})_2\text{dppz}]^{2+}$  shows different staining of the fixed cells with the  $\Delta$ dppz-complex only staining the nucleus whereas the  $\Lambda$ -complex additionally also shows weaker cytoplasm staining. The highest intensities for this complex are, however, found in the nucleus and nucleolus, see Figure 6.10. The study was further extended with two enantiomers of a bipyridine complex with two dppz derivate ligands, T3 (Figure 6.9), and for this highly lipophilic complex both enantiomers show high membrane preference *in vitro* and stain the cytoplasm of fixed cells. The  $\Delta$ -complex seems, however, also to localize in the nucleolus. These new unpublished results show that the ability of ruthenium complexes to stain fixed cells can, in addition to variation of the lipophilicity, also be tuned by their stereochemistry.

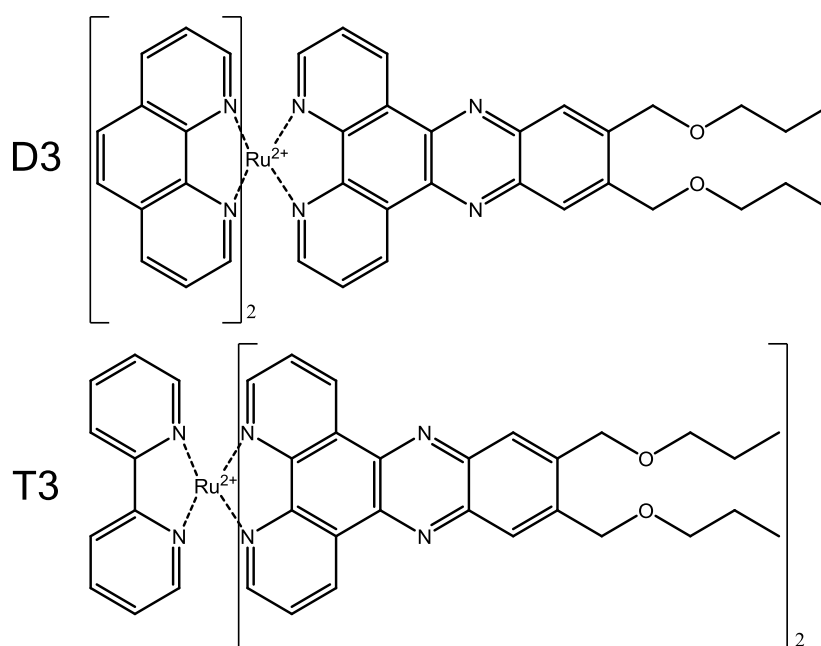


**Figure 6.9.** The structure of the complexes D3 and T3. The enantiomers of the complexes were used in binding preference and cellular localization studies (unpublished data).

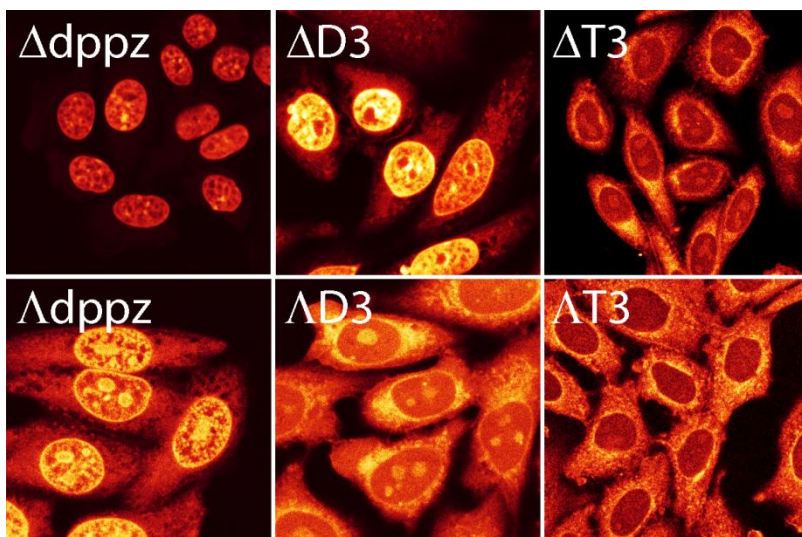


**Figure 6.10.** CLSM images of methanol fixed CHO-K1 cells stained with the enantiomers of the ruthenium complexes D3 and T3 and the parent  $[Ru(phen)_2dppz]^{2+}$  ( $10 \mu M$ ). The PMT gain is adjusted for each image and therefore the intensities should not be compared between the images.

In summary, the binding preferences and cellular localization are highly affected by the lipophilicity of the complexes, with higher relative affinity for membranes for the more lipophilic complexes. In addition, the stereoisomers of the complexes show distinctly different cellular localization since the  $\Delta$ -enantiomers prefer DNA over membrane binding whereas the opposite is true for the  $\Lambda$ -enantiomers. Although the complexes can be used as probes for the different sites in fixed cells, their cellular uptake is highly restricted by the plasma membrane. Interestingly, the more lipophilic complexes show two different ways of internalizing cells. Incubation in dark resulted in a punctuate staining pattern that indicate endocytotic uptake mechanism and further internalization also can occur by photoactivated uptake.

## 6.2 Membrane Interaction of Voltage-Sensitive Dyes

*Although voltage-sensitive dyes have been used to probe the potential over cell membranes for decades, the mechanism behind the spectral shifts is still under debate. Electrochromic effects have for a long time been the major suggested mechanisms but more recently the possibility of solvatochromic mechanisms has been investigated. We studied three styryl dyes, di-4-ANEPPS, di-8-ANEPPS and RH421 and their membrane interactions as well as their spectral properties in different solvents in Paper III, to further examine and compare the dyes and the environmental sensitivity of their spectra.*

### 6.2.1 Dye Dimerization Can Explain Unexpected Spectral Shifts

The absorbance and fluorescence spectra of di-4-ANEPPS, di-8-ANEPPS and RH421 were measured in a series of alcohols of different polarity, ranging from methanol to decanol, as well as in water, LUVs and lamellar liquid crystals (LLC), see Figure 6.11. For all dyes the trend was the same, the absorption maximum became red-shifted and the fluorescence blue-shifted and, additionally, showed an increased intensity with decreased polarity. The polarity seems thus to be important for the spectral properties of the dyes. However, two exceptions to these trends were found. Firstly, the decanol and membrane model absorptions for all dyes are blue-shifted compared to methanol and, secondly, the fluorescence in water for di-8-ANEPPS is blue-shifted compared to methanol. The unexpected blue-shift in membrane environment has been observed before for a similar dye and was then explained by

differential solvation of the chromophore[63]. We were, however, interested in further investigating this observation. The membrane environment provides a decreased polarity but also an increased viscosity compared to the extracellular fluid. The spectral properties of the dyes were further studied in samples with different glycerol content. Generally the absorption of the dyes red-shifted and the fluorescence blue-shifted and increased in intensity with increased glycerol content but the emission wavelength of di-8-ANEPPS did not follow this trend. Samples with different glycerol content differ not only in viscosity but also in polarity and therefore the effect of temperature variation was also investigated. The viscosity of water is decreased with the temperature whereas the polarity does only slightly vary. The trends are opposite to the experiment with increased glycerol content with blue-shifted absorption and red-shifted and decreased intensity of the fluorescence. Again, the dye di-8-ANEPPS is not following the trend. The viscosity does indeed change the spectral properties of the dyes but the wavelength shifts due to increased viscosity are reinforcing the red-shifts obtained by decreased polarity and cannot explain the unexpected blue-shift of the absorption found for the dyes in decanol and membrane models.

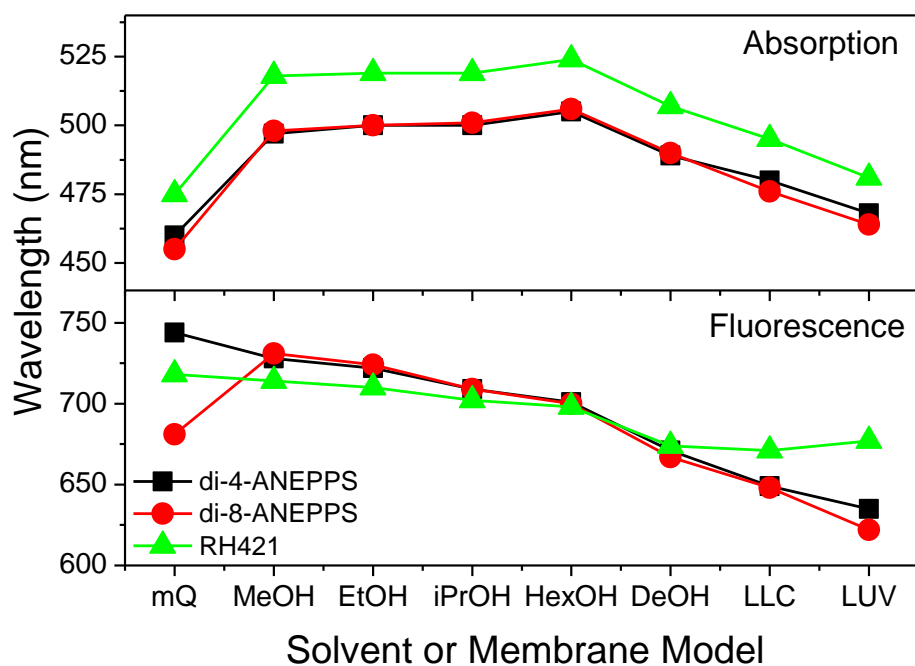


**Figure 6.11.** Wavelengths of absorption and emission maximum for di-4-ANEPPS, di-8-ANEPPS and RH421 in different solvents or membrane environment. Generally, the emission wavelength shows a blue-shift with the decreased polarity whereas the absorption red-shifts. The absorption wavelengths of the dyes in DeOH, octanoate-decanol lamellar liquid crystals (LLC) and DOPC/DOPG (4:1) LUVs are, however, blue-shifted compared to the other alcohols.

In the search for an explanation to the unexpected blue-shifted absorption of the dyes in membrane environments, theoretical calculations were performed. These calculations showed that the chromophore of ANEPPS dyes in apolar environments such as decanol and heptane would in monomeric form give an absorption maximum at longer wavelengths compared to the one in ethanol. Dye dimers, however, could explain the blue-shifts since both a parallel (p) and an anti-parallel dimer (ap) were found to have blue-shifted absorption maximums in decanol and heptane relative to ethanol, see Table 6.2. The membrane interaction of an anti-parallel ANEPPS dimer is schematically illustrated in Figure 6.12.

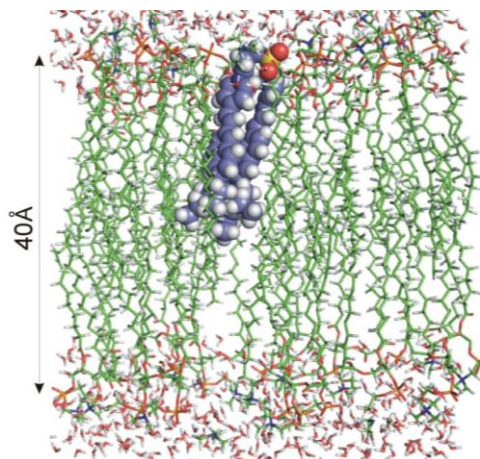


**Table 6.2.** Calculated wavelength shifts of the ANEPPS chromophore in nm with respect to ethanol environment.

	mono	ap dimer	p dimer	exp
DeOH	+10	-19	-37	-11
Heptane	+21	-11	-44	
Water	-3	-25	-38	-41
LLC				-20
LUV				-32

The abbreviations are *mono* – monomer, *ap* – antiparallel, *p* – parallel, *exp* – experimental, LC – liquid crystal

**Figure 6.12.** Estimated binding of an antiparallel ANEPPS dimer to the lipid bilayer of LUVs and calculated wavelength shifts compared to the experimentally obtained for the ANEPPS chromophore.

### 6.2.2 Membrane Binding Kinetics Differ Between Dyes but Binding Geometry is Similar

The trends seen for the variations of the spectral properties were very clear for di-4-ANEPPS and RH421 whereas di-8-ANEPPS was found to break the pattern, especially in water environment. Therefore the dye was investigated in a series of buffer solutions with different content of ethanol. Decreased ethanol content was shown to correlate with increased light scattering, indicating the presence of dye aggregates in solution. All dyes are likely to form dimers or small aggregates in water, and also in lipid membranes as concluded from the theoretical calculations but di-8-ANEPPS seems to form even larger aggregates in aqueous solution. It is not surprising that the dye is more prone to aggregate since it is more hydrophobic compared to di-4-ANEPPS and the deviations of the spectral properties trends can be because of this effect. Further, aggregation could also explain the fact that binding to LUVs was very much slower for di-8-ANEPPS compared to the other two dyes. This was seen in an experiment where the increase in fluorescence intensity, as a consequence of membrane binding, was monitored with time, see Figure 6.13. The dyes di-4-ANEPPS and RH421 showed a rapid increase in fluorescence intensity and hence bind almost instantly whereas the process was very slow for di-8-ANEPPS. The binding kinetics can, however, be enhanced by the presence of pluronic F127 which is a polymer that probably increases the solubility of the dye in buffer solution.

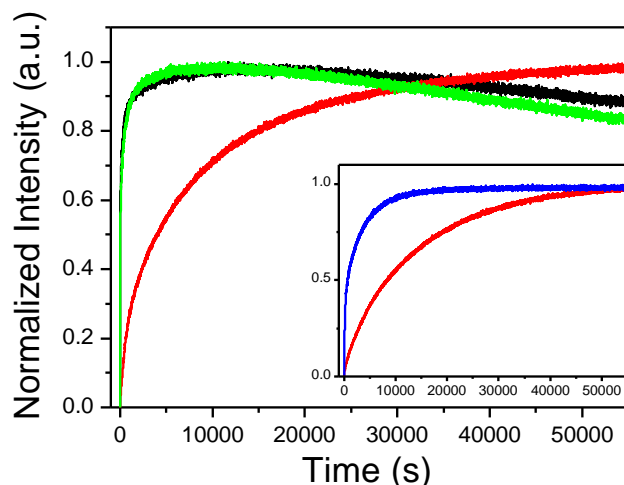


**Figure 6.13.** Emission intensity variation with time for di-4-ANEPPS (black), di-8-ANEPPS (red), and RH421 (green) ( $1 \mu\text{M}$ ) after addition of DOPC/DOPG (4:1) LUVs ( $600 \mu\text{M}$ ). The binding kinetics is much slower for di-8-ANEPPS than for the other two probes. The inset compares the binding kinetics of di-8-ANEPPS with (blue) and without (red) pluronic F127.

The binding geometry of the styryl dyes in lipid membranes has been debated. Probe orientations varying from perfectly aligned to angles of  $63^\circ$  with respect to the membrane normal have been reported. We used LD to study the orientation of the dyes when bound to LUVs (DOPC:DOPG ratio of 4:1) and octanoate-decanol-water lamellar liquid crystals. From the LD spectra, see Figure 6.14, it was concluded that the orientation of the dyes is preferentially parallel with the membrane normal and not with the membrane surface since a negative LD signal was achieved. By normalizing LD with respect to the absorption spectra the  $LD_r$  was obtained and the binding angles of the dyes were calculated using an orientation factor ( $S$ ) estimated from experiments with retinoic acid as a reference for the orientation of the membrane normal (assuming binding angle of  $0^\circ$ ). The binding angles are presented in Table 6.3 (note that this is the angle of the transition dipole moment that is polarized nearly parallel with the long axis of the molecule).

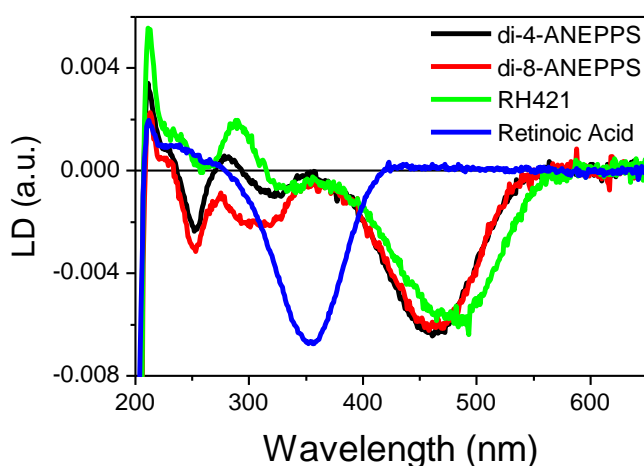


**Table 6.3.** Apparent binding angles of the dyes in LUVs.

Dye	$\alpha_{\text{app}}$
di-4-ANEPPS	$14^\circ (\pm 4^\circ)$
di-8-ANEPPS	$18^\circ (\pm 4^\circ)$
RH421	$21^\circ (\pm 4^\circ)$

**Figure 6.14.** LD spectra for di-4-ANEPPS, di-8-ANEPPS, RH421 ( $3 \mu\text{M}$ ), and retinoic acid ( $4 \mu\text{M}$ ) when bound to DOPC/DOPG (4:1) LUVs ( $1.25 \text{ mM}$ ) and the calculated apparent binding angles of the transition dipole moment of the dyes.

In conclusion, the three voltage-sensitive styryl dyes were found to have spectral properties sensitive to their microenvironment and all seem to dimerize in aqueous solution and lipid membranes. The binding kinetics to lipid membranes are fast for di-4-ANEPPS and RH421 whereas di-8-ANEPPS show very slow binding, an effect presumably due to formation of even larger aggregates in water solution. Lastly, the binding geometry was studied by LD and apparent binding angles of about 14-21° were obtained.

### 6.3 Amino Acid Sequence Affects the Cellular Uptake of Cell-Penetrating Peptides

*CPPs have been proposed as drug delivery vectors since they are able to transverse the cell membrane and simultaneously bring a cargo into the cell. Among this diverse category of peptides, arginine rich peptides have gained certain interest because they show especially efficient cell internalization. In Paper IV, we investigate the cellular uptake and lipid membrane interaction of a series of arginine- and tryptophan-rich peptides in order to systematically examine the effect of the number of tryptophans and their location in the sequence to obtain further insights in the sequence-cellular uptake relationship of CPPs.*

The sequences of the peptides used in this study are presented in Table 6.4. All of them contain eight arginines and one to four tryptophans, which are placed either in the N-terminus, in the middle of the sequence, or scattered throughout the sequence.

**Table 6.4.** *The sequences of the examined CPPs*

Peptide	Sequence
WR <sub>8</sub>	WRRRRRRRR
W <sub>2</sub> R <sub>8</sub>	WWRRRRRRRR
W <sub>3</sub> R <sub>8</sub>	W WWRRRRRRRR
W <sub>4</sub> R <sub>8</sub>	WW WWRRRRRRRR
RWR	RRRRWWWRRRR
RW <sub>mix</sub>	RWRRWRRWRRWR

#### 6.3.1 Sequence Dependence of Cellular Uptake Efficiency and Internalization Mechanism

The cellular uptake of the peptides is highly dependent on the number of tryptophans and the exact amino acid sequence. Generally, peptides with a low number of tryptophans did not internalize cells as efficiently as the peptides with higher number of tryptophan residues, see Figure 6.15. RW<sub>mix</sub>, with the scattered sequence, showed the highest cellular uptake followed by RWR whereas the peptides with N-terminal tryptophans did not have as efficient cellular uptake. Interestingly, the peptide W<sub>4</sub>R<sub>8</sub> showed a lower uptake than W<sub>3</sub>R<sub>8</sub>. Furthermore, W<sub>4</sub>R<sub>8</sub> was also the peptide that diverges from the low toxicity displayed by the others with somewhat higher levels of necrotic and apoptotic cells. The low uptake could in fact be a result of the higher toxicity if higher uptake results in cell death since dead cells were excluded from the analysis. Another explanation is that the primary amphipathicity of the peptide could disturb the endocytosis process by adherence of endosomes to the cell membrane or endosome aggregation.

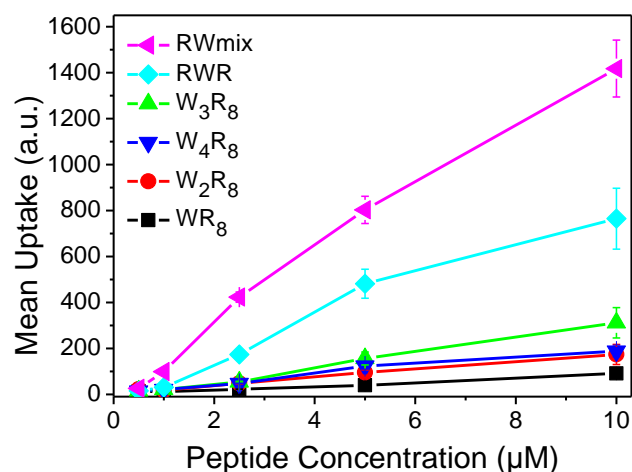


**Figure 6.15.** Cellular uptake of 5-FAM-labeled peptides in live CHO-K1 cells after incubation for 1 h at 37 °C. The uptake is measured as the mean cellular fluorescence from flow cytometry measurements of all live cells positive for the fluorophore. The background level (mean cellular fluorescence for untreated cells) is 10–15 a.u., and hence the uptake at concentrations of 0.5 and 1 µM are hard to detect. Error bars are standard errors of the mean ( $n = 6$ ).

To further investigate the cellular uptake we performed CLSM imaging of live cells incubated with peptides during 1 hour, see Figure 6.16. The peptides WR<sub>8</sub>, W<sub>3</sub>R<sub>8</sub>, W<sub>4</sub>R<sub>8</sub>, and RWmix show punctuate staining intracellularly, which usually is seen for molecules that internalize cells by endocytotic pathways. In addition to this punctuate staining, W<sub>3</sub>R<sub>8</sub>, W<sub>3</sub>R<sub>8</sub>, and RWmix stain the cells in a more diffuse and homogenous manner. This staining pattern indicates that the peptides, in parallel to endocytosis, facilitate cellular uptake via direct penetration mechanisms. W<sub>3</sub>R<sub>8</sub> and RWR are diffusely staining the cells and interestingly, the cell nucleus shows somewhat higher intensity. Since endocytosis is highly reduced when the cells are subjected to lower incubation temperatures, the cellular uptake of the peptides in cells incubated at 4°C during 1 hour was also examined. All peptides stain the cells diffusely and the punctuate staining is highly reduced, this is true even for the peptide WR<sub>8</sub> which at 37°C only showed punctuate staining. The peptide W<sub>4</sub>R<sub>8</sub> shows, however, very weak diffuse staining intracellularly and for some cells only plasma membrane interaction at 4°C which indicate that endocytotic pathways seem to be its main route of entry. The other peptides were concluded to internalize via direct translocation since they showed a significant diffuse staining at low incubation temperature, which is common for arginine-rich peptides [83,85], but WR<sub>8</sub>, W<sub>3</sub>R<sub>8</sub>, W<sub>4</sub>R<sub>8</sub>, and RWmix might use endocytosis in parallel. RWmix colocalize with the commercial dye Lysotracker red, indicating that the peptide is internalized by endocytosis and transported to the lysosome compartments whereas this was not seen for the other peptides. Since the uptake is different between W<sub>4</sub>R<sub>8</sub>, RWR, and RWmix, the uptake mechanism seems thus to depend on the peptide sequence and not on the number of positive charges, a conclusion which agrees with a study of the internalization mechanism of other well-studied peptides [88].

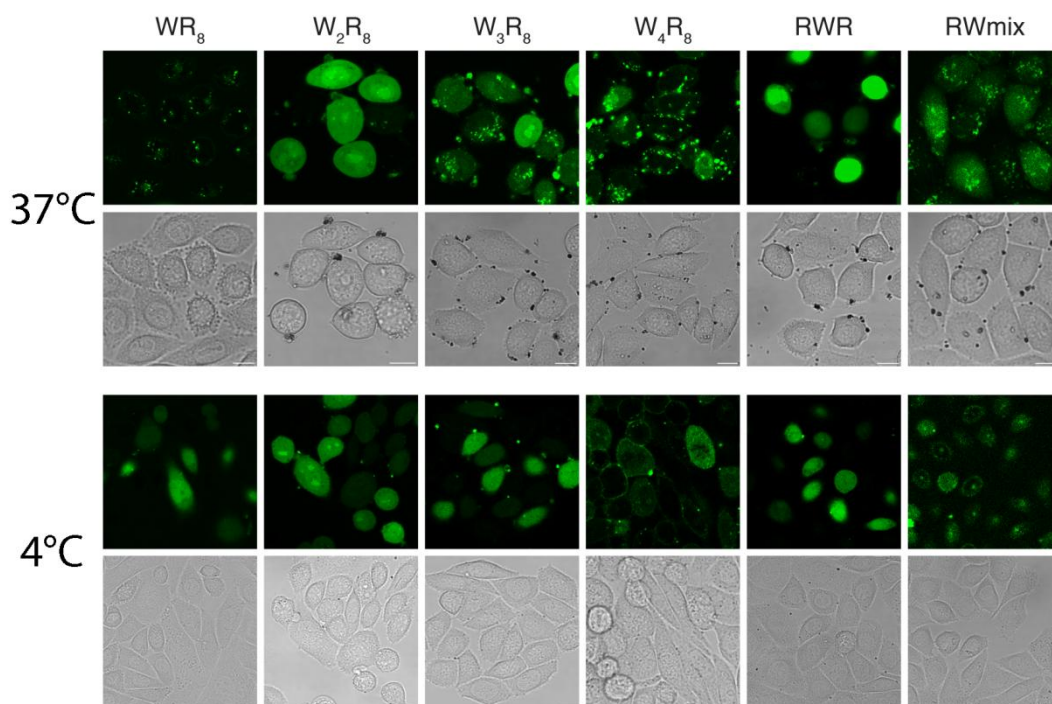


**Figure 6.16.** Confocal imaging of live CHO-K1 cells incubated with 5-FAM-labeled peptides (5  $\mu$ M) during 1 h at 37°C or 4°C and the corresponding transmission images. The laser intensity and PMT gain have been adjusted for each image and the intensities are thus not directly comparable.

### 6.3.2 Membrane Affinity is Similar for All Peptides

There is thus a difference in both the quantity and the route of internalization for the six peptides. In the search for an explanation to this effect we investigated the affinity to lipid membranes by monitoring the variations of the tryptophan fluorescence upon LUV titrations (note that 5% pegylated lipids were used since the peptides, especially  $W_4R_8$ , seemed to induce LUV aggregation). Using the pseudoinverse command (pinv) in MATLAB and spectra of peptide free in solution and presumably bound to membranes, the fraction of bound peptide was estimated for each titration step, see Figure 6.17. A simple one-site binding model, assuming that the liposomes have binding sites consisting of  $n$  lipids, was used to estimate the binding constants of the peptides (Table 6.5). The binding curves for  $WR_8$  and  $W_2R_8$  were not sufficiently saturated and it was therefore not possible to estimate their binding constants. For the other peptides, the binding constants were found to be very similar and the difference in uptake of the peptides can, hence, not be attributed to differences in lipid membrane affinities. Using a helical-wheel projection, RWmix was predicted to be able to form an  $\alpha$ -helical structure because of the suitable spacing between the tryptophan residues and, more recently, Rydberg et al showed that RWmix is indeed adopting  $\alpha$ -helical conformation when interacting with LUVs whereas the other peptides do not [170]. This conformation could be the reason for its much higher cellular uptake.

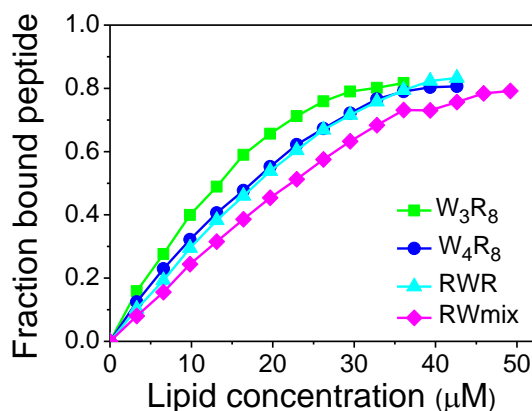


**Table 6.5.** Apparent binding constant to LUVs and number of lipids per peptide for the CPPs.

Peptide	$K_{app}$ ( $\times 10^6$ M <sup>-1</sup> )	n
W <sub>3</sub> R <sub>8</sub>	10	19
W <sub>4</sub> R <sub>8</sub>	5	16
RWR	8	14
RWmix	13	24

**Figure 6.17.** Binding curves for the association of RWR, W<sub>4</sub>R<sub>8</sub>, W<sub>3</sub>R<sub>8</sub>, and RWmix with POPC/POPG/DSPE-MPEG (16:3:1) liposomes and their apparent binding constants.

To summarize, the number of tryptophans and their position in the sequence influence the cellular uptake of the peptides. The efficiency of internalization was increased by higher number of tryptophans and a scattered amino acid sequence, even though the affinity to lipid membranes was similar for all peptides. The mechanism of uptake was mainly direct penetration but some of the peptides also seem to use endocytotic pathways in parallel.

## 6.4 Proteoglycans Enhance the Cellular Uptake of the Antisecretory Peptide AF-16

The antisecretory and anti-inflammatory peptide AF-16 has remarkable properties making it promising as a peptide-based drug against diseases such as diarrhea. Although the physiological effects of the peptide have been extensively studied, the mechanisms behind its activities are, however, still not known and additionally little is known about its interactions at molecular and cellular level. In Paper V we investigate the interaction with cells of the peptide, with particular interest in membrane-associated proteoglycans, in order to examine its cellular uptake.

The cellular uptake of AF-16 was investigated by CLSM using a fluorescently labeled peptide (Figure 6.18). After one hour of incubation the peptide was found intracellularly with a punctuate staining pattern in the cytoplasm. This pattern is often seen for endocytosed molecules when they are entrapped in the endosomes and since endocytotic pathways are reduced when cells are stressed for instance by lowering the incubation temperature, a similar experiment was performed at 4°C. A highly reduced uptake was observed as a consequence of the lower incubation temperature and hence endocytotic pathways are probable involved in the cellular uptake of AF-16. In comparison to the arginine- and tryptophan rich peptides in Paper IV, the decrease in uptake is striking.

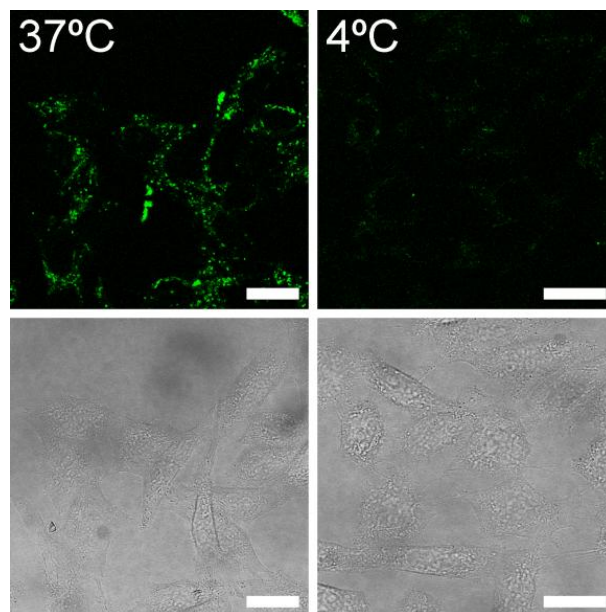


**Figure 6.18.** CLSM pictures of live CHO-K1 cells incubated with Alexa Fluor 488-labeled AF-16 (10  $\mu$ M) during 1 h at 37°C and 4°C (top panel) and the corresponding transmission images (bottom panel). The uptake is highly reduced when the temperature is decreased indicating cellular uptake by endocytosis.

#### 6.4.1 Electrostatic Interaction of AF-16 and Heparin

In *Paper IV*, we used the tryptophan fluorescence to probe the affinity of CPPs to LUVs. For AF-16 this is not possible without modification of the peptide sequence and hence we used ITC to study the interaction of the peptide with membrane components. Initial studies with zwitterionic DOPC LUVs showed poor affinity (see below), therefore the binding of AF-16 to proteoglycans was addressed. ITC experiments with AF-16 and heparin was performed and at pH 5 and 10 mM NaCl exothermic peaks were obtained when peptide is titrated into a heparin solution. By fitting a one-site model to the binding curve a binding constant of about  $10^5$   $M^{-1}$  was obtained (Figure 6.19A). The stoichiometry constant  $n$  estimates that one peptide is bound per four heparin units ( $n$  is the estimated ratio peptide:heparin at equilibrium), which means that the system has not reached charge saturation at equilibrium. The binding curve obtained by a similar titration at pH 7.4 had a smaller magnitude of the slope, indicating a lower binding constant (Figure 6.19B). The one-site model generates a rather poor fitting to this curve but a rough estimation is that the binding constant is about 60 times lower ( $\sim 1.5 \cdot 10^3$   $M^{-1}$ ) than at pH 5. This is reasonable since the net charge of the peptide is +1 at pH 7.4 whereas it is +2 at pH 5 and the heparin molecule is highly negatively charged.

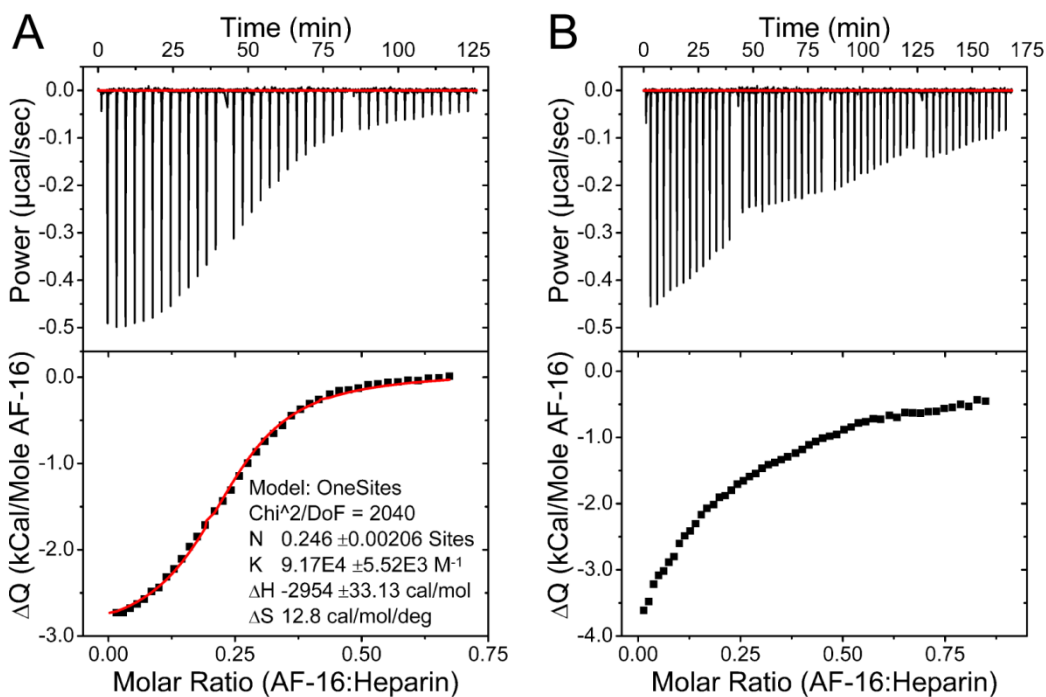


**Figure 6.19.** ITC measurements of (A) AF-16 (0.5 mM) to heparin (0.55 mM) at pH 5 (buffer: 10 mM citrate-phosphate/10 mM NaCl) and (B) AF-16 (0.4 mM) to heparin (0.5 mM) at pH 7.4 (buffer: 10 mM Na-phosphate/10 mM NaCl). Top panels represent the power recorded during the titration and bottom panels the integrated heats per mole peptide obtained by integration of the peaks in the power plot.

Titration of peptide to heparin at higher ionic strength was also performed. The binding curves for experiments performed at pH 5 in buffer containing 10 mM, 50 mM and 150 mM NaCl are compared in Figure 6.20A. The magnitude of the released heat is clearly decreased in buffers with higher salt concentrations, indicating that less peptide is binding and hence the affinity is decreased. This is expected for an electrostatic interaction since at high ionic strength the NaCl is screening the charges of the peptide and heparin. Moreover, the nature of the binding can be further characterized by performing the same titration at different temperatures. Generally a hydrophobic effect of the binding would generate a negative change in heat capacity [98] which means that the binding enthalpy is decreasing with the temperature. In contrast, electrostatic contributions to the binding heat capacity are either very small [171] or, for systems where charge neutralization is reached, have a positive sign [172]. For the interaction between AF-16 and heparin the binding enthalpy was indeed not affected by variation of the temperature (in the internal 15-37°C, Figure 6.20B). The binding of AF-16 to heparin was therefore concluded to have a mainly electrostatic nature since it is affected by pH and ionic strength but not by temperature variation.

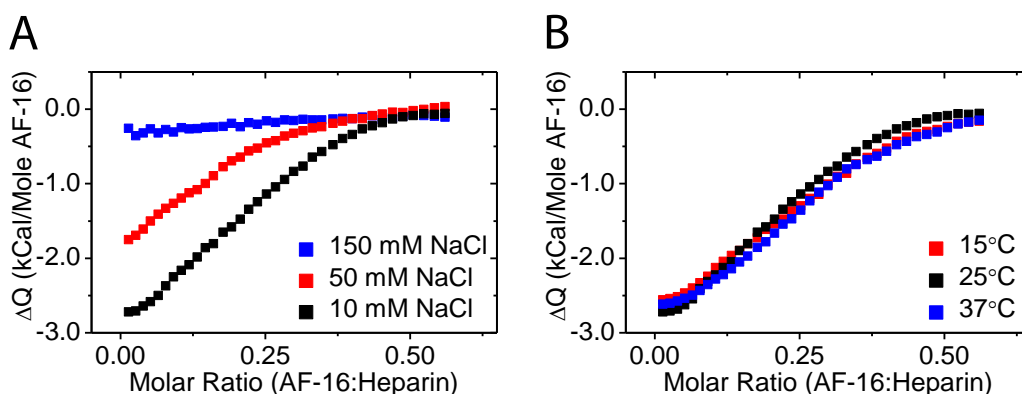


**Figure 6.20.** ITC measurements of AF-16 (0.5 mM) to heparin (0.55 mM) (A) in buffer with different NaCl concentrations (10 mM citrate-phosphate, pH 5) and (B) at different temperatures (buffer: 10 mM citrate-phosphate/10 mM NaCl, pH 5).

Many peptides change conformation upon binding with LUVs or GAGs which can be an important step in their cellular uptake. CD experiments of AF-16 in buffer solution show that the peptide has a major random coil structure with a small fraction of  $\alpha$ -helix and that this conformation does not change upon addition of heparin. Molecular modeling confirmed the result and the small  $\alpha$ -helical region was predicted to be close to the N-terminus, see Figure 6.21. This is further in accordance with a prediction of the AF protein, in which the AF-16 sequence is found in the end of a helical structure and extends into a turn. The modeling showed also that it is possible for all cationic residues to simultaneously interact with a heparin molecule and that the negatively charged glutamic acid seems to interact with the arginine residue.

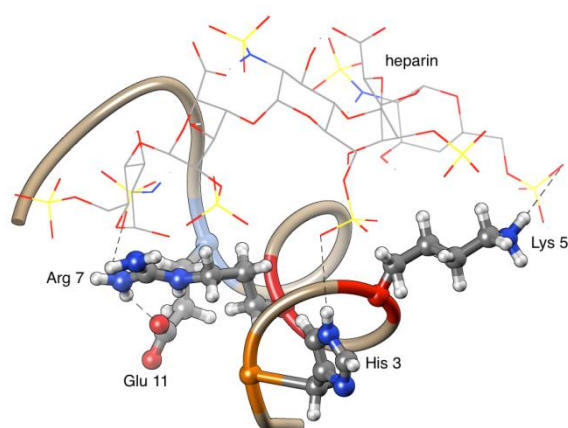


**Figure 6.21.** Predicted AF-16 secondary structure by molecular dynamics simulation. The peptide is able to interact with the negatively charged groups of heparin with its positively charged lysine and arginine in physiological pH and, additionally, with its histidine residue at pH 5. For simplicity only the peptide backbone and charged side chains as well as 2.5 disaccharide units of heparin are shown.

#### 6.4.2 Binding to Proteoglycans Enhances Cellular Uptake

Does the potential interaction with proteoglycans affect the cellular uptake? We compared the uptake in wild type (CHO-K1) and proteoglycan deficient (A745) cells and the results showed a reduced uptake in the cells without cell-surface proteoglycans. Both cell types display a linear dependence of the uptake with time (incubation times 15 min – 6 h, see Figure 6.22A) and external peptide concentration (1-10  $\mu$ M, see Figure 6.22B). Some CPPs

show a rapid cellular uptake with saturation within 1 hour [89,97] and some peptides change mechanism of internalization depending on the extracellular concentration [81,87,89,97,99]. AF-16, however, does not show this saturation of the cellular uptake and seems to only facilitate endocytotic internalization based on CLSM experiments at different concentrations and times. The uptake in the mutant A745 cells is, however, also likely to be via endocytosis as indicated by the punctuate staining intracellularly that is reduced at low incubation temperatures (not shown). The cellular uptake is therefore either a result of several different endocytotic mechanisms in parallel or dependent on one mechanism which is enhanced by cell-surface proteoglycans. Many cationic peptides bind and cluster proteoglycans as part of their internalization [97–99], especially direct penetration appears to be promoted by the clustering, whereas CPPs that bind proteoglycans without clustering generally show endocytotic uptake [99]. AF-16 is likely using endocytosis and does not show any clustering of heparin molecules which agrees well with the low binding constant to heparin and the fact that charge neutralization is not obtained. That the affinity for heparin is increased with lower pH and ionic strength is interesting from a physiological point of view since these factors are disturbed during antisecretory and anti-inflammatory diseases and hence the cellular uptake of the peptide during these conditions could be enhanced. High membrane binding affinity and high cellular uptake have, however, been shown to not always correlate for some CPPs [88,97,173,174].

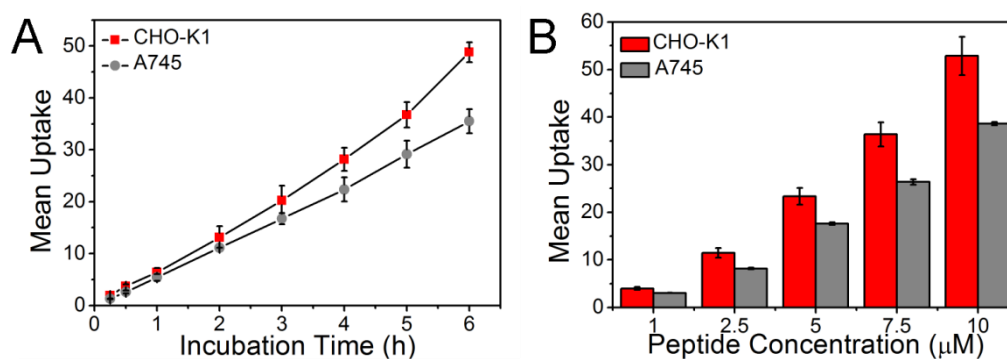


**Figure 6.22.** Cellular uptake of AF-16 (Alexa Fluor 488-labeled) in live wild type CHO-K1 and proteoglycan deficient A745 cells (A) as function of incubation time at a concentration of 10  $\mu\text{M}$  (the lines are added as a guide for the eye) and (B) as a function of concentration after 6 h incubation at 37°C. The uptake is measured as mean fluorescence by flow cytometry and the auto-fluorescence is subtracted from the data. Error bars are standard deviation of mean ( $n=3$ ).

### 6.4.3 AF-16 Interacts with Negatively Charged Lipid Membranes

With the knowledge that AF-16 binds to heparin with a large electrostatic contribution, we were interested in knowing if the peptide also interacts with negatively charged lipid membranes. ITC experiments where DOPG LUVs were titrated to AF-16 were performed at pH 5 and 25°C, see Figure 6.23. The titrations indeed showed a change in heat significantly larger than the dilution heat as expected when interaction occurs. The change in heat for a similar experiment using DOPC LUVs is very small with very small signal-to-noise ratio and it is not really possible to detect any binding event. Interestingly, the peaks in the experiment with DOPG LUVs are initially endothermic and decrease in magnitude and in the end exothermic peaks are achieved. The power plot and binding curve are thus very different from the ones obtained for the heparin experiments. The experiment with DOPG LUVs was repeated at 15 and 37°C and the initial heat change per mole,  $\Delta Q$ , was notably different, with larger endothermic peaks at 15°C compared to at 25°C whereas the peaks at

37°C were exothermic. The apparent binding enthalpy at all temperatures are found in Table 6.6 (due to the lack of initial plateau for the experiment at 37°C, the binding enthalpy cannot accurately be determined but is instead based on  $\Delta Q$  for the initial titration). The interaction also seemed to be associated with a fast and a slow process when the interaction becomes more exothermic. The slow process could be due to liposome aggregation but since the size of the LUVs was found to be approximately the same before and after titration with dynamic light-scattering, this can be ruled out.

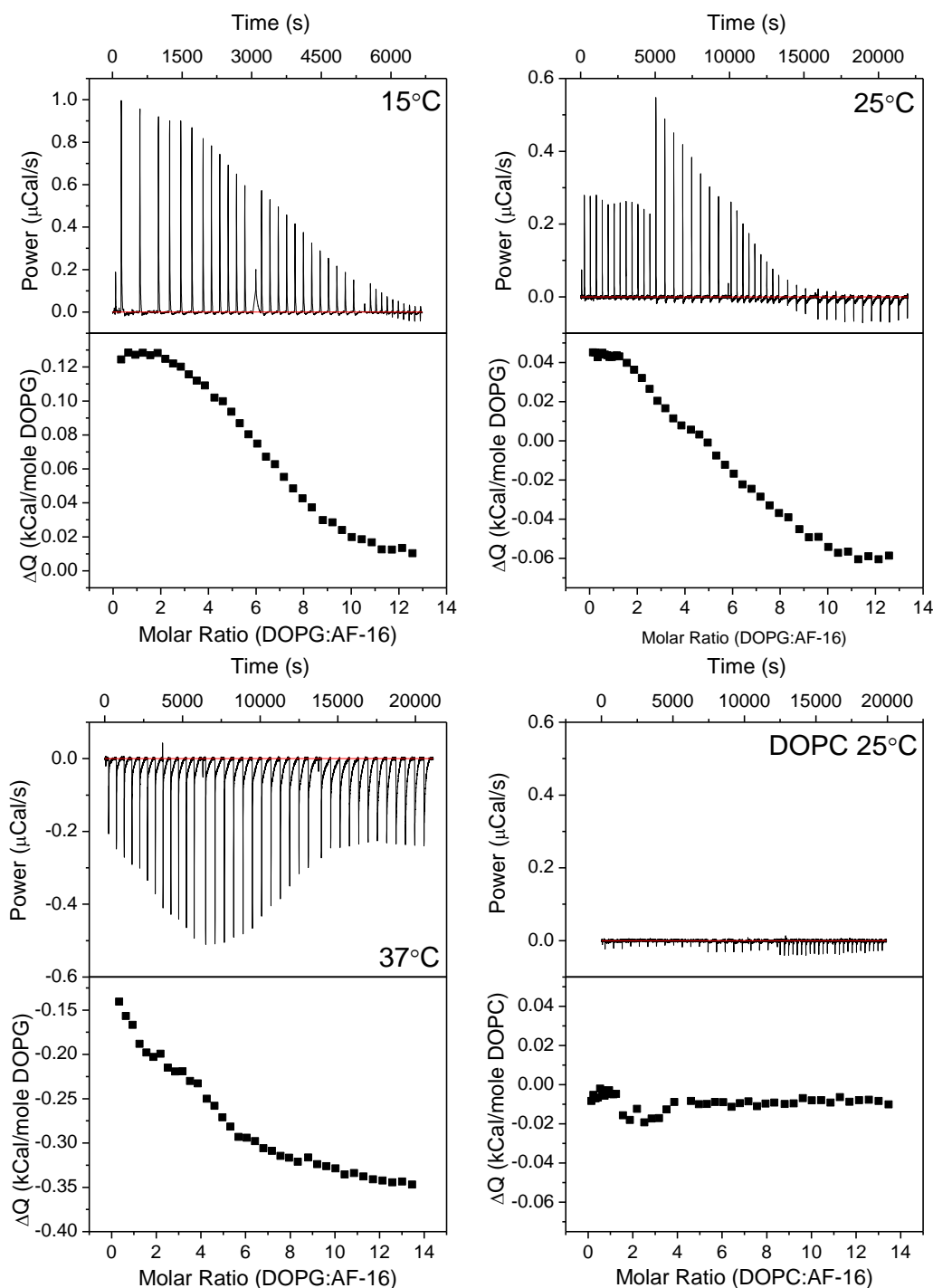


**Figure 6.23.** ITC measurement of AF-16 (1 mM) titrated with DOPG LUVs (20 mM) at 15, 25 and 37°C. The buffer used was 10 mM citrate-phosphate/10 mM NaCl, pH 5. To gain the initial plateau for the 25°C experiment the initial injections are smaller, this was also done in the 37°C experiment but without success. An identical experiment with DOPC LUVs at 25°C is also included for comparison.

By plotting the binding enthalpy versus the temperature and fitting the data with a linear function, the change in heat capacity can be estimated from the slope. The change in heat capacity upon binding to LUVs is a result of dehydration of the membrane. Negative binding heat capacity is due to loss of water from the hydrophobic regions whereas water release from hydrophilic areas generates a positive sign of the heat capacity change. The binding heat capacity was found to be  $-12.1 \text{ calmol}^{-1}\text{K}^{-1}$  ( $-50.6 \text{ Jmol}^{-1}\text{K}^{-1}$ ), see Figure 6.24, but is probably somewhat less negative since the binding enthalpy value for  $37^\circ\text{C}$  is likely overestimated. Nevertheless, the calculated value is about 20-60 times smaller compared to the well-known antibacterial peptide melittin upon binding LUVs of different lipid composition [175,176] but similar to the two arginine rich peptides RW9 (RRWWRRWRR-NH<sub>2</sub>) and RL9 (RRLRLRLRR-NH<sub>2</sub>) upon binding POPG LUVs (negatively charged) [177]. The difference in magnitude of binding heat capacity between melittin and RW9/RL9 can be explained by the fact that melittin more embedded in the hydrophobic region of the membrane [178] whereas the RW9 and RL9 peptides seem to bind more parallel to the membrane surface and mainly interact with the polar head groups. The fact that the binding heat capacity is negative shows that hydrophobic effects contribute to the interaction between AF-16 and DOPG LUVs and the small magnitude indicates that it is bound to the surface. The interaction must, however, have an electrostatic contribution since the peptide seems to not interact with DOPC LUVs. In general, the electrostatic contribution to the binding heat capacity is small in comparison to the contribution of the hydrophobic effects [171] which could be the explanation to that the binding heat capacity still has a negative sign. CD measurement of AF-16 in the presence of LUVs composed of either DOPG or DOPC also showed no conformational change compared to peptide in buffer (not shown) which is the same result as obtained in the heparin experiment. AF-16 is thus interacting both with glycosaminoglycans and negatively charged lipid bilayers which could be of interest in the research of its antiseptory and anti-inflammatory activity. The peptide might be more likely to target the sick sites in the body due to changes of the cell membrane composition associated with the diseases. For instance, cancer cells have an increased number of negatively charged lipids [179] and display changes in the glycan composition [180] compared to healthy cells. Furthermore, inflammation is also associated with a change of the cell-surface glycans as well as secretion of proteoglycans by mast cells in the extracellular space [181,182].

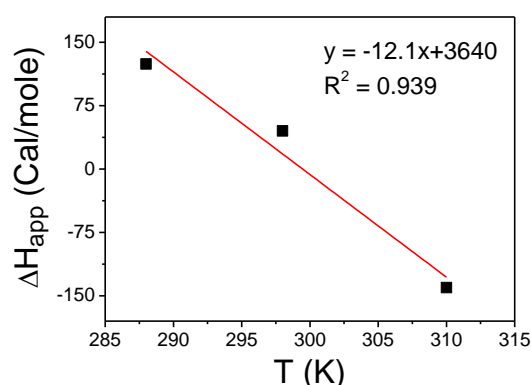


**Figure 6.24.** The apparent binding enthalpy from Figure 6.23 as a function of the temperature fitted with linear regression. The slope is the change in heat capacity upon binding.

**Table 6.6.** Apparent binding enthalpies for the different temperatures.

T (°C)	ΔH <sub>app</sub> (Cal/mole)
15	124
25	45.1
37	-140 <sup>a</sup>

<sup>a</sup>due to the lack of initial plateau the initial value of change in heat per mole was used as apparent binding enthalpy for this temperature.

In summary, the antisecretory and anti-inflammatory peptide AF-16 has been shown to enter cells by endocytosis, which is enhanced by proteoglycans. Moreover, AF-16 binds to heparin and the affinity is higher at low pH and ionic strength with a primary electrostatic contribution to the interaction. Electrostatic effects are also important in its binding to lipid membranes since interaction with negatively charged bilayers occurs whereas no binding was detected for zwitterionic bilayers. The secondary structure of the peptide is mainly random coil with a small  $\alpha$ -helical structure and it does not change upon binding to heparin or lipid membranes.

# Conclusions

---

*The work presented in this thesis has concerned two types of dyes for cell imaging, lipophilic ruthenium dppz complexes and voltage-sensitive styryl dyes, as well as arginine- and tryptophan-rich peptides for drug delivery and the antisecretory peptide AF-16. Although the examined molecules are of different character they all are intended for cellular applications and are interesting in a membrane interaction context.*

For the series of lipophilic ruthenium complexes in *Paper I* and *II*, the binding preferences and localization in fixed cells were found to be highly affected by slight structural changes. It was concluded that the relative affinity for membrane structures increased with the complex lipophilicity but is also highly affected by the enantiomeric form. Furthermore, the plasma membrane was found to restrict the cellular uptake and hence the useful staining patterns seen for fixed cells were not obtained in live cells. The more lipophilic complexes were, however, found to internalize live cells in two different ways. Firstly, by a mechanism that could be of endocytotic nature since the complexes were found in punctuate structures in the cytoplasm when cells were incubated in dark. Secondly, by a photoactivated uptake in which the complexes were able to translocate the membrane upon laser illumination. The possibility to tune the affinity of the complexes for biomolecules and biomembranes gives great opportunities for one important criteria for cellular dyes, to selectively stain a certain area of the cell. The poor internalization is, however, a problem that has to be solved if imaging of live cells is desired. The complexes used in this thesis are indeed not useful for those applications but can be used to highlight areas in fixed cells since they display beautiful and distinct staining patterns.

In *Paper III*, three voltage-sensitive dyes were found to have spectral properties highly dependent on the microenvironment. All dyes show a red-shifted absorption with decreased polarity of the solvent but with an unexpected blue-shift in membrane environments that we assigned to dimerization of the dyes. The most hydrophobic dye, di-8-ANEPPS, had a very slow binding kinetics to lipid membranes which probably is an effect of even larger aggregates. This fact might be important to consider since either long incubation times followed by sample washing or co-incubation with surfactants is needed if this dye is used. The study suggested solvatochromic effects as likely response for membrane potential variations but further studies need to be done to conclude if electrochromic effects are also involved in the voltage-sensing mechanism.

The effect of peptide sequence on the membrane affinity and cellular uptake was systematically investigated in *Paper IV* for a series of arginine- and tryptophan-rich peptides. We concluded that although the peptides displayed similar membrane affinity the uptake efficiency was remarkably different for the different peptides. Generally, the uptake seems to increase with the number of tryptophans in the peptide sequence and their position was, additionally, found to be central for the uptake efficiency. The scattered distribution of the residues results in a highly enhanced uptake compared to a coherent tryptophan position, which could be due to both the possibility for  $\alpha$ -helix formation and a favorable backbone spacing between the arginine residues. The uptake mechanism was also found to vary with the sequence but not following any general trend. Most peptides, however, appear to use direct penetration mechanisms as main internalization route which can be an advantage for drug delivery systems compared to endocytotic uptake, where the drug also expectantly needs to escape endosomal entrapment in order to reach the intracellular target.

The antisecretory and anti-inflammatory peptide, AF-16, studied in *Paper V*, was found to utilize endocytosis as cellular uptake mechanism which was enhanced by the presence of cell-surface proteoglycans. Since the affinity of the peptide to heparin was increased with decreased pH and ionic strength, the cellular uptake could be further enhanced in the secretory and inflammatory diseases, in which these factors are decreased from the physiological values. Interaction with negatively charged lipid bilayers was also established whereas no binding was found to zwitterionic lipid bilayers, which strengthen the conclusion of a major electrostatic interaction both for lipid bilayers and proteoglycans. The interaction with negatively charged lipids and proteoglycans is important since the composition of these molecules on the cell-surface is also changed in many of the conditions cured by AF therapy and they may therefore be part of peptide recruitment. The knowledge about these molecular interactions and the cellular uptake of AF-16 might be important for revealing the mechanism behind its activity and is vital for further drug development.

The results from the different studies emphasize the importance of membrane interaction studies. To design and develop cellular dyes, drug delivery vectors and peptide-based drugs it is essential to understand the molecular interactions and cellular mechanisms as well as how structural changes and external factors influence their functions. As seen for the ruthenium complexes and the voltage-sensitive dyes, small alterations of the structure can result in significant changes in the membrane binding properties. Moreover, the cellular uptake can be highly influenced by structural differences although the membrane interaction seem to be similar, as seen for the peptides studied in *Paper IV*.

Furthermore, this thesis has also highlighted that large charged and hydrophobic molecules, such as the ruthenium complexes and the arginine- and tryptophan-rich peptides, are able to transverse the membrane barrier. The peptide AF-16 is positively charged and does not have a hydrophobic character but it contains an arginine residue which is seen as a key to cellular uptake. Interestingly, ruthenium dppz complexes conjugated with an oligoarginine sequence has been shown to have enhanced cellular uptake compared to the corresponding unconjugated complex [183,184], which demonstrates that these different fields can be combined to improve cellular interaction and uptake of molecules. Cells are complex systems to study and therefore biophysical studies on molecules mimicking part of the cells are often essential for gaining insights into molecular interactions. Although it is possible to find correlations between the cellular response and molecular properties, it is not always as intuitive as expected and therefore combination of biophysical and cellular studies, or even studies on organism level, are needed to achieve a comprehensive understanding.

# Acknowledgements

---

I would like to express my gratitude to all persons that contributed directly or indirectly to this thesis, a special thanks to...

...my supervisors: **Bengt Nordén**, for your enthusiasm and for believing in me, **Sandra Rocha**, for outstanding help, all encouragement and your thoughtfulness, and **Per Lincoln**, for valuable discussions, help with MATLAB, and images of Ru-enantiomers in Figure 3.1.

...**Frida Wilhelmsson (Svensson)**, for fun times in the lab and for teaching me about ruthenium complexes, cells, lab procedures, and writing papers but also about life.

...**Nils “Nisse” Carlsson**, for wonderful days in the lab, discussions about spectral properties, light-scattering and linear dichroism.

...all other coauthors: **Anna Reymer**, **Kristina Fant**, **Hanna Rydberg**, **Helene Åmand Malmberg**, **Elin Esbjörner-Winters**, **Tamás Beke-Somfai**, and **Minna Li**, for great work, collaborations, and support.

...**Catherine Kitts**, for valuable discussions about spectral properties of dyes.

...**Stefan Lange**, **Ivar Lönnroth**, **Eva Jennische**, **Ewa Johansson**, and **Ingela Jonsson**, for the opportunity to work with the AF-16 project and fruitful discussions.

...my **bachelor students** for the synthesis of the stereoisomer of the complexes D3 and T3 and binding preference studies of them and my master student **Chun Man**, for hard work with AF-16 – the knowledge we gained was valuable to me in so many ways.

...**Maria Abrahamsson**, **Helene Åmand Malmberg**, **Johanna Andersson**, **Frida Wilhelmsson (Svensson)**, **Sandra Rocha**, and **Kristina Fant**, for your valuable advices, your support, friendship and for being great role models.

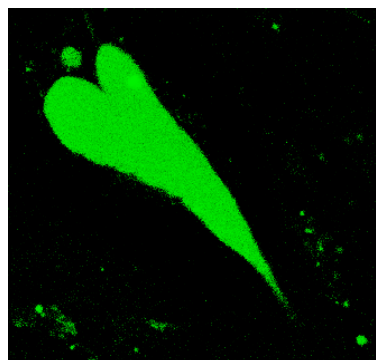
...**Lena Nyberg**, for always helping me when I was in need of an abstract proofreader and for being a great friend.

...**Sandra Rocha**, **Bengt Nordén**, **Per Lincoln**, and **Kristina Fant** for proof-reading this thesis.

...All **present and former colleagues** at physical chemistry, for help with science or lab matters and for great company.

...My **family**, for helping me overcome difficulties, supporting me in the choices I have made and always being there for me.

...my husband **Damir Džebo** for helping me with all kind of matters during my PhD studies (including the cell cartoon in Figure 2.1), for making me laugh every day, and for always being on my side in all challenges that life offers. Together we are strong. *I love you!*



*This CLSM image of cells incubated with AF-16 was one of a kind. I want to dedicate it to my husband, Damir, since it was taken shortly before our wedding.*



# List of References

---

- [1] Alberts B, Johnson A, Lewis J, Raff M, Roberts K, Walter P (2002) *Molecular Biology of the Cell*, Garland Science, Taylor and Francis Group, New York, USA.
- [2] Mathews CK, van Holde KE, Ahern KG (2000) *Biochemistry*, Addison Wesley Longman, Inc., San Francisco, USA.
- [3] Gennis RB (1989) *Biomembranes - Molecular Structure and Function*, Springer-Verlag, New York, USA.
- [4] Bloomfield VA, Crothers DM, Tinoco I (2000) *Nucleic Acids: Structures, Properties and Function*, University Science Books, Sausalito, USA.
- [5] Boisvert F-M, van Koningsbruggen S, Navascués J, Lamond AI (2007) The multifunctional nucleolus. *Nat. Rev. Mol. Cell Biol.* **8**, 574–85.
- [6] Van Meer G, Voelker DR, Feigenson GW (2008) Membrane lipids: where they are and how they behave. *Nat. Rev. Mol. Cell Biol.* **9**, 112–124.
- [7] Munro S (2003) Lipid Rafts: Elusive or Illusive? *Cell* **115**, 377–388.
- [8] Owen DM, Magenau A, Williamson D, Gaus K (2012) The lipid raft hypothesis revisited - New insights on raft composition and function from super-resolution fluorescence microscopy. *Bioessays* **34**, 739–747.
- [9] Simons K, Gerl MJ (2010) Revitalizing membrane rafts: new tools and insights. *Nat. Rev. Mol. Cell Biol.* **11**, 688–99.
- [10] Sarrazin S, Lamanna WC, Esko JD (2011) Heparan sulfate proteoglycans. *Cold Spring Harb. Perspect. Biol.* **3**, 1–33.
- [11] Walrant A, Alves ID, Sagan S (2012) Molecular partners for interaction and cell internalization of cell-penetrating peptides: how identical are they? *Nanomedicine* **7**, 133–144.
- [12] Poon GMK, Gariépy J (2007) Cell-surface proteoglycans as molecular portals for cationic peptide and polymer entry into cells. *Biochem. Soc. Trans.* **35**, 788–793.
- [13] Rabenstein DL (2002) Heparin and heparan sulfate: structure and function. *Nat. Prod. Rep.* **19**, 312–331.
- [14] Silverstein SC, Steinman RM, Cohn ZA (1977) Endocytosis. *Annu. Rev. Biochem.* **46**, 669–772.
- [15] Conner SD, Schmid SL (2003) Regulated portals of entry into the cell. *Nature* **422**, 37–44.
- [16] Doherty GJ, McMahon HT (2009) Mechanisms of endocytosis. *Annu. Rev. Biochem.* **78**, 857–902.
- [17] McMahon HT, Boucrot E (2011) Molecular mechanism and physiological functions of clathrin-mediated endocytosis. *Nat. Rev. Mol. Cell Biol.* **12**, 517–533.
- [18] Mayor S, Pagano RE (2007) Pathways of clathrin-independent endocytosis. *Nat. Rev. Mol. Cell Biol.* **8**, 603–612.

- [19] El-Sayed A, Harashima H (2013) Endocytosis of gene delivery vectors: from clathrin-dependent to lipid raft-mediated endocytosis. *Mol. Ther.* **21**, 1118–1130.
- [20] Huotari J, Helenius A (2011) Endosome maturation. *EMBO J.* **30**, 3481–3500.
- [21] Schmid SL, Carter LL (1990) ATP is required for receptor-mediated endocytosis in intact cells. *J. Cell Biol.* **111**, 2307–2318.
- [22] Larsson K (1994) *Lipids - Molecular organization, physical functions and technical applications*, The Oily Press LTD, Dundee, UK.
- [23] Vos JG, Kelly JM (2006) Ruthenium polypyridyl chemistry; from basic research to applications and back again. *Dalton Trans.* 4869–83.
- [24] Barton JK, Danishefsky AT, Goldberg JM (1984) Tris(phenanthroline)ruthenium(II): Stereoselectivity in Binding to DNA. *J. Am. Chem. Soc.* **106**, 2172–2176.
- [25] Biver T, Secco F, Venturini M (2008) Mechanistic aspects of the interaction of intercalating metal complexes with nucleic acids. *Coord. Chem. Rev.* **252**, 1163–1177.
- [26] Erkkila KE, Odom DT, Barton JK (1999) Recognition and reaction of metallointercalators with DNA. *Chem. Rev.* **99**, 2777–2796.
- [27] Hiort C, Lincoln P, Nordén B (1993) DNA binding of  $\Delta$ - and  $\Lambda$ -[Ru(phen)<sub>2</sub>dppz]<sup>2+</sup>. *J. Am. Chem. Soc.* **115**, 3448–3454.
- [28] Holmlin RE, Stemp EDA, Barton JK (1998) Ru(phen)<sub>2</sub>dppz<sup>2+</sup> luminescence: dependence on DNA sequences and groove-binding agents. *Inorg. Chem.* **37**, 29–34.
- [29] Lincoln P, Broo A, Nordén B (1996) Diastereomeric DNA-binding geometries of intercalated ruthenium(II) trischelates probed by linear dichroism: [Ru(phen)<sub>2</sub>dppz]<sup>2+</sup> and [Ru(phen)<sub>2</sub>bdppz]<sup>2+</sup>. *J. Am. Chem. Soc.* **118**, 2644–2653.
- [30] Mei H, Barton JK (1986) Chiral probe for A-form helices of DNA and RNA: Tris(tetramethylphenanthroline)ruthenium(II). *J. Am. Chem. Soc.* **108**, 7414–7416.
- [31] Barton JK, Basile LA, Danishefsky A, Alexandrescu A (1984) Chiral probes for the handedness of DNA helices: Enantiomers of tris(4,7-diphenylphenanthroline)ruthenium(II). *Proc. Natl. Acad. Sci. U. S. A.* **81**, 1961–1965.
- [32] Hiort C, Nordén B, Rodger A (1990) Enantiopreferential DNA Binding of [Ru(II)(1,10-phenanthroline)<sub>3</sub>]<sup>2+</sup> studied with linear and circular dichroism. *J. Am. Chem. Soc.* **112**, 1971–1982.
- [33] Friedman AE, Chambron J-C, Sauvage J, Turro NJ, Barton JK (1990) A molecular “light switch” for DNA: Ru(bpy)<sub>2</sub>(dppz)<sup>2+</sup>. *J. Am. Chem. Soc.* **112**, 4960–4962.
- [34] Gill MR, Thomas JA (2012) Ruthenium(II) polypyridyl complexes and DNA - from structural probes to cellular imaging and therapeutics. *Chem. Soc. Rev.* **41**, 3179–3192.
- [35] Fernández-Moreira V, Thorp-Greenwood FL, Coogan MP (2010) Application of d6 transition metal complexes in fluorescence cell imaging. *Chem. Commun.* **46**, 186–202.
- [36] McKinley AW, Lincoln P, Tuite EM (2011) Environmental effects on the photophysics of transition metal complexes with dipyrido[2,3-a:3',2'-c]phenazine (dppz) and related ligands. *Coord. Chem. Rev.* **255**, 2676–2692.

- [37] Wilhelmsson LM, Westerlund F, Lincoln P, Nordén B (2002) DNA-binding of semirigid binuclear ruthenium complex  $\Delta, \Delta$ - $[\mu$ -(11,11'-bidppz)(phen)<sub>4</sub>Ru<sub>2</sub>]<sup>4+</sup>: extremely slow intercalation kinetics. *J. Am. Chem. Soc.* **124**, 12092–12093.
- [38] Ardhammar M, Lincoln P, Nordén B (2001) Ligand substituents of ruthenium dipyridophenazine complexes sensitively determine orientation in liposome membrane. *J. Phys. Chem. B* **105**, 11363–11368.
- [39] Svensson FR, Li M, Nordén B, Lincoln P (2008) Luminescent dipyridophenazine-ruthenium probes for liposome membranes. *J. Phys. Chem. B* **112**, 10969–10975.
- [40] Luedtke NW, Hwang JS, Glazer EC, Gut D, Kol M, Tor Y (2002) Eilatin Ru(II) complexes display anti-HIV activity and enantiomeric diversity in the binding of RNA. *ChemBiochem* **3**, 766–771.
- [41] Luedtke NW (2003) The DNA and RNA specificity of eilatin Ru(II) complexes as compared to eilatin and ethidium bromide. *Nucleic Acids Res.* **31**, 5732–5740.
- [42] O'Connor NA, Stevens N, Samaroo D, Solomon MR, Martí AA, Dyer J, Vishwasrao H, Akins DL, Kandel ER, Turro NJ (2009) A covalently linked phenanthridine-ruthenium(II) complex as a RNA probe. *Chem. Commun.* 2640–2642.
- [43] Spillane CB, Smith JA, Buck DP, Collins JG, Keene FR (2007) Dinuclear ruthenium(II) complexes as potential probes for RNA bulge sites. *Dalt. Trans.* **2**, 5290–5296.
- [44] Xu H, Liang Y, Zhang P, Du F, Zhou B-R, Wu J, Liu J-H, Liu Z-G, Ji L-N (2005) Biophysical studies of a ruthenium(II) polypyridyl complex binding to DNA and RNA prove that nucleic acid structure has significant effects on binding behaviors. *J. Biol. Inorg. Chem.* **10**, 529–538.
- [45] Xu H, Deng H, Zhang Q-L, Huang Y, Liu J-Z, Ji L-N (2003) Synthesis and spectroscopic RNA binding studies of [Ru(phen)<sub>2</sub>MHPiP]<sup>2+</sup>. *Inorg. Chem. Commun.* **6**, 766–768.
- [46] Rajendiran V, Palaniandavar M, Periasamy VS, Akbarsha MA (2010) [Ru(phen)<sub>2</sub>(dppz)]<sup>2+</sup> as an efficient optical probe for staining nuclear components. *J. Inorg. Biochem.* **104**, 217–220.
- [47] Gill MR, Garcia-Lara J, Foster SJ, Smythe C, Battaglia G, Thomas J a (2009) A ruthenium(II) polypyridyl complex for direct imaging of DNA structure in living cells. *Nat. Chem.* **1**, 662–667.
- [48] Örnfelt B, Göstring I, Lincoln P, Nordén B, Örnfelt A (2002) Cell studies of the DNA bis-intercalator  $\Delta$ - $\Delta$  [ $\mu$ -C<sub>4</sub>(cpdppz)<sub>2</sub>(phen)<sub>4</sub>Ru<sub>2</sub>]<sup>4+</sup>: toxic effects and properties as a light emitting DNA probe in V79 Chinese hamster cells. *Mutagenesis* **17**, 317–320.
- [49] Zava O, Zakeeruddin SM, Danelon C, Vogel H, Grätzel M, Dyson PJ (2009) A cytotoxic ruthenium tris(bipyridyl) complex that accumulates at plasma membranes. *ChemBioChem* **10**, 1796–800.
- [50] Gill MR, Cecchin D, Walker MG, Mulla RS, Battaglia G, Smythe C, Thomas JA (2013) Targeting the endoplasmic reticulum with a membrane-interactive luminescent ruthenium(II) polypyridyl complex. *Chem. Sci.* **4**, 4512–4519.
- [51] Jiménez-Hernández ME, Orellana G, Montero F, Portolés MT (2000) A ruthenium probe for cell viability measurement using flow cytometry, confocal microscopy and time-resolved luminescence. *Photochem. Photobiol.* **72**, 28–34.
- [52] Chemla S, Chavane F (2004) Voltage-sensitive dye imaging: Technique review and models. *J. Physiol.* **104**, 40–50.

- [53] Grinvald A, Hildesheim R (2004) VSDI: a new era in functional imaging of cortical dynamics. *Nat. Rev. Neurosci.* **5**, 874–885.
- [54] Zochowski M, Wachowiak M, Falk C (2000) Imaging membrane potential with voltage-sensitive dyes. *Biol. Bull.* **198**, 1–21.
- [55] Loew LM (1996) Potentiometric dyes: Imaging electrical activity of cell membranes. *Pure Appl. Chem.* **68**, 1405–1409.
- [56] Fromherz P, Müller CO (1994) Cable properties of a straight neurite of a leech neuron probed by a voltage-sensitive dye. *Proc. Natl. Acad. Sci. U. S. A.* **91**, 4604–4608.
- [57] Gogan P, Schmiedel-Jakob I, Chitti Y, Tyc-Dumont S (1995) Fluorescence imaging of local membrane electric fields during the excitation of single neurons in culture. *Biophys. J.* **69**, 299–310.
- [58] Canepari M, Campani M, Spadavecchia L, Torre V (1996) CCD imaging of the electrical activity in the leech nervous system. *Eur. Biophys. J.* **24**, 359–370.
- [59] Bartolommei G, Devaux N, Tadini-Buoninsegni F, Moncelli M, Apell H-J (2008) Effect of clotrimazole on the pump cycle of the Na<sup>+</sup>,K<sup>+</sup>-ATPase. *Biophys. J.* **95**, 1813–1825.
- [60] Habeck M, Cirri E, Katz A, Karlish SJ, Apell H-J (2009) Investigation of electrogenic partial reactions in detergent-solubilized Na<sup>+</sup>,K<sup>+</sup>-ATPase. *Biochemistry* **48**, 9147–9155.
- [61] Pratap PR, Robinson JD (1993) Rapid kinetic analyses of the Na<sup>+</sup>/K<sup>+</sup>-ATPase distinguish among different criteria for conformational change. *Biochim. Biophys. Acta* **1151**, 89–98.
- [62] Clarke RJ, Apell H-J, Kong BY (2007) Allosteric effect of ATP on Na<sup>+</sup>/K<sup>+</sup>-ATPase conformational kinetics. *Biochemistry* **46**, 7034–7044.
- [63] Loew LM, Simpson L, Hassner A, Alexanian V (1979) An unexpected blue shift caused by differential solvation of a chromophore oriented in a lipid bilayer. *J. Am. Chem. Soc.* **101**, 5439–5440.
- [64] Loew LM, Simpson LL (1981) Charge-shift probes of membrane potential: a probable electrochromic mechanism for p-aminostyrylpyridinium probes on a hemispherical lipid bilayer. *Biophys. J.* **34**, 353–365.
- [65] Loew L, Scully S, Simpson L, Waggoner A (1979) Evidence for a charge-shift electrochromic mechanism in a probe of membrane potential. *Nature* **281**, 497–499.
- [66] Visser N V, van Hoek A, Visser AJ, Frank J, Apell HJ, Clarke RJ (1995) Time-resolved fluorescence investigations of the interaction of the voltage-sensitive probe RH421 with lipid membranes and proteins. *Biochemistry* **34**, 11777–11784.
- [67] Ries RS, Choi H, Blunck R, Bezanilla F, Heath JR (2004) Black lipid membranes: Visualizing the structure, dynamics, and substrate dependence of membranes. *J. Phys. Chem. B* **108**, 16040–16049.
- [68] Greeson JN, Raphael RM (2010) Application of fluorescence polarization microscopy to measure fluorophore orientation in the outer hair cell plasma membrane. *J. Biomed. Opt.* **12**, 021002.
- [69] Lambacher A, Fromherz P (2001) Orientation of hemicyanine dye in lipid membrane measured by fluorescence interferometry on a silicon chip. *J. Phys. Chem. B* **105**, 343–346.

- [70] Antosova Z, Mackova M, Kral V, Macek T (2009) Therapeutic application of peptides and proteins: parenteral forever? *Trends Biotechnol.* **27**, 628–635.
- [71] Danquah M, Agyei D (2012) Pharmaceutical applications of bioactive peptides. *OA Biotechnol.* **1**, 1–7.
- [72] Langel Ü (2007) *Handbook of Cell-Penetrating Peptides*, CRC Press, Taylor and Francis, Boca Raton, US.
- [73] Lange S, Lönnroth I (2001) The antisecretory factor: synthesis, anatomical and cellular distribution, and biological action in experimental and clinical studies. *Int. Rev. Cytol.* **210**, 39–75.
- [74] Ulgheri C, Paganini B, Rossi F (2010) Antisecretory factor as a potential health-promoting molecule in man and animals. *Nutr. Res. Rev.* **23**, 300–313.
- [75] Frankel AD, Pabo CO (1988) Cellular uptake of the tat protein from human immunodeficiency virus. *Cell* **55**, 1189–1193.
- [76] Joliot a, Pernelle C, Deagostini-Bazin H, Prochiantz A (1991) Antennapedia homeobox peptide regulates neural morphogenesis. *Proc. Natl. Acad. Sci. U. S. A.* **88**, 1864–1868.
- [77] Green M, Ishino M, Loewenstein PM (1989) Mutational analysis of HIV-1 Tat minimal domain peptides: identification of trans-dominant mutants that suppress HIV-LTR-driven gene expression. *Cell* **58**, 215–223.
- [78] Vivès E, Brodin P, Lebleu B (1997) A truncated HIV-1 Tat protein basic domain rapidly translocates through the plasma membrane and accumulates in the cell nucleus. *J. Biol. Chem.* **272**, 16010–16017.
- [79] Derossit D, Joliot AH, Chassaing G, Prochiantz A (1994) The third helix of the antennapedia homeodomain translocates through biological membranes. *J. Biol. Chem.* **269**, 10444–10450.
- [80] Milletti F (2012) Cell-penetrating peptides: classes, origin, and current landscape. *Drug Discov. Today* **17**, 850–860.
- [81] Madani F, Lindberg S, Langel U, Futaki S, Gräslund A (2011) Mechanisms of cellular uptake of cell-penetrating peptides. *J. Biophys.* **2011**, 414729.
- [82] Morris MC, Depollier J, Mery J, Heitz F, Divita G (2001) A peptide carrier for the delivery of biologically active proteins into mammalian cells. *Nat. Biotechnol.* **19**, 1173–1176.
- [83] Futaki S, Nakase I, Tadokoro A, Takeuchi T, Jones AT (2007) Arginine-rich peptides and their internalization mechanisms. *Biochem. Soc. Trans.* **35**, 784–787.
- [84] Fotin-Mleczek M, Fischer R, Brock R (2005) Endocytosis and cationic cell-penetrating peptides - A merger of concepts and methods. *Curr. Pharm. Des.* **11**, 3613–3628.
- [85] Ter-Avetisyan G, Tünnemann G, Nowak D, Nitschke M, Herrmann A, Drab M, Cardoso MC (2009) Cell entry of arginine-rich peptides is independent of endocytosis. *J. Biol. Chem.* **284**, 3370–3378.
- [86] Lindgren M, Hällbrink M, Prochiantz A, Langel Ü (2000) Cell-penetrating peptides. *Trends Pharmacol. Sci.* **21**, 99–103.
- [87] Bechara C, Sagan S (2013) Cell-penetrating peptides: 20 years later, where do we stand? *FEBS Lett.* **587**, 1693–1702.

- [88] Jiao C-Y, Delaroche D, Burlina F, Alves ID, Chassaing G, Sagan S (2009) Translocation and endocytosis for cell-penetrating peptide internalization. *J. Biol. Chem.* **284**, 33957–33965.
- [89] Mano M, Teodósio C, Paiva A, Simões S, Pedroso de Lima MC (2005) On the mechanisms of the internalization of S4(13)-PV cell-penetrating peptide. *Biochem. J.* **390**, 603–612.
- [90] Magzoub M, Kilk K, Eriksson LEG, Langel Ü, Gräslund A (2001) Interaction and structure induction of cell-penetrating peptides in the presence of phospholipid vesicles. *Biochim. Biophys. Acta* **1512**, 77–89.
- [91] Christiaens B, Symoens S, Vanderheyden S, Engelborghs Y, Joliot A, Prochiantz A, Vandekerckhove J, Rosseneu M, Vanloo B (2002) Tryptophan fluorescence study of the interaction of penetratin peptides with model membranes. *Eur. J. Biochem.* **269**, 2918–2926.
- [92] Persson D, Thorén PEG, Herner M, Lincoln P, Nordén B (2003) Application of a novel analysis to measure the binding of the membrane-translocating peptide penetratin to negatively charged liposomes. *Biochemistry* **42**, 421–429.
- [93] Thorén PEG, Persson D, Esbjörner EK, Goksör M, Lincoln P, Nordén B (2004) Membrane binding and translocation of cell-penetrating peptides. *Biochemistry* **43**, 3471–3489.
- [94] Caesar CEB, Esbjörner EK, Lincoln P, Nordén B (2006) Membrane interactions of cell-penetrating peptides probed by tryptophan fluorescence and dichroism techniques: Correlations of structure to cellular uptake. *Biochemistry* **45**, 7682–7692.
- [95] Jobin M-L, Bonnafous P, Tamsamin H, Dole FF, Grelard A, Dufourc EJ, Alves ID, Tamsamani H, Grélard A (2013) The enhanced membrane interaction and perturbation of a cell penetrating peptide in the presence of anionic lipids: toward an understanding of its selectivity for cancer cells. *Biochim. Biophys. Acta* **1828**, 1457–1470.
- [96] Bechara C, Pallerla M, Zaltsman Y, Burlina F, Alves ID, Lequin O, Sagan S (2013) Tryptophan within basic peptide sequences triggers glycosaminoglycan-dependent endocytosis. *FASEB J.* **27**, 738–749.
- [97] Åmand HL, Rydberg HA, Fornander LH, Lincoln P, Nordén B, Esbjörner EK (2012) Cell surface binding and uptake of arginine- and lysine-rich penetratin peptides in absence and presence of proteoglycans. *Biochim. Biophys. Acta* **1818**, 2669–2678.
- [98] Ziegler A, Seelig J (2008) Binding and clustering of glycosaminoglycans: a common property of mono- and multivalent cell-penetrating compounds. *Biophys. J.* **94**, 2142–2149.
- [99] Ziegler A, Seelig J (2011) Contributions of glycosaminoglycan binding and clustering to the biological uptake of the nonamphipatic cell-penetrating peptide WR9. *Biochemistry* **50**, 4650–4664.
- [100] Walrant A, Correia I, Jiao C-Y, Lequin O, Bent EH, Goasdoué N, Lacombe C, Chassaing G, Sagan S, Alves ID (2011) Different membrane behaviour and cellular uptake of three basic arginine-rich peptides. *Biochim. Biophys. Acta* **1808**, 382–393.
- [101] Mitchell DJ, Kim DT, Steinman L, Fathman CG, Rothbard JB (2000) Polyarginine enters cells more efficiently than other polycationic homopolymers. *J. Pept. Res.* **56**, 318–325.
- [102] Maiolo JR, Ferrer M, Ottinger EA (2005) Effects of cargo molecules on the cellular uptake of arginine-rich cell-penetrating peptides. *Biochim. Biophys. Acta* **1712**, 161–172.
- [103] Rothbard JB, Kreider E, VanDeusen CL, Wright L, Wylie BL, Wender PA (2002) Arginine-rich molecular transporters for drug delivery: Role of backbone spacing in cellular uptake. *J. Med. Chem.* **45**, 3612–3618.

- [104] Johansson E, Lönnroth I, Jonson I, Lange S, Jennische E (2009) Development of monoclonal antibodies for detection of Antisecretory Factor activity in human plasma. *J. Immunol. Methods* **342**, 64–70.
- [105] Lönnroth I, Lange S (1986) Purification and characterization of the antisecretory factor: a protein in the central nervous system and in the gut which inhibits intestinal hypersecretion induced by cholera toxin. *Biochim. Biophys. Acta* **883**, 138–144.
- [106] Johansson E, Lönnroth I, Lange S, Jonson I, Jennische E, Lönnroth C (1995) Molecular cloning and expression of a pituitary gland protein modulating intestinal fluid secretion. *J. Biol. Chem.* **270**, 20615–20620.
- [107] Johansson E, Jennische E, Lange S, Lönnroth I (1997) Antisecretory factor suppresses intestinal inflammation and hypersecretion. *Gut* **41**, 642–645.
- [108] Davidson T, Hickey W (2004) Antisecretory factor expression is regulated by inflammatory mediators and influences the severity of experimental autoimmune encephalomyelitis. *J. Leukoc. Biol.* **74**, 835–844.
- [109] Björck S, Bosaeus I, Ek E, Jennische E, Lönnroth I, Johansson E, Lange S (2000) Food induced stimulation of the antisecretory factor can improve symptoms in human inflammatory bowel disease: a study of a concept. *Gut* **46**, 824–829.
- [110] Lange S, Lönnroth I (1984) Passive transfer of protection against cholera toxin in rat intestine. *FEMS Microbiol. Lett.* **24**, 165–168.
- [111] Lönnroth I, Lange S (1984) Purification and characterization of a hormone-like factor which inhibits cholera secretion. *FEBS Lett.* **177**, 104–108.
- [112] Lönnroth I, Lange S, Jennische E, Johansson E, Jonson I, Torres J (2003) Cholera toxin protects against action by Clostridium difficile toxin A. The role of antisecretory factor in intestinal secretion and inflammation in rat. *APMIS* **111**, 969–977.
- [113] Lönnroth I, Lange S, Skadhauge E (1988) The antisecretory factors: inducible proteins which modulate secretion in the small intestine. *Comp. Biochem. Physiol.* **90**, 611–617.
- [114] Lönnroth I, Lange S (1985) A hormone-like protein from the pituitary gland inhibits intestinal hypersecretion induced by cholera toxin. *Regul. Pept. Suppl.* **4**, 216–218.
- [115] Johansson E, Lange S, Lönnroth I (1997) Identification of an active site in the antisecretory factor protein. *Biochim. Biophys. Acta* **1362**, 177–182.
- [116] Zaman S, Mannan J, Lange S, Lönnroth I, Hanson L-A (2007) B 221, a medical food containing antisecretory factor reduces child diarrhoea: a placebo controlled trial. *Acta Paediatr.* **96**, 1655–1659.
- [117] Jennische E, Bergström T, Johansson M, Nyström K, Tarkowski A, Hansson H-A, Lange S (2008) The peptide AF-16 abolishes sickness and death at experimental encephalitis by reducing increase of intracranial pressure. *Brain Res.* **1227**, 189–197.
- [118] Al-Olama M, Wallgren A, Andersson B, Gatzinsky K, Hultborn R, Karlsson-Parra A, Lange S, Hansson H-A, Jennische E (2011) The peptide AF-16 decreases high interstitial fluid pressure in solid tumors. *Acta Oncol.* **50**, 1098–1104.
- [119] Svensson K, Lange S, Lönnroth I, Widström A-M, Hanson L (2004) Induction of anti-secretory factor in human milk may prevent mastitis. *Acta Paediatr.* **93**, 1228–1231.

- [120] Hanner P, Jennische E, Lange S, Lönnroth I, Wahlström B (2004) Increased antiseecretory factor reduces vertigo in patients with Ménière's disease: a pilot study. *Hear. Res.* **190**, 31–36.
- [121] Young P, Deveraux Q, Beal RE, Pickart CM, Rechsteiner M (1998) Characterization of two polyubiquitin binding sites in the 26 S protease subunit 5a. *J. Biol. Chem.* **273**, 5461–5467.
- [122] Johansson E, Jonson I, Bosaeus M, Jennische E (2008) Identification of flotillin-1 as an interacting protein for antiseecretory factor. *Regul. Pept.* **146**, 303–309.
- [123] Lange S, Malmberg P, Nygren H (2013) Binding of the VCHSKT peptide to ceramide-rich and cholesterol-rich domains of cell membranes in rat pancreatic glands. *Surf. Interface Anal.* **45**, 268–272.
- [124] Statistics of Child Mortality 2008, World Health Organisation, [www.who.int](http://www.who.int), accessed 2012-03-18.
- [125] National Encyklopedin, [www.ne.se](http://www.ne.se), accessed 2014-10-20.
- [126] Hollas JM (2007) *Modern Spectroscopy*, John Wiley and Sons Ltd, Chichester, UK.
- [127] Parson WW (2007) *Modern Optical Spectroscopy*, Springer-Verlag Berlin Heidelberg, Heidelberg, Germany.
- [128] Lakowicz JR (2006) *Principles of Fluorescence Spectroscopy*, Springer Science, New York, USA.
- [129] Nordén B, Rodger A, Dafforn T (2010) *Linear dichroism and circular dichroism - A textbook on polarized-light spectroscopy*, RSC Publishing, Cambridge, U.K.
- [130] Pawley JB (2006) *Handbook of Biological Confocal Microscopy*, Springer Science, New York, USA.
- [131] Marcey MG (2007) *Flow Cytometry - Principles and Applications*, Humana Press Inc., Totowa, USA.
- [132] Freyer MW, Lewis EA (2008) Isothermal titration calorimetry: experimental design, data analysis, and probing macromolecule/ligand binding and kinetic interactions. *Methods Cell Biol.* **84**, 79–113.
- [133] Rodino S, Butu M, Golea D, Butu A (2012) Fundamentals of Isothermal Titration Calorimetry and Some Applications. *Banat. J. Biotechnol.* **3**, 18–22.
- [134] Saboury AA (2006) A review on the ligand binding studies by isothermal titration calorimetry. *J. Iran. Chem. Soc.* **3**, 1–21.
- [135] Reichardt C (1994) Solvatochromic dyes as solvent polarity indicators. *Chem. Rev.* **94**, 2319–2358.
- [136] Schoonover JR, Bates WD, Meyer TJ (1995) Application of resonance raman spectroscopy to electronic structure in metal complex excited states. Excited-state ordering and electron delocalization in Dipyrrodo[3,2-a:2',3'-c]phenazine (dppz): Complexes of Re(I) and Ru(II). *Inorg. Chem.* **43**, 6421–6422.
- [137] Olofsson J, Önfelt B, Lincoln P (2004) Three-state light switch of [Ru(phen)<sub>2</sub>dppz]<sup>2+</sup>: Distinct excited-state species with two, one, or no hydrogen bonds from solvent. *J. Phys. Chem. A* **108**, 4391–4398.

- [138] Önfelt B, Olofsson J, Lincoln P, Nordén B (2003) Picosecond and Steady-State Emission of [Ru(phen)<sub>2</sub>dppz]<sup>2+</sup> in Glycerol: Anomalous Temperature Dependence. *J. Phys. Chem. A* **107**, 1000–1009.
- [139] Olson EJC, Hu D, Hörmann A, Jonkman AM, Arkin MR, Stemp EDA, Barton JK, Barbara PF (1997) First observation of the key intermediate in the “light-switch” mechanism of [Ru(phen)<sub>2</sub>dppz]<sup>2+</sup>. *J. Am. Chem. Soc.* **119**, 11458–11467.
- [140] Fluhler E, Burnham VG, Loew LM (1985) Spectra, membrane binding, and potentiometric responses of new charge shift probes. *Biochemistry* **24**, 5749–5755.
- [141] Kuhn B, Fromherz P (2003) Anellated hemicyanine dyes in a neuron membrane: Molecular stark effect and optical voltage recording. *J. Phys. Chem. B* **107**, 7903–7913.
- [142] Callis PR (2010) Electrochromism and solvatochromism in fluorescence response of organic dyes: A nanoscopic view. In *Advanced Fluorescence Reporters in Chemistry and Biology I: Fundamentals and Molecular Design, Springer Series on Fluorescence, Volume 8*, Demchenko AP, ed. Springer Berlin Heidelberg, Berlin, Heidelberg, pp. 309–330.
- [143] Clarke RJ, Zouni A, Holzwarth JF (1995) Voltage sensitivity of the fluorescent probe RH421 in a model membrane system. *Biophys. J.* **68**, 1406–1415.
- [144] Osakai T, Sawada J, Nagatani H (2009) Potential-modulated fluorescence spectroscopy of the membrane potential-sensitive dye di-4-ANEPPS at the 1,2-dichloroethane/water interface. *Anal. Bioanal. Chem.* **395**, 1055–1061.
- [145] Fromherz P, Lambacher A (1991) Spectra of voltage-sensitive fluorescence of styryl-dye in neuron membrane. *Biochim. Biophys. Acta* **1068**, 149–156.
- [146] Pham THN, Clarke RJ (2008) Solvent dependence of the photochemistry of the styrylpyridinium dye RH421. *J. Phys. Chem. B* **112**, 6513–6520.
- [147] Le Goff G, Vitha MF, Clarke RJ (2007) Orientational polarisability of lipid membrane surfaces. *Biochim. Biophys. Acta* **1768**, 562–570.
- [148] Li H, Mao G, Singer KD, Lu Z, Weber R, Twieg RJ (2007) Solvent effects on the nonlinear optical response of a potentiometric biological imaging dye. *J. Opt. Soc. Am. B* **24**, 1310–1318.
- [149] Mishra A, Behera G., Krishna MM., Periasamy N (2001) Time-resolved fluorescence studies of aminostyryl pyridinium dyes in organic solvents and surfactant solutions. *J. Lumin.* **92**, 175–188.
- [150] Clarke RJ, Schrimpf P, Schöneich M (1992) Spectroscopic investigations of the potential-sensitive membrane probe RH421. *Biochim. Biophys. Acta* **1112**, 142–152.
- [151] Wolfbeis O (1995) Fluorescence-based ion sensing using potential-sensitive dyes. *Sensors Actuators B Chem.* **4005**, 140–147.
- [152] Ephardt H, Fromherz P (1991) Anilinopyridinium: solvent-dependent fluorescence by intramolecular charge transfer. *J. Phys. Chem.* **95**, 6792–6797.
- [153] Ephardt H, Fromherz P (1993) Fluorescence of amphiphilic hemicyanine dyes without free double bonds. *J. Phys. Chem.* **97**, 4540–4547.
- [154] Krishna M, Periasamy N (1998) Fluorescence of organic dyes in lipid membranes: site of solubilization and effects of viscosity and refractive index on lifetimes. *J. Fluoresc.* **8**, 81–91.

- [155] Visser N, van Hoek A, Visser A, Clarke R, Holzwarth J (1994) Time-resolved polarized fluorescence of the potential-sensitive dye RH421 in organic solvents and micelles. *Chem. Phys. Lett.* **231**, 551–560.
- [156] Fromherz P, Schenk O (1994) Voltage-sensitive fluorescence of amphiphilic hemicyanine dyes in a black lipid membrane of glycerol monooleate. *Biochim. Biophys. Acta* **1191**, 299–308.
- [157] Fromherz P, Müller CO (1993) Voltage-sensitive fluorescence of amphiphilic hemicyanine dyes in neuron membrane. *Biochim. Biophys. Acta* **1150**, 111–122.
- [158] Schmid F (2001) Biological macromolecules: UV-visible spectrophotometry. *Encycl. Life Sci.* 1–4.
- [159] Pace CN, Vajdos F, Fee L, Grimsley G, Gray T (1995) How to measure and predict the molar absorption coefficient of a protein. *Protein Sci.* **4**, 2411–2423.
- [160] Smith PK, Krohn RI, Hermanson GT, Mallia AK, Gartner FH, Provenzano MD, Fujimoto EK, Goeke NM, Olson BJ, Klenk DC (1985) Measurement of protein using bicinchoninic acid. *Anal. Biochem.* **150**, 76–85.
- [161] Wiechelman KJ, Braun RD, Fitzpatrick JD (1988) Investigation of the bicinchoninic acid protein assay: identification of the groups responsible for color formation. *Anal. Biochem.* **175**, 231–237.
- [162] Ardhammar M, Lincoln P, Nordén B (2002) Invisible liposomes: Refractive index matching with sucrose enables flow dichroism assessment of peptide orientation in lipid vesicle membrane. *Proc. Natl. Acad. Sci. U. S. A.* **99**, 15313–15317.
- [163] Semwogerere D, Weeks ER (2005) Confocal Microscopy. In *Encyclopedia of Biomaterials and Biomedical Engineering* Taylor and Francis, London, UK.
- [164] Lingler FS, Kim JS. (2010) *The Microflow Cytometer*, Pan Stanford Publishing, Singapore.
- [165] Puckett CA, Barton JK (2007) Methods to explore cellular uptake of ruthenium complexes. *J. Am. Chem. Soc.* **129**, 46–47.
- [166] Gill MR, Derrat H, Smythe CGW, Battaglia G, Thomas JA (2011) Ruthenium(II) metallo-intercalators: DNA imaging and cytotoxicity. *ChemBiochem* **12**, 877–880.
- [167] Puckett CA, Barton JK (2008) Mechanism of cellular uptake of a ruthenium polypyridyl complex. *Biochemistry* **47**, 11711–11716.
- [168] Dobrucki JW (2001) Interaction of oxygen-sensitive luminescent probes Ru(phen)<sub>3</sub><sup>2+</sup> and Ru(bipy)<sub>3</sub><sup>2+</sup> with animal and plant cells *in vitro*. Mechanism of phototoxicity and conditions for non-invasive oxygen measurements. *J. Photochem. Photobiol. B.* **65**, 136–144.
- [169] Svensson FR, Abrahamsson M, Strömberg N, Ewing AG, Lincoln P (2011) Ruthenium(II) Complex Enantiomers as Cellular Probes for Diastereomeric Interactions in Confocal and Fluorescence Lifetime Imaging Microscopy. *J. Phys. Chem. Lett.* **2**, 397–401.
- [170] Rydberg HA, Carlsson N, Nordén B (2012) Membrane interaction and secondary structure of de novo designed arginine- and tryptophan peptides with dual function. *Biochem. Biophys. Res. Commun.* **427**, 261–5.
- [171] Gallagher K, Sharp K (1998) Electrostatic contributions to heat capacity changes of DNA-ligand binding. *Biophys. J.* **75**, 769–776.

- [172] Gonçalves E, Kitas E, Seelig J (2005) Binding of oligoarginine to membrane lipids and heparan sulfate: structural and thermodynamic characterization of a cell-penetrating peptide. *Biochemistry* **44**, 2692–2702.
- [173] Burlina F, Sagan S, Bolbach G, Chassaing G (2005) Quantification of the cellular uptake of cell-penetrating peptides by MALDI-TOF mass spectrometry. *Angew. Chem. Int. Ed. Engl.* **44**, 4244–4247.
- [174] Alves ID, Bechara C, Walrant A, Zaltsman Y, Jiao C-Y, Sagan S (2011) Relationships between membrane binding, affinity and cell internalization efficacy of a cell-penetrating peptide: penetratin as a case study. *PLoS One* **6**, e24096.
- [175] Klocek G, Schulthess T, Shai Y, Seelig J (2009) Thermodynamics of melittin binding to lipid bilayers. Aggregation and pore formation. *Biochemistry* **48**, 2586–2596.
- [176] Fernández-Vidal M, White SH, Ladokhin AS (2011) Membrane partitioning: “classical” and “nonclassical” hydrophobic effects. *J. Membr. Biol.* **239**, 5–14.
- [177] Walrant A, Vogel A, Correia I, Lequin O, Olausson BES, Desbat B, Sagan S, Alves ID (2012) Membrane interactions of two arginine-rich peptides with different cell internalization capacities. *Biochim. Biophys. Acta* **1818**, 1755–1763.
- [178] Bernèche S, Nina M, Roux B (1998) Molecular dynamics simulation of melittin in a dimyristoylphosphatidylcholine bilayer membrane. *Biophys. J.* **75**, 1603–1618.
- [179] Ran S, Downes A, Thorpe PE, Vessels B (2002) Increased exposure of anionic phospholipids on the surface of tumor blood vessels. *Cancer Res.* **62**, 6132–6140.
- [180] Dube DH, Bertozzi CR (2005) Glycans in cancer and inflammation--potential for therapeutics and diagnostics. *Nat. Rev. Drug Discov.* **4**, 477–488.
- [181] Delehedde M, Allain F, Payne SJ, Borgo R, Vanpouille C, Fernig DG, Deudon E (2002) Proteoglycans in inflammation. *Curr. Med. Chem. Anti Inflamm. Anti Allergy Agents* **1**, 89–102.
- [182] Parish CR (2006) The role of heparan sulphate in inflammation. *Nat. Rev. Immunol.* **6**, 633–643.
- [183] Puckett CA, Barton JK (2010) Targeting a ruthenium complex to the nucleus with short peptides. *Bioorg. Med. Chem.* **18**, 3564–3569.
- [184] Puckett CA, Barton JK (2009) Fluorescein redirects a ruthenium-octaarginine conjugate to the nucleus. *J. Am. Chem. Soc.* **131**, 8738–8739.

